Predictive Dynamic Simulation of Cycling Using Olympic Cyclist and Bicycle Models

by

Conor Jansen

A thesis
presented to the University of Waterloo
in fulfillment of the
thesis requirement for the degree of
Master of Applied Science
in
Systems Design Engineering

Waterloo, Ontario, Canada, 2018

I hereby declare that I am the sole author of this thesis. This is a true copy of the thesis, including any required final revisions, as accepted by my examiners.

I understand that my thesis may be made electronically available to the public.

Abstract

Predictive dynamic simulation is a useful tool for analyzing human movement and optimizing performance. Such simulations do not require experimental data collection and provide the opportunity to analyze a variety of potential scenarios. This presents interesting possibilities for investigating the optimal technique in sports applications, such as cycling. Much of the previous research on modeling and simulation of cycling has focused on seated pedaling and models the bicycle or ergometer with an effective resistive torque and inertia. This study was focused on modeling standing starts, a component of certain track cycling events in which the cyclist starts from rest and attempts to accelerate to top speed as quickly as possible. A useful model would need to incorporate bicycle dynamics, including tire models, and complete cyclist dynamics, including the upper body.

A ten degree-of-freedom, two-legged cyclist and bicycle model was developed using MapleSim and utilized for predictive simulations of standing starts. A joint torque model was incorporated to represent musculoskeletal dynamics, including scaling based on joint angle and angular velocity to represent the muscle force-length and force-velocity relationships. Tire slip for the bicycle model was represented by the Pacejka tire model for wheel-ground contact. GPOPS-II, a direct collocation optimal control software, was used to solve the optimal control problem for the predictive simulation.

First, a modified version of this model was used to simulate ergometer pedaling. The model was validated by comparing simulated ergometer pedaling against ergometer pedaling performed by seven Olympic-level track cyclists from the Canadian team. A kinematic data tracking approach was used to assess the abilities of the model to match experimental data. Following the successful matching of experimental data, a purely predictive simulation was performed for seated maximal start-up ergometer pedaling with an objective function of maximizing the crank progress. These simulations produce joint angles, crank torque, and power similar to experimental results, indicating that the model was a reasonable representation of an Olympic cyclist.

Subsequently, experimental data were collected for a single member of the Canadian team performing standing starts on the track. Data collected included crank torque, cadence, and joint kinematics. Predictive simulations of standing starts were performed using the combined cyclist and bicycle model. Key aspects of the standing start technique, including the drive and reset, were captured in the predictive simulations. The results show that optimal control can be used for predictive simulation with a combined cyclist and bicycle model. Future work to improve upon the current model is discussed.

Acknowledgements

I would like to thank my supervisor, Professor John McPhee, for the opportunity to conduct this research and for his guidance and support throughout this project.

I would also like to thank Mike Patton and Will George at Cycling Canada for their assistance and for sharing their knowledge of track cycling. Additional thanks goes out to Canadian Sport Institute Ontario, Cycling Canada, and the members of the Canadian track cycling team for their support and participation in experiments.

Finally, I would like to thank all the members of the Motion Research Group at the University of Waterloo for their suggestions and feedback over the past two years.

This research was financially supported by the Natural Sciences and Engineering Research Council of Canada and the Canada Research Chairs program.

Table of Contents

List of Tables

List of Figures

Chapter 1

Introduction

1.1 Background

Track cycling is a highly competitive sport, especially at the Olympic level, with races often being decided by fractions of seconds. Track cycling takes place in a velodrome, an arena (usually indoors) that consists of an oval-shaped track with steeply banked ends. For a velodrome that meets Olympic standards, the track is 250 meters long with 42-degree banked bends and 13-degree banked straights. For indoor velodromes, the track itself is typically made of pine. Figure 1.1 shows the velodrome at the Mattamy National Cycling Centre in Milton, Ontario, one of two velodromes in North America capable of hosting Olympic, Paralympic, and elite world championship events.

Figure 1.1: The velodrome at the Mattamy National Cycling Centre in Milton, Ontario [5]

Figure 1.2: A track cycling sprint bicycle [6]

There are various different events in track cycling, some of which are performed as a team and some individually. Track cycling events can generally be split into two categories: sprint events and endurance events. Sprint events are shorter and much more focused on speed so the cyclists are trying to generate as much power as possible. In endurance events, efficiency and pacing are a greater concern.

The bicycles used in track cycling are a feat unto themselves, with engineers and developers always striving to make their bicycles as lightweight and efficient as possible. For Olympic-level cyclists, the frame is typically made of carbon fiber, which is rigid and lightweight (see Figure 1.2). Track cycling wheels are also predominantly made of carbon fiber, although aluminum spokes are often used during practice. The Union Cycliste Internationale (UCI), track cycling's governing body, mandates that bicycles must exceed a minimum total weight of 6.8 kg. Most bicycle manufacturers are capable of manufacturing bicycles at less than that weight, so a track bicycle is usually designed to that specification. Aerodynamics plays an important role in track cycling, as the cyclists can achieve speeds of over 70 km/h. In addition to riding a bicycle that has been designed to be as aerodynamic as possible, cyclists will wear tight-fitting aerodynamic suits and helmets. In track cycling, bicycles with a fixed high gear ratio are used so the cyclists can generate as much power as possible at high speeds. The fixed gear ratio means the pedal motion is directly connected to the wheel motion (i.e. there is no "freewheeling"). The cyclists clip their feet into the pedals, ensuring their feet are always in contact with the pedals. The tires used in track cycling are tubular tires that are typically inflated to approximately 200 psi to reduce rolling resistance (for comparison, road cycling tires are usually inflated to 90-125 psi). They are made to be as light as possible and are made from a softer compound that has better grip than road tires.

(a) Pre-launch (b) Gate Release (c) Drive (d) Reset

Figure 1.3: A standing start performed by a member of the Canadian team

In certain events, such as the team sprint, the cyclists start from a stand-still and then accelerate to their top speed as quickly as possible, a maneuver referred to as a standing start. The lead cyclist on each team starts in the gate, which fixes the bicycle position (Figure 1.3a). During the pre-launch, the cyclist rocks their hips back and then launches forward in an attempt to have as much forward momentum as possible when the countdown reaches 0 and the bicycle is released from the gate (Figure 1.3b). As they launch out of the gate, they drive their hips forward relative to the bicycle (Figure 1.3c). This allows them to get their hips over the bottom bracket, thus using their weight to generate more torque at the crank. As the crank approaches a vertical position (referred to as top dead center), they enter a mechanically inefficient position. It is difficult to generate torque with the crank in this position, so the cyclist wants to spend as little time as possible in this position. To overcome this mechanically inefficient position, they shift their hips backwards relative to the frame, in the process pushing their bike forward underneath them and propelling the crank through the top dead center position (Figure 1.3d). After passing through top dead center, the cyclist drives forward again, getting up over the bottom bracket. The cyclist will complete this periodic motion several times, growing less pronounced with each pedal stroke, until they have increased the angular velocity of the crank to its top speed.

1.2 Motivation and Research Goals

Over the years, significant work has been put into optimizing track cycling performance by studying the effects of various bicycle designs and cycling techniques. Much of the research has been focused on making the bicycle more mechanically efficient (e.g. reducing the weight of the bicycle) and making the cyclist and bicycle more aerodynamic. Previously, there have been few efforts to model the multibody dynamics of both the cyclist and bicycle together.

The overarching goal of this work was to develop a dynamical model of a cyclist and bicycle that can be used for predictive simulations of cycling. The idea is that such a model would be reasonably easy to adapt to various cycling questions. The development of a predictive dynamic simulation of cycling would allow for various aspects of cycling such as seat and handlebar positions, gear ratios, pedaling rates, and general biomechanical technique to be tested much more quickly than with experiments. Predictive computer simulation is useful in this regard because it allows for numerous trials under various conditions in a relatively short period of time, and it does not rely on previous experimental data. The challenge with a forward dynamics model is in finding the appropriate simplifications to get a useful model: too much detail and the model is overly complex; too simple and the model is not an accurate representation of real life.

The focus of this project was prompted by discussions with members of Cycling Canada, who are interested in two main points regarding standing starts in track cycling. They want to know, in general, what defines the "optimal" kinematics in a standing start. They are also interested in finding the optimal crank angle at which to start. The standing start can be broken down into two phases: pre-launch and launch. The pre-launch phase consists of the portion up until the gate release, and the launch phase is the portion from gate release up until the cyclist enters the first turn (approximately 30 m). The goals within the pre-launch are to (1) maximize initial forward velocity at the time of gate release, (2) time the gate release so that forward progress begins as the gate releases, and (3) optimize the body position for the start of the launch phase [7]. The goals for the launch phase are much less concrete at this time. In general, the goal is to rise from the seat and use the additional degrees of freedom to maximum advantage. By shifting the body relative to the crank, one can optimize the body relative to the crank in a position best for producing torque. Another hypothesis is that the ability to engage different muscle groups might play an important role for maximizing torque production during the standing start [7].

To summarize, the goal was to model a standing start to gain a better understanding of the optimal kinematics, including aspects such as the initial pose. The initial objective was to develop a model that is a faithful representation of a cyclist and bicycle. Once the model was developed, it was validated using results from experimental analysis of ergometer pedaling and a model representing those experimental conditions. The bicycle and cyclist model was then utilized for predictive simulations of standing starts. These simulation results were compared against experimental results for a standing start on the track.

1.3 Thesis Structure

- Chapter 1 provides background on track cycling, discusses the motivation and research goals, and outlines the main contributions of this work.
- Chapter 2 contains a review of relevant literature regarding modeling of cycling and bicycle dynamics.
- Chapter 3 contains details on the development of the cyclist and bicycle model, and describes the optimal control process used in all the predictive simulations.
- Chapter 4 contains experimental results from ergometer testing for members of the Canadian track cycling team. It explains how the model was modified to represent ergometer pedaling. A data tracking approach was utilized to test the model's ability to match experimental results. Predictive simulations were performed to compare how the optimal result for the ergometer pedaling model compared to experiments performed under similar conditions.
- Chapter 5 contains the experimental methods and results from standing starts on the velodrome track. The cyclist and bicycle model was utilized for predictive simulations of standing starts. The results from the experiments and simulations are compared.
- Chapter 6 contains a summary of the work and a discussion of the key findings. It concludes with suggestions for future work.

1.4 Contributions

- A multibody dynamics model of a cyclist and bicycle that reflects the capabilities of an Olympic cyclist and bicycle
- A predictive simulation of ergometer pedaling using direct collocation optimal control
- An implementation of a tire model with a bicycle model that includes a dynamic cyclist
- An experimental analysis of a standing start including crank torque, crank kinematics, and joint kinematics
- A predictive simulation of a track cycling standing start using direct collocation optimal control

Chapter 2

Literature Review

2.1 General Competitive Track Cycling Research

There are several different aspects of cycling that can be analyzed to understand the factors that contribute to performance. These could generally be broken down into two categories: optimization of the cyclist (e.g. technique, strategy, and physiological capabilities) and optimization of the equipment (e.g. bicycle, suit, and helmet). With the suit and helmet, the primary goal is to make them as aerodynamic as possible. With the bicycle, the goals are to be aerodynamic and mechanically efficient (e.g. optimizing the weight of the bicycle, rolling resistance, frame stiffness, bearing and chain efficiency, etc.). For the cyclist, researchers have investigated factors affecting power production and fatigue, with the goal usually focused on optimizing cycling position and pacing strategies.

Several mathematical models [8, 9, 10, 11] have been developed that look at fatigue and pacing strategies, in addition to examining the effect of changing bicycle parameters. These generally use an experimentally-measured power as the input to the model and neglect cyclist biomechanics. Flyger et al. [12] took the work of Martin et al. [9] and replaced the power data input with a model of physiological energy supply. Again the dynamics of the cyclist were not analyzed, and they simply utilized the torque that the cyclist was generating at the crank. One of their modifications was to add an initial velocity for the center of mass that essentially represents the outcome of the pre-launch in the standing start technique. There have been relatively few studies focused specifically on the starting technique in track cycling. Janssen and Cornelissen [13] collected pedal forces during standing starts for BMX and track cyclists and reported the maximum forces during each of the first two pedal strokes. The experimental studies most relevant to

this work were the experiments of Padulo et al. [14, 15], who investigated the starting conditions for track cycling, but were limited to two conditions for starting crank angle (71° and 47°), hand position, and seated/standing. Of the configurations they tested, the best performance was achieved when in the standing position with the hands on the upper bar of the handlebar and an initial crank angle of 71°.

The limitation of experimental analysis is that numerous tests have to be conducted and it is not always clear how various factors affect each other. A limitation of the power-based and energy-based mathematical models is that they do not aid in understanding how the cyclist is interacting with the bicycle. In many cases, extensive testing is required to understand this interaction and ongoing testing is still required. A biomechanical model is useful in this regard because it allows one to investigate the biomechanics of the cyclist and the interactions between the cyclist and the bicycle. The idea is that once testing has been conducted and the model has been validated, numerous different experimental conditions could be tested.

2.2 Multibody Dynamic Analysis: Inverse Dynamics versus Forward Dynamics

Relatively little work has been done regarding musculoskeletal modeling and dynamic simulations specific to competitive track cycling. One of the key distinctions to make for biomechanical analysis is between inverse dynamics and forward dynamics. Both inverse and forward dynamics can be useful, depending on the questions you are trying to answer. For inverse dynamics, one uses experimentally-measured external kinetics and kinematics to find the torques and forces acting on various joints. For forward dynamics models on the other hand, the model is driven using torques or forces. Forward dynamics usually requires some form of optimization to find the actuations that achieve the desired goal. Within forward dynamics, there are different methods of driving the simulations. One is to collect experimental data and then drive the model to match this data; this is referred to as "data tracking" simulation in this thesis. With the use of experimental data, it is closer in nature to inverse dynamics and is often used to find the muscle activations and forces required for a given experimentally-measured motion. Alternatively, one can have simulations that are purely predictive in nature. In such simulations, no experimental data are used to drive the simulation, and the model is driven using a representative objective function, such as achieving the maximum distance.

2.2.1 Inverse Dynamics of Cycling

Inverse dynamics is not the focus of this work, so only a brief overview of relevant literature will be discussed. In 2009, Bini and Diefenthaeler [16] conducted a review of the various studies on mechanical work in cycling. One of the findings they discussed was that different joints should be playing different roles during the pedaling motion; each joint is not focused only on force production. For example, at times in pedaling, the primary use of the ankle joint seems to be to provide stiffness and transmit the mechanical energy produced by the hips and knees to the crank. Wangerin et al. [17] conducted inverse dynamics analysis for four cyclists who were were asked to maintain a power output of 350W at a cadence of 90 revolutions per minute (rpm). They were investigating the influence of pedaling rate and power on joint moments. Martin and Brown [18] were interested in the effects of fatigue on joint kinematics and power. In their study, thirteen trained cyclists performed a 30-second maximal cycling trial at 120 rpm. They found that changes in power were related to the decrease in amount of time spent extending the legs due to fatigue, as the extending motion is more powerful than the flexing motion. More recently, in 2016, Yamazaki and Matsuda found the inverse dynamics for amateur male cyclists producing 200W at 90 rpm [19].

This is just a sample of the inverse dynamics analyses that have been conducted. Pure inverse dynamics analysis has somewhat reduced in popularity, as now there is more focus on what is happening at the muscular level, rather than only the joint level. The main limitations of inverse dynamics are the potential for errors in data collection and the simplifications made in developing the model. Furthermore, data collection can be time-consuming and expensive. For example, one of the primary interests in experimental data collection for cycling, and a key necessity of inverse dynamics, is pedal force data. This requires pedal force sensors, which can be expensive, especially for ones that give accurate and reliable measurements. This example is used to show that there are limitations to inverse dynamics and reliable results can be difficult, time-consuming, and expensive to obtain. Forward dynamics is more dependent on accurate modeling, but can be less dependent on experimental data. When it comes to optimization and trying to improve performance, forward dynamics and predictive simulation is more useful.

2.2.2 Musculoskeletal Modeling and Forward Dynamics of Cycling

In forward dynamics, the model is driven using a force or torque activation as the inputs. The kinematics are then solved for from these forces or torques. In their paper on developing musculoskeletal models, Hicks et al. [1] present the flowchart in Figure 2.1 that

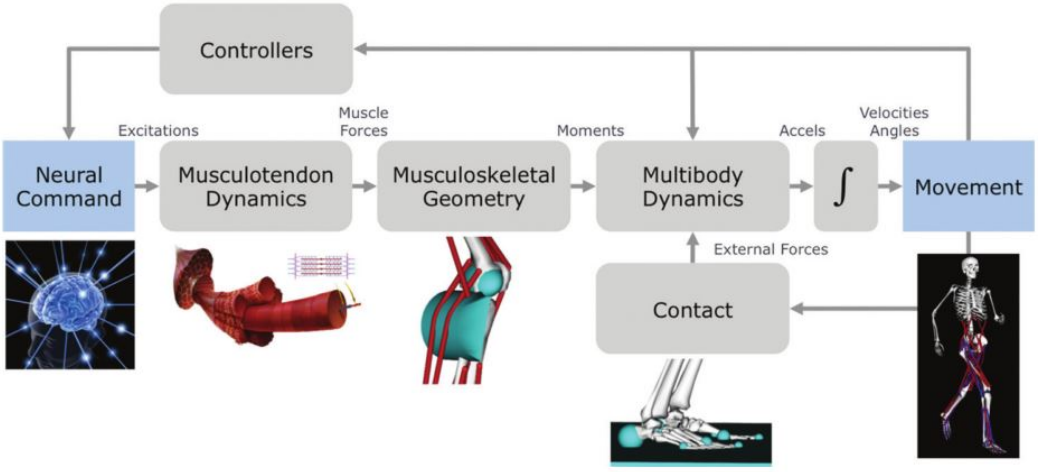

Figure 2.1: Flowchart of forward dynamics presented by Hicks et al. [1]. Reproduced with permission from American Society of Mechanical Engineers.

displays the forward dynamics process in a straightforward manner. One of the challenges with forward dynamics is determining the best place to enter the process flow. There are two main ways to drive a biomechanical model using forward dynamics. One is to include individual muscles and to activate them using muscle excitations (entering at the far left of the flow chart in Figure 2.1). Using forward dynamics on a musculoskeletal level allows one to identify individual muscle contributions and investigate muscle coordination [20, 21, 22]. However, this can become computationally intensive when using optimal control methods because of the increased number of state variables. An alternative is to use applied torques (entering in the middle of the process flow, at the step labeled "Moments" in Figure 2.1) to represent the combination of muscle forces on a joint and activate them using a representative excitation. This reduces the number of variables and simplifies the optimal control problem.

Muscle models

Various muscle models have been developed starting with the simple muscle model developed by Hill [23]. Advancements and adaptations have been made over the years (see [24] for one version), but the focus of these models is accurately capturing musculotendon dynamics. Muscle models usually consist of a contractile element representing the muscle body, a series elastic component representing the tendon and everything acting in series to the muscle, and a parallel elastic component representing the ligament, connective tis-

sue around the muscle, and other passive elastic components. Muscle forces are scaled based on the muscle force-length and force-velocity curve that has been experimentally determined. Activation dynamics are included as well to represent the neural excitation to muscle activation process.

In lower limb models developed specifically for cycling [20, 22, 25, 26, 27, 28], generally 9-15 muscles per leg have been included in the model. This has been accepted as an accurate method of modeling the lower limb. The primary drawback of this approach is the number of variables it entails. In predictive simulations, the number of excitations is the number of controls that need to be computed. Improving the fidelity by modeling individual muscles means there are more controls to consider in the problem. As the model increases in number of segments (e.g. adding upper body movement), the more redundant actuators would be required, resulting in a more complex optimization problem and long simulation times.

Joint torque models

An alternative to modeling individual muscles is to use applied torques to represent the combination of muscle forces on a joint. This reduces the number of variables and simplifies the optimal control problem. Generally, the joint torque model consists of a passive and active torque. The active torque represents the combination of active muscle forces acting on a joint and is scaled based on joint angle and angular velocity to represent the force-length and force-velocity relationship of muscles. Alexander [29] was one of the first to employ this method when it was used to study the take-off technique for high and long jumps. Subsequent researchers expanded on this model to include detailed passive torque models, which represent the forces produced by the passive stretching of muscle tissue, tendons, and ligaments. Joint torque models have been implemented previously in predictive simulation of human movement, especially with sports applications [30, 31, 32, 2].

The key trade-off with joint torque models, as with many models, is between accuracy and computation time. Muscle models are more realistic and are the standard in musculoskeletal modeling. However, for some studies such as this one, it is not reasonable based on the increased computation time it would require. In general, the extra parameters make the model that much more difficult to work with, tune, and debug, which was a major issue already based on the simulation times. Additionally, the primary focus of this work was on finding the optimal kinematics of the standing start, and there was less concern with the individual muscles forces required to achieve the motion. For this reason, a detailed muscle model was not required, only sufficient constraints to limit the movements and torques to what is physiologically possible.

Once the musculoskeletal model has been developed and validated, it is time to use it in simulations. The key for the simulations is determining the best way to solve for the activations, i.e. the method of driving the simulation. Generally this is formulated as an optimization problem with an objective function of trying to match experimental data or to achieve a certain goal.

2.3 Forward Dynamics Applications to Human Movement: Kinematic Data Tracking versus Predictive Simulation

Various methods have been used to actuate forward dynamic simulations of human movement. A commonly used approach in forward dynamic simulations of human movement is to employ optimal control methods.

2.3.1 Optimal Control

Two frequently-used numerical approaches to solving optimal control problems are direct methods and indirect methods. Indirect methods utilize Pontryagin's minimum principle and the problem becomes a boundary value problem. One downside is that the co-state equations have to be derived. It can be challenging to solve because it needs an initial guess for the co-state variables, which often do not have a physical meaning.

Direct methods do not require analytical derivation of the co-state equations. In direct methods, the control and/or state variables are approximated with a polynomial function, and the optimal control problem is transcribed to a non-linear programming problem (NLP). The NLP problem is then solved using a NLP solver. Direct methods can be further broken down into shooting methods (single or multiple shooting) and collocation (local or global orthogonal) methods. In shooting methods, only the control variables are parameterized. In collocation methods, both the control and state variables are parameterized. In collocation methods, the differential equations are essentially treated as constraints such that the derivatives of the states from the polynomial functions must be equal to the state derivatives calculated from the model dynamics.

In direct shooting, the dynamic equations are simulated by solving sequentially. This can lead to issues with states being very sensitive to the controls due to the time duration of a simulation. Solving sequentially often leads to longer computation times as well. In

2001, Anderson and Pandy [33] used direct shooting for gait and took 10,000 hours for half the gait cycle. Also in 2001, Kaplan compared direct collocation with a numerical gradient approach and found that direct collocation was more efficient and converged to a solution in fewer iterations. Later, Porsa et al. [34] compared direct shooting and direct collocation for maximum-height jumping. They found that direct collocation converged to essentially the same optimal solution up to 249 times faster than direct shooting. These results indicated the advantages of direct collocation over direct shooting and subsequent researchers have used direct collocation in other applications. DeGroote et al. [35] evaluated the capabilities of direct collocation optimal control with human movement for solving the muscle redundancy problem. They used GPOPS-II, an orthogonal collocation optimal control software, with two and three dimensional models of human gait in a formulation they refer to as "muscle dynamic optimization." In this approach they performed an inverse dynamics analysis to obtain the skeletal dynamics, which were then prescribed in the optimization. They were able to obtain much shorter computation times than previously seen, but some of the decrease in computation time was a result of only evaluating muscle dynamics in the optimization. They achieved promising results, and they recommended future work to assess the capabilities for predictive simulations involving skeletal dynamics.

Using optimal control has the benefit of finding optimal profiles for the inputs. It is free to take any value within the given bounds. An alternative approach is to have the joints maximally activated every time [31, 30, 36, 28]. In these approaches, the on/off activation times are solved for, and the force or torque profiles are defined based on those activation times. This can produce effective simulations for shorter or repetitive motions, but solving for multiple different activation times over a longer or more complex simulation becomes cumbersome and less effective. Based on the advantages of optimal control, it can be an effective tool for simulations of human movement. There are many robust and ready-to-use optimization algorithms (NLP solvers) available. Optimal control has previously been applied to forward dynamics simulations of pedaling [20, 26, 2], which is ideal for such methods due to the constrained nature of the movement. However, one challenge with pedaling models in these types of setups is that the legs + crank form a closed kinematic chain, which results in dynamic equations that are differential algebraic equations (DAEs) rather than ordinary differential equations (ODEs).

2.3.2 Forward Dynamics Utilizing Experimental Data

Some forward dynamics simulations are formulated as an experimental data tracking problem. This is classified as forward dynamics, but it still requires experimental data to run the simulation so it is not predictive in nature. As with inverse dynamics, it is reliant on

collecting accurate experimental data. Essentially, the forward dynamic optimization is run to determine what combination of muscle forces cause a given movement. With the inclusion of muscles and their forces, this type of setup can be useful for understanding what is happening internally during an experiment and give better estimates of joint reaction forces and stress on different internal structures such as ligaments. Several researchers have used this method or similar methods [26, 27, 22, 37, 38] in a range of applications like gait, jumping, and pedaling. They use several different optimization techniques, but their approaches are similar in that they are driving a model to match experimental results.

Hull and his colleagues were involved in several of the pioneering studies in cycling biomechanics throughout the 1980s and 1990s. In 1986, Redfield and Hull [38] utilized a single leg model with a fixed hip joint center to predict pedal forces with an optimization routine. Their kinematic inputs were the experimentally measured angular position, velocity, and acceleration of the crank and the angular position, velocity, and acceleration of the foot relative to the crank. An additional constraint prevented the knee joint from extending past the straight leg position. Optimized pedal force profiles based on a Fourier series were determined for two cost functions: one based on joint moments and one based on muscle stress. They removed the complication of handling the muscle redundancy problem by lumping the muscles into functional groups (i.e. flexors and extensors). After comparing to experimental pedal forces it was determined that both cost functions offered reasonable predictions of pedal forces; however, the muscle stress cost function better predicted joint moments. A few years later, Gonzalez and Hull [39] used experimental data and a model to examine the optimal pedaling rate, crank arm length, seat tube angle, seat height, and longitudinal foot position on the pedal.

In the 1990s, Fregly and Zajac [40] were interested in how energy was generated and transferred between segments during the pedaling motion. They developed a three degree-of-freedom, two-legged model of stationary ergometer pedaling. Each leg was a five bar mechanism with hip center and crank center both fixed. Their degrees of freedom were the crank angle and the angles of the feet. The ergometer was modeled by a resistive torque that represented the inertia of the flywheel, along with other resistive torques that would be experienced by a cyclist. They calculated net muscle joint torques using an inverse dynamics analysis and then utilized a parameter optimization algorithm to track the experimental joint torques. They presented interesting results regarding the roles of each joint in generating, absorbing, or transferring energy throughout the pedaling motion. The general result was that the hip joint torques are generating energy and delivering it to the limb segments, and the ankle joint torque serves to transfer that energy to the crank.

In a continuation of Hull's cycling research, Kautz and Hull [41] simulated sub-maximal steady-state cycling at 90 rpm and 225 W for a two-legged model with hip joint centers

fixed and the feet rigidly attached to the pedal. The pedal angle was prescribed as the experimental pedal angle, leaving the crank angle as the only degree of freedom. The hip and knee torques were the inputs. They used Fregly and Zajac's method of modeling the ergometer where the ergometer was modeled by an effective resistance. One application they considered for their model was optimizing the shape of the chainring to see if an ellipsoidal chainring could reduce the joint moments. They used a direct shooting-type approach, in which the controls were parameterized. Neptune and Hull [22] followed up on the work of Kautz and Hull using a similar model; however, the knee was given two translational degrees of freedom that were defined based on the knee flexion angle. Instead of joint torques, it was driven by 15 muscle actuators per leg. Their optimization was set up to find the muscle excitations that resulted in matching the experimental data for seven different combinations of the crank and pedal kinetics and kinematics, joint moments, and timing of muscle excitations. They converted the optimal control formulation into a parameter optimization problem and utilized a simulated annealing algorithm. They had the most success utilizing the objective function matching all the experimental data (kinetic and kinematic data and electromyography (EMG) timing).

Kaplan and Heegaard [26] focused on a new algorithm they developed using direct collocation. Their model consisted of 7 total segments with the hip joint center fixed and 18 independent muscle groups (9/leg). They were trying to find the muscle activations that maintained a constant cadence of 60 rpm and matched pedal angles experimentally determined by Ting et al. [25]. Kaplan and Heegaard were comparing their method against the work previously done by Ting et al. [25], who used a numerical gradient approach on a model with 9 muscles and 27 unknowns. As mentioned previously, the direct collocation performed better than the numerical gradient approach. Various optimal control softwares have become available since then, so these types of problems can now be analyzed without developing one's own optimal control formulation.

Thelen et al. [27] demonstrated an implementation of their computed muscle control using a pedaling model. They included 15 muscles per leg and even included the patella in their model of the lower leg. The hip and ankle were revolute joints, but, similar to Neptune and Hull, their knee joint was a planar kinematic joint that allowed two degrees of freedom that were defined based on the knee flexion angle. The pelvis location was fixed, leaving the model with 3 degrees of freedom. Based on Fregly and Zajac [40], the load was modeled by an equivalent inertial and resistive torque. The objective in their optimization was to find the muscle excitations that drive the model to match the pedal angles, crank angle, and radial pedal forces.

Lai et al. [42] investigated the effects of including multiple types of motor units in the muscles controlling the ankle during pedaling. Previous musculoskeletal models did

not account for the activation dynamics of different types of motor units (slower or faster activations). These models often had to have their force-producing capabilities scaled up in order to match experimental data for tasks requiring high force outputs. Lai et al. modeled the ankle as a universal joint with the appropriate musculature surrounding it, but now both fast and slow motor units were included. They neglected the thigh motion and prescribed the translations and rotations of the shank using the experimental results. Their forward dynamic simulations were run for cadences ranging from 60 to 140 rpm and a constant average crank torque. They found that the excitation required to match the ankle kinematics was reduced by as much as 23% when they included the two types of motor units. These results suggest that incorporating multiple types of motor units can increase the force-producing capabilities of a model.

Farahani et al. [37] utilized what they refer to as an inverse-inverse dynamics method. They also refer to this approach as predictive dynamics, although it is not entirely predictive in nature. In this approach, the movement is the independent variable and is parameterized using functions that specify the motion of the various degrees of freedom. The muscle excitations are determined that result in the kinematics and external forces that are specified by the parameterization functions. They developed a similar model to previous researchers with a fixed upper body, and their degrees of freedom were crank angle and ankle angle. The independent inputs of the cycling optimization problem were the foot motion and crank torque. To simplify the problem, they assumed the crank angular velocity was constant and the foot motion was symmetric and offset by 180 degrees. These simplifications allowed them to neglect the crank inertial load and to only optimize for one set of variables. These assumptions are reasonable for the steady-state pedaling in this study, but for start-up pedaling, there is too much variation from one pedal stroke to the next to make these simplifications. The foot motion was described by a Fourier series due to its cyclic nature. Crank torque was described by a sinusoidal function, which is a reasonable approximation for their experimental power output and constant cadence. The objective function was the minimization of muscle activity. While their simulations could be considered predictive in terms of the muscle activations required and the fact they are not directly using experimental data, the independent inputs have a predefined form that can only change based on the parameters.

A variety of approaches have been used in modeling the biomechanics of pedaling, ranging from two legs with 15 muscles per leg to models that focus specifically on the ankle but include multiple types of motor units. These methods are all useful for understanding the muscle forces required for a movement, but they can only examine what is happening in previously recorded movements. They are unable to study what would happen under different conditions or how the existing movements could be improved.

2.3.3 Predictive Simulation of Human Movement

Forward dynamics using experimental data tracking can be contrasted with purely predictive simulation, in which there is no experimental data used. Purely predictive simulation is useful because it does not necessarily require the detailed data collection that experimental tracking does. Additionally, numerous different simulations can be run with various different parameters to see how the optimal solution changes. Predictive simulation is useful for running "What if?" simulations to get an idea of what happens when various components of the model are changed. This can be used to reduce the number of physical experiments that need to be run and therefore find the best techniques more quickly.

One of the challenges of predictive simulations, regardless of the optimization method used, is determining an approximate objective function. Predictive simulation of submaximal movements will generally have objective functions that include both high-level and low-level objectives (e.g. maintain a certain cadence while minimizing energy expenditure). For walking, objective functions such as maintaining a certain metabolic energy per unit distance have been used. In maximal exertion movements, the objective function is usually a maximization of a final condition. Ashby and Delp [43] studied maximal long jump and maximized the horizontal postion of the toe at landing. Pandy et al. [44] used the vertical position and velocity of the CoM at moment of take-off for maximum-height vertical jumping. Raasch et al. [20], a study that will be discussed further in the following paragraphs, used total crank progression as the objective function for maximal start-up pedaling on an ergometer. Essentially, in maximal exertion studies, the primary, and often only, objective is to maximize some final condition.

Around the time of the Fregly and Zajac analyses using kinematic data, Raasch and Zajac were also investigating pedaling. In 1993, Raasch et al. [20] used optimal control with a musculoskeletal model for maximal start-up pedaling (i.e. starting with zero velocity). Their model had two legs with the hip positions fixed and the feet rigidly attached to the pedals, similar to the other models that have been discussed. All the joints were revolute joints except the knee, which had two translational degrees of freedom that were defined based on the knee flexion angle. Initially, they were seeing large amounts of ankle dorsiflexion in the first downstroke, so there was additional stiffness added at the boundaries of the normal range of motion to prevent this. The method used by Fregly et al. [40] for modelling the effective ergometer load was implemented in this model as well. They used 15 muscles per leg that were broken into 9 muscle sets, or synergies. Activations were applied to a set so all the muscles in a set received the same signal. They utilized a constrained optimal control algorithm to find the excitations to the muscle sets that maximized the total crank progress. The initial state for the simulation was found by allowing the musculoskeletal

model to come to rest with all muscles off. In 1999, Raasch and Zajac [21] followed up on this work using the same model and looked at the muscle groups further to find the functional muscle groups and the neuromuscular strategy for pedaling. Mehrabi and McPhee [45] also used muscle synergies to reduce the optimal control problem for the predictive simulation of pedaling. They included muscle fatigue in their simulations to examine the effects of fatigue on steady-state cycling, as opposed to the start-up pedaling investigated by Raasch and Zajac.

The work of Van Soest and Casius [36] is an example of predictive simulation not using optimal control. They used a parallel genetic algorithm for their optimization. Their goal was to maximize the average power for pedaling at a designated fixed crank angular velocity. They prescribed the crank angular velocity, which allowed them to mechanically decouple the crank and only model one leg, actuated by eight muscle groups. The joints were all frictionless revolute joints, and, as with other models, the hip joint center and upper body orientation were fixed. The inputs to the model were the muscle excitations. They made the assumption that the muscles were always maximally activated anytime they were stimulated. Their optimization was attempting to find the on/off crank angle for each muscle group that maximized average power output over a full pedal stroke at a constant crank angular velocity. The optimization method used by van Soest and Casisus, and subsequently by Bobbert et al., works well for steady state pedaling. It does not work as well for start-up pedaling because the on/off angles will be changing with each pedal stroke as the cadence increases.

Bobbert et al. [28] followed up on VanSoest's work using the same simulation model and optimization approach, now looking specifically at why the relationship between pedal force and crank angular velocity was not hyperbolic like the relationship between muscle force and contraction velocity. They simulated at different crank angular velocities and varied inertial properties and model dynamics to see what effect they had on the relationship between pedal force and crank angular velocity. They were investigating a previous hypothesis that the linear relationship between pedal force and crank angular velocity was a result of segmental dynamics canceling out muscle forces as velocity increased. The results of Bobbert et al. indicated segmental dynamics were not playing a noticeable role in pedal force reduction in cycling. What they noticed, rather, was the linear relationship between torque and cadence seemed to be a result of the activation/deactivation dynamics. Because the model needed time to deactivate the muscles, they had to be deactivated earlier in the pedal stroke as cadence increased, which led to a reduction in the maximum amount of pedal force that could be produced. Both studies by this group reached similar conclusions that activation dynamics have a major effect on the optimal pedaling rate and the maximum pedal force that can be produced. This effect is captured in the model

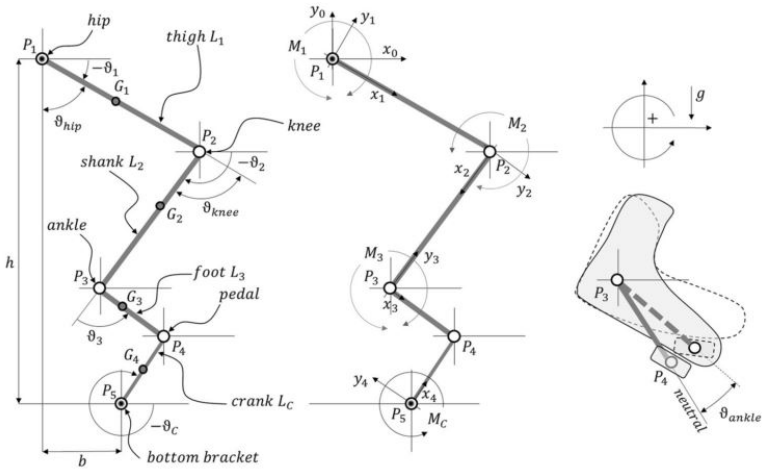

Figure 2.2: Model developed by Zignoli et al. [2]. Reproduced with permission from Springer Nature. Similar components are seen in other models such as the fixed hip location and rigid connection between the pedal and the toe.

presented in this thesis.

Zignoli et al. [2] recently used optimal control with a joint torque-driven model for predictive dynamics of sub-maximal ergometer cycling. Figure 2.2 displays the framework of their model. They implemented a joint torque model with active and passive torques applied to each of the joints. The hip position was fixed and all joints were revolute joints with a damping of 0.1 N·m/(rad/s). Similar to previous researchers, the crank-load was modeled by an effective inertial and resistive torque. In a change from what had previously been commonly used in optimal control, they used indirect methods rather than direct methods. They focused on sub-maximal exertion and tried to match a cadence while minimizing joint torques and jerks. They achieved good agreement with experimental results indicating that indirect methods can also be an effective method for predictive simulations of human movement.

A common theme among previous dynamic models is that many have focused on ergometer pedaling or steady-state cycling and have used some form of equivalent resistive torque and/or effective inertia to provide the resistance at the crank [20, 22, 27, 2]. They do not model the bicycle itself because, for steady-state cycling and ergometer pedaling, the resistance at the crank can be modeled more easily in the aforementioned ways. Furthermore, they all considered the hip to be fixed and did not include upper body motion in their models. There has been limited research done in which both the cyclist and bicycle are modeled.

2.4 Bicycle Dynamics

Modeling the bicycle allows one to incorporate the bicycle dynamics when examining the effects of the cyclist shifting body positions. This becomes important when considering standing starts in track cycling. Schwab and Meijaard [46] conducted a review on previous bicycle dynamics research, which is largely focused on bicycle stability and control methods for balance and steering. The Carvallo-Whipple model has been the basis of models for studying bicycle dynamics since the early 1900s.

2.4.1 Carvallo-Whipple Model

The Carvallo-Whipple model consists of a rear frame, steering assembly (front fork + handlebars) and two wheels. These four rigid bodies are connected by three revolute joints. The model is simplified by making several assumptions. The wheels are treated as contacting the ground at a knife-edge, and it is assumed there is no longitudinal or lateral tire slip. In many cases, the rider is ignored or treated to be rigidly attached to the frame at the seat. If given movement, the model was typically only given upper body lean for stability and not lower limb movement for propulsion. Although fairly simple, the Carvallo-Whipple is a reasonably accurate model of a rider-less bicycle, and Kooijman et al. [47] were able to validate it for speeds ranging from 3 to 6 m/s. Subsequent researchers added to the model by incorporating various different components such as toroidal wheels and forward acceleration. The Carvallo-Whipple model and other models of a similar nature are accurate at lower speeds and can give a general idea of bicycle dynamics under ideal conditions. However, it does not consider the effect of the rider's movement, and the simplified tire model is not accurate at higher speeds.

There has been considerable research done into the process by which the rider steers the bike. Various controllers have been developed that aim to accurately represent steering and balancing. When developing a controller for a cyclist, it is often desired that there is both balancing and path following, so a multi-loop controller is required for such studies. Some models have added a degree of freedom for upper body lean and control this with the controller as well. Schwab et al. [48] used optimal control in their study and allowed for upper body lean, but treated the legs as being fixed.

As mentioned, most previous researchers ignore the cyclist or treat the cyclist as being fixed when investigating bicycle dynamics. Part of the reason this is done is due to the difficulties caused by adding moving legs. The pedaling motion means the leg masses are constantly oscillating. This leads to resultant moments about the frame's longitudinal

axis. Connors and Hubbard [49] investigated the effects of leg movement on the steering controller. As the cyclist pedals, the bicycle rolls side-to-side as a result of the leg movement, and the bicycle will tend to oscillate in relation to the pedaling frequency. Connors and Hubbard found that by shifting gears the cyclist could minimize the oscillations and make the bicycle easier to control. They incorporated a geared bike that would allow for lower pedaling rates at higher speeds, but this is not possible for track cycling models due to their fixed gear ratio. In general, during the standing start, the cyclist is moving in a straight line with the bicycle frame upright. Developing a controller that accurately models a cyclist steering and balancing can be complex, so for the purposes of this project focused on straight-line cycling, it was ignored. The additional complexity of the controller would increase computation time, which is already large due to the nature of the model.

2.4.2 Tire Modeling

An important aspect of modeling a bicycle is accurately modeling the wheel-ground contact. Researchers often make the assumption there is no slip and use nonholonomic constraints for the wheel-ground contact. This is not a good assumption when studying an accelerating bicycle, especially when looking at start-up cycling. A study by Sharp [50] showed that at higher speeds the simplified nonholonomic tire models employed in the Carvallo-Whipple model are not accurate. For more detailed wheel-ground contact, researchers employ a tire model. Various different tire models are available, but the most common for multibody vehicle dynamics is the Pacejka tire model. The Pacejka tire model fits model parameters to experimentally-measured tire forces and moments acting on the wheel hub. Implementing a Pacejka tire model for a bicycle would allow for more accurate representation of the tire dynamics than that of the basic Carvallo-Whipple model. It is a highly accurate model, but requires experimental testing to determine the parameters.

Unfortunately, there is relatively little research that has been done on bicycle tires and their force properties. Two of the more recent studies are those by Dressel and Rahman [51] and by Doria et al. [52], but these were primarily for road bicycles. The study by Doria et al. collected tire data and used a curve-fit approach to find parameters for the basic form of the Pacejka tire model. Bulsink et al. [53] investigated rider stability with a fixed rider and utilized the results of Doria et al. to implement the Pacejka tire model for wheel-ground contact, a novel method for bicycle dynamics. Bulsink et al. [53] is one of the only ones to use the Pacejka tire model in a model of bicycle dynamics, partially due to the difficulties of obtaining the necessary data.

2.5 Opportunities for Novel Research

Based on the analysis of previous literature and the research interests of Cycling Canada, there are several opportunities for novel research. Studies focused on musculoskeletal modeling of the cyclist have not considered bicycle dynamics and generally focus on ergometer pedaling. Studies focused on bicycle dynamics have not included the cyclist dynamics and generally treat the cyclist as being rigid. There is a lack of models that take into account both cyclist and bicycle dynamics simultaneously. Furthermore, with regards to modeling the bicycle, there has been limited application of tire models. This is important for maneuvers involving significant longitudinal acceleration. Adding a tire model presents an expansion on the work done in modeling bicycle dynamics. These gaps in literature mean there is the potential need for modeling and simulation that take both cyclist and bicycle dynamics into account. There is also the need for more detailed experimental studies of standing starts on the track. This includes high-frequency torque and power measurements as well as a kinematic analysis of the cyclist. Gathering such data is important for making comparisons and drawing conclusions from the results of predictive simulations.

There have been several studies, but not an extensive use of predictive simulation for pedaling. There is the potential for novel applications of direct collocation, specifically the software GPOPS-II, to predictive simulation. An additional benefit of this work is the use of predictive simulation of human movement in a more unique application such as the standing start. Hopefully this work can be used by future researchers as a resource when approaching their own project involving predictive simulation of human movement.

The purpose of this work was to develop a model of a cyclist and bicycle that can be used for predictive simulations of Olympic-level track cycling using optimal control methods. To our knowledge, there is no previous modeling and simulation study of track cycling standing starts. The model should be able to replicate experimental joint angles for seated start-up pedaling on an ergometer and observe similar patterns in crank torque, cadence, and power. During standing starts, cyclists are off the seat and shift their bodies longitudinally relative to the bicycle to obtain more efficient positions to generate more torque. For this reason, it is necessary to include the upper body in any model of a standing start. The goal is to use predictive simulations to gain a better understanding of what the optimal full body kinematics might look like for standing starts, including the starting pose.

Chapter 3

Bicycle and Cyclist Model Development and Optimal Control Formulation

The model was developed using MapleSim because its multi-domain capabilities allowed the bicycle and cyclist to be modeled in the same software. Additionally, its optimized code generation capabilities make it an excellent choice for developing and exporting computationally-efficient forward dynamics models. Two primary versions of the model were used, one including the bicycle representing cycling on the track (referred to as the combined cyclist and bicycle model or the track model) and one without the bicycle representing ergometer pedaling (referred to as the ergometer model).

3.1 Bicycle Model

The bicycle model consisted of four bodies: the rear wheel, the front wheel, the crank and the frame/fork/handlebars (see Figure 3.1). Revolute joints connected the rear wheel to the frame and the front wheel to the fork. The crank was modeled as a single link connected to the frame by a revolute joint. The rear wheel motion was connected to the crank motion using an ideal gear with a 50:14 (3.57:1) gear ratio that was the same as the fixed gear ratio used by the cyclist in the on-track experiments. The focus for this model was on the initial portion of the team sprint event up until the cyclist enters the first turn. During a standing start, the cyclist is in the straightaway of the track and is traveling in

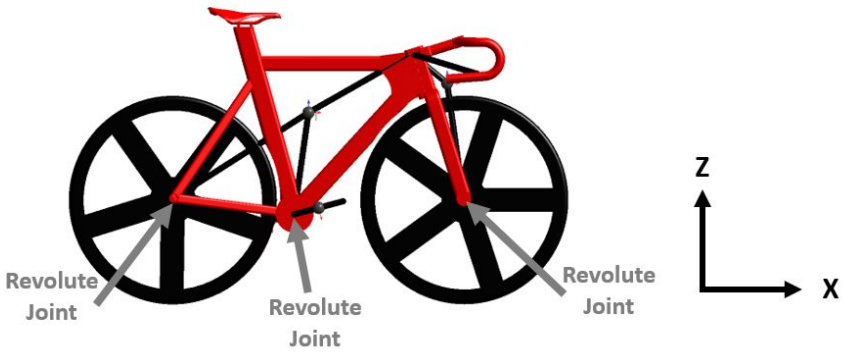

Figure 3.1: Image of the bicycle model in MapleSim.

a relatively straight path. To simplify the model for straight-line cycling, a revolute joint was not included between the frame and the front fork/handlebars, and the bicycle was constrained to remain upright and follow a straight path. These simplifications were made to eliminate the need for steering or balancing controllers. Adding a steering or balancing controller was not the main focus of the study and would have added complexity to the problem, thus increasing computation time. With these simplifications, the bicycle model had five degrees of freedom: crank rotation, front wheel rotation, longitudinal and vertical translation, and pitch (frame rotation about the y axis).

The setup of the bicycle model, including overall bicycle dimensions as well as handlebar position and crank length, was set to match that of the bicycle used by the cyclist in the experiments. The dimensions of the bicycle frame were determined from the Look L96 track cycling bicycle frame used by the cyclist and from dimensions given on the Look product website. Moment of inertia and center of mass locations were determined using a SolidWorks model of a bicycle frame that was developed using these dimensions. The only moment of inertia that has an effect is the moment of inertia about the y-axis (pitch). The bike is undergoing minimal pitch so slight errors in this value were not a significant concern. Center of mass location for the frame also does not play a significant role as the cyclist mass is more than 10x that of the bicycle.

To simplify the model, several factors such as aerodynamic drag, frame compliance, and chain and bearing efficiency were ignored. In reality, there is some energy lost due to chain and bearing inefficiencies, and a bicycle frame would have some level of compliance. However, Olympic cyclists, especially sprinters, use very stiff frames so the energy losses are relatively small, with a previous study estimating frame efficiency at approximately

99% [8]. The efficiency of the chain drive train is between 95% and 98.5% and the bearing efficiency is between 99.64-99.84% according to [8]. Overall, these various factors would affect the performance, but with such high efficiencies, it is not anticipated that they would significantly affect the selected technique for a standing start. For these reasons, they were neglected in this project.

Aerodynamic drag was also not considered in this model as the effects are negligible when traveling at low speeds during start-up cycling. The basic equation for drag force is

$$F_D = \frac{1}{2}\rho v^2 C_D A \tag{3.1}$$

where ρ is the air density, v is the relative velocity, C_D is the drag coefficient, and A is the cross sectional area. To give an idea of the drag forces, a quick calculation can be done with some approximate values of $\rho = 1.225$ kg/m^3 and $C_D A = 0.33$ m^2 [66]. After 15 meters the cyclist will typically have a velocity of approximately 7 m/s. At this speed, the drag force is approximately 10 N, for a resistive power of 70 W. When compared to an average power output typically over 1200 W at the same point in the standing start, the aerodynamic drag force is not a major factor. In order for the drag forces to affect the optimal standing start technique found in the simulations, the drag equations would need to take into account different body positions and segment velocities for both upper body and lower body. Having a simple drag force solely dependent on overall velocity would not affect the technique being used, only the overall performance in terms of distance covered. Even with more complex drag models, the effects would be minimal at low speeds, so drag was neglected in order to reduce the level of complexity of the model.

3.2 Tire Model

One of the key differences that separates this work from previous cycling models is the implementation of a tire model for modeling wheel-ground contact. MapleSim contains built-in tire model components that were used for formulating the tire force and moment equations. For the purpose of this project, a tire model was chosen with the goal of being as accurate as possible using model parameters that were available in literature. The Pacejka model is the most commonly used tire model in literature for modeling multibody vehicle systems. Unfortunately, the lack of testing done on bicycle tires meant the available results were limited. Pacejka parameters have not been reported for track cycling tires so parameters for road tires from Bulsink et al. were used [53], with the exception of the rolling resistance coefficient, which has been experimentally determined for track cycling

tires [54]. Tire parameters from Bulsink et al. were for road tires, which are high-durability tires usually inflated to around 90-125 psi. Tires used on the track are tubular tires that are typically inflated to around 200 psi. They are made to be as light as possible and are made from a softer compound that has better grip. The different bonding agents used to attach the tires to the rims likely have an effect on tire parameters as well. Based on these differences, there are likely noticeable differences in the slip parameters between road cycling tires and track cycling tires, but it is unknown to what extent and whether they would have a noticeable effect on the results of the simulation.

For a purely longitudinal model (2D with no lateral forces), the forces and moments that come into play are the vertical reaction force, longitudinal force, and rolling resistance moment. A velodrome has a sloped surface throughout the entire track (42-degree banked bends and 13-degree banked straights for an Olympic-category velodrome) so there is always a camber angle, even in the straights. For simplicity, the surface for the straights was modeled as being flat in this study. Camber forces could have been included, but they would have had minimal effect when the model was constrained to remain upright.

MapleSim implements the 2002 Pacejka tire model [55], which requires 117 parameters that are determined by linear regression to experimental data. This can make it difficult to work with, but it can give highly accurate tire models when the appropriate data are available. The parameters reported by Bulsink et al. were not for the 2002 Pacejka tire model but rather a simplified version of the Pacejka tire model. The equations for the basic Pacejka model are of the form in Equation 3.2.

$$F_x(\epsilon) = F_z D \sin(C \arctan(B\epsilon - E(B\epsilon - \arctan(B\epsilon)))) \tag{3.2}$$

Table 3.1: Pacejka tire model parameters used by Bulsink et al. [53]

B	C	D	E	K
$\frac{K}{CD}$	1	1.642 N	0	12 N

where F_x is the longitudinal force acting on the wheel; F_z is the vertical force acting on the wheel; ϵ is longitudinal slip; and C, D, E, and K are the parameters determined experimentally. C is the shape factor for longitudinal force, D is the longitudinal friction μ_x at the nominal wheel load F_{z0}, K is the longitudinal slip stiffness at F_{z0}, and E is the longitudinal curvature at F_{z0}. The parameter values used in these equations were those reported by Bulsink et al. (see Table 3.1).

The Pacejka tire model also contains equations for determining the tire vertical force, F_z, and the tire slip, ϵ, that are required for calculating the longitudinal force in Equation 3.2. The simplified equation for the tire vertical force is

$$F_z = k_z\rho + c_z\dot{\rho} \tag{3.3}$$

where k_z is the linear vertical tire stiffness, c_z is the tire damping, and ρ is the tire deflection. The basic equation for tire slip is

$$\epsilon = \frac{\Omega R_{eff} - V_x}{|V_x|} \tag{3.4}$$

where ϵ is longitudinal slip, R_{eff} is the effective tire radius, V_x is the translational velocity of the wheel center, and Ω is the spin rate of the tire. However, when performing starting maneuvers, the zero initial translational velocity results in a slip that is infinity. To use the tire models when starting at zero velocity, relaxation lengths have to be included, which is demonstrated in equation 3.5

$$\frac{d\epsilon}{dt} = \frac{\Omega R_{eff} - V_x}{B_{long}} - \frac{\epsilon|V_x|}{B_{long}} \tag{3.5}$$

where B_{long} is the relaxation length. For simplicity, constant relaxation lengths of 0.3 were used in this study. A more complex model for determining the relaxation lengths known as a stretched string model [55] was considered, but ultimately not used in the final simulation because there were no experimentally determined parameters for the model available for bicycle tires.

In the 2002 Pacejka model, the parameters C, D, E, and K are a function of other parameters and variables. They are generally determined using linear regression from experimental results and do not necessarily have a physical meaning. Ideally, by simplifying the 2002 Pacejka model, a direct relationship between 2002 Pacejka parameters and basic Pacejka parameters can be found. This would be done by setting some parameters in the 2002 Pacejka model to 0 or 1 to reduce the number of parameters that show up in the equations. For example, the rolling resistance moment used by the Pacejka model is

$$M_y = R_0F_z[q_{Sy1} + q_{Sy3}\frac{F_x}{F_{z0}} + q_{Sy3}\left|\frac{V_x}{V_{ref}}\right| + q_{Sy4}(\frac{V_x}{V_{ref}})^4] \tag{3.6}$$

which can be simplified as

$$M_y = R_0F_zC_{rr} \tag{3.7}$$

where R_0 is the unloaded tire radius, q_{Sy1} is the rolling resistance moment coefficient C_{rr}, and q_{Sy3} and q_{Sy4} are assumed to be 0. Generally, the parameters q_{Sy3} and q_{Sy4} are quite small so that is a reasonable assumption. The coefficient of rolling resistance for track cycling tires is approximately 0.0023-0.0024 depending on the brand of tire being used [8, 54]. This simplification process was applied to the other Pacejka 2002 equations in MapleSim and was made more straightforward by the fact that side-slip and camber were ignored so only the longitudinal force equations needed to be simplified.

The tire body component in MapleSim contains stiffness and damping parameters to represent the stiffness and damping of the tire. The appropriate stiffness was based on the properties for radial structural behaviour of racing bicycle wheels reported by Petrone and Giubilato [56]. They found radial stiffness was in the range of 1.7e5 to 2e5 N/m, while the damping was not experimentally determined. Bulsink et al. used a damping of 5.4e3 N/(m/s) to achieve supercritical responses, and this value was used as a reference when determining the range of values to consider. The tire damping was included as part of the optimization, with bounds being 1e2 to 1e5 and an initial guess of 2.5e3 N/(m/s).

3.3 Cyclist Model

The cyclist model consisted of ten rigid bodies: two feet, two shanks, two thighs, upper arm, forearm, hand, and the head + trunk (see Figure 3.2). Based on video analysis of a standing start, the upper limb motion was assumed to be symmetric so the arms were lumped together into one upper arm, one forearm, and one hand. Revolute joints were used to represent the shoulder, elbow, wrist, hips, knees, and ankles. To approximate the spinal curvature that was observed in the cyclist during the standing start, there was a fixed angle of 25 degrees between the abdomen and the thorax in the trunk segment. The cyclist's hands were rigidly fixed to the handle bars at a 45-degree angle. The cyclists feet were clipped into the pedals using toe clips, thus allowing the foot/pedal to be constrained to the crank with a revolute joint. The combined cyclist and bicycle track cycling model was modeled by fourteen generalized coordinates coupled by four algebraic constraints, resulting in ten degrees of freedom (for a list of the degrees of freedom, see Appendix A). Limb properties, including segment length, mass, center of mass location, and moment of inertia, were set using anthropometric data from de Leva [57]. The anthropometric properties were scaled to match one of the subjects (from here on referred to as Cyclist X) in an attempt to have a more relevant comparison between simulation results and experimental results.

The sign conventions and joint coordinate systems for the cyclist model are detailed in

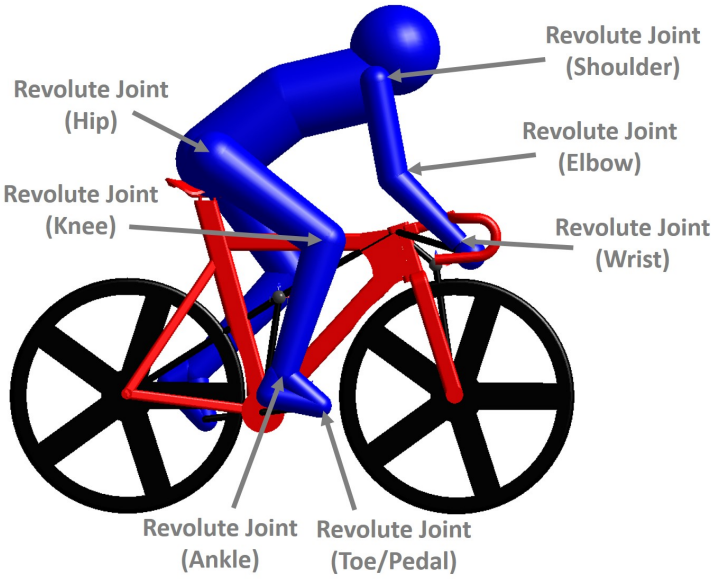

Figure 3.2: The combined cyclist and bicycle model in MapleSim

Figure 3.3 and Table 3.2. The zero joint angles were considered to be when the body was in the neutral position. The neutral position was defined as the position corresponding to having both feet flat on the ground, the legs straight, and the arms hanging straight at the sides. This meant that for all joints except the ankle, the zero degree angle corresponded to a straight limb. The zero degree angle for the ankle corresponded to the bottom of the foot being perpendicular to the shank.

3.4 Joint Torques

3.4.1 Active Joint Torques

The cyclist model was driven using active joint torques, which represent the combination of muscle forces acting on a joint. Anderson et al. [58] developed a joint torque model for the lower limb that was implemented here. In Anderson et al.'s model, the active joint torque that can be applied at the joint is scaled based on the joint angle and angular velocity, representing the muscle force-length and force-velocity relationship. The scaling function is piecewise to account for both concentric and eccentric muscle contractions. Concentric

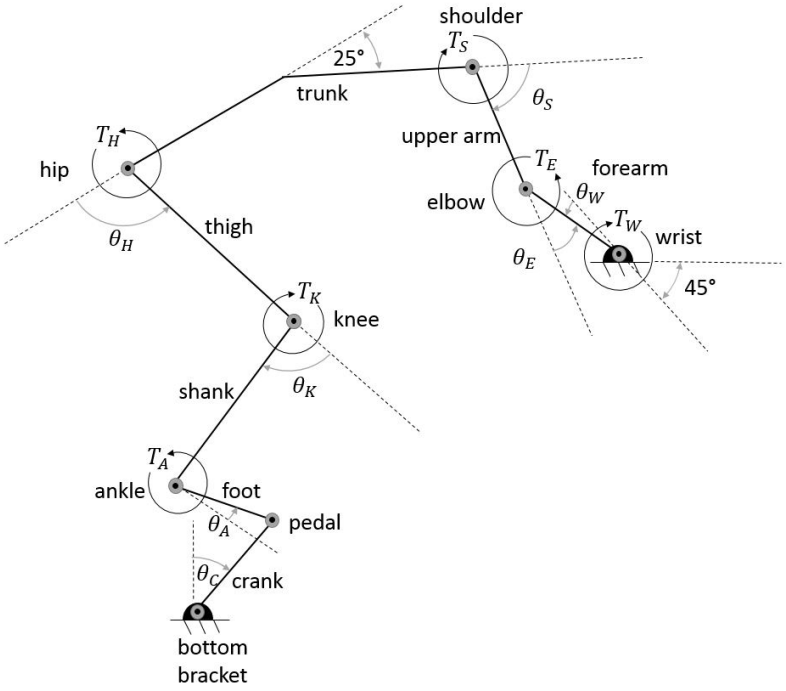

Figure 3.3: Diagram of the cyclist in the track model

Table 3.2: Sign conventions for each joint in the model

Joint	Movement	Torque	Angle
Wrist	Radial Deviation	+	> 0, increasing
	Ulnar Deviation	-	< 0, decreasing
Elbow	Flexion	+	increasing
	Extension	-	decreasing
Shoulder	Flexion	+	increasing
	Extension	-	decreasing
Hip	Flexion	+	increasing
	Extension	-	decreasing
Knee	Flexion	+	increasing
	Extension	-	decreasing
Ankle	Dorsiflexion	+	> 0, increasing
	Plantar Flexion	-	< 0, decreasing

contractions are when the muscle is contracting and shortening (i.e. when the joint torque and angular velocity have the same sign). Eccentric contractions are when the muscle is contracting and lengthening. This occurs when the muscle is counteracting a motion in the opposite direction (i.e. when the joint torque and angular velocity have different signs). Equation 3.8 contains the torque scaling equations and Table 3.3 contains the parameters that were used. Figure 3.4 displays the torque scaling profiles for each of the lower limb movements.

The parameters for Anderson et al. were for "average" 18-25 year old males. Olympic cyclists are far from average so it is not clear how well these scaling parameters represent the force-velocity and force-length relationships of their muscles. For the maximum torque values, Kordi et al. [59] measured the maximum isometric joint torques for competitive cyclists for the hip extensor, knee flexor and extensor, and ankle extensor. Values were chosen at the upper end of these ranges as these would likely be the approximate capabilities of an Olympic-level cyclist. For the hip flexor and ankle flexor, the extensor torque limits were scaled from values in Kordi et al. based on the relationship seen in Anderson et al.[58]

A simpler joint torque scaling model that only scales based on joint angular velocity was used for the upper limb joint torques. This torque scaling method has been implemented in previous upper limb joint torque applications [31] and was based on the work done by van Soest et al. [60]

$$T_{active} = \begin{cases} T_{iso}\left(\frac{\dot{\theta}_{max}-\dot{\theta}}{\dot{\theta}_{max}+\Gamma\dot{\theta}}\right) & \dot{\theta} \geq 0 \\ \\ T_{iso}\left(\frac{(1-T_r)\dot{\theta}_{max}+S\dot{\theta}T_r(\Gamma+1)}{(1-T_r)\dot{\theta}_{max}+S\dot{\theta}(\Gamma+1)}\right) & \dot{\theta} < 0 \end{cases} \tag{3.9}$$

where T_{iso} is the isometric torque, $\dot{\theta}$ is the maximum angular velocity where torque can be applied, Γ is a shape factor, S is the slope factor, which determines the slope of the transition between concentric and eccentric torque, and T_r is the ratio between the maximum eccentric and isometric force. A slope factor of 2 and a force ratio of 1.5, values determined by van Soest et al. [60], were used in this model. The shape factor was 3, the value used by Alexander [29]. For simplicity, it was assumed the maximum angular velocity of the joint is the same for both concentric and eccentric contractions and a value of 10 rad/s was used. Maximum upper limb joint torque values were taken from Garner and Pandy's study of the upper limb [61].

Each joint for both upper and lower limbs had its own maximum torque rate of change that was based on muscle activation and deactivation time constants [24]. For simplicity, it was assumed maximum rates of change were the same for both activation and deactivation.

$$T_{active} = \begin{cases} C_1 cos(C_2(\theta - C_3)) \frac{2C_4C_5 + \dot{\theta}(C_5 - 3C_4)}{2C_4C_5 + \dot{\theta}(2C_5 - 4C_4)} & \dot{\theta} \geq 0 \\ \\ C_1 cos(C_2(\theta - C_3)) \frac{2C_4C_5 - \dot{\theta}(C_5 - 3C_4)}{2C_4C_5 - \dot{\theta}(2C_5 - 4C_4)} (1 - C_6\dot{\theta}) & \dot{\theta} < 0 \end{cases} \tag{3.8}$$

Table 3.3: Active torque scaling parameters obtained from Anderson, et al. [58].

	Units	Definition
C_1	N·m	Maximum isometric joint torque
C_2	–	π divided by the theoretical range of joint angles in which active muscle force is present
C_3	rad	Joint angle at maximum isometric torque
C_4	rad/s	Angular velocity when torque is 75% of isometric torque
C_5	rad/s	Angular velocity when torque is 50% of isometric torque
C_6	–	Defines eccentric torque relative to concentric torque

	Hip Ext.	Hip Flex.	Knee Ext.	Knee Flex.	Plantar Flexion	Dorsiflexion
C_1*	380	320	330	225	210	90
C_2	0.958	0.738	1.258	0.869	1.391	1.510
C_3	0.932	-0.214	1.133	0.522	0.408	-0.187
C_4	1.578	2.095	1.517	2.008	0.987	0.699
C_5	3.190	4.267	3.952	5.233	3.558	1.940
C_6	0.242	0.218	0.095	0.304	0.295	0.828

*Row C_1 is based on values from Kordi et al. [59], which better represent the strength of an Olympic track cyclist

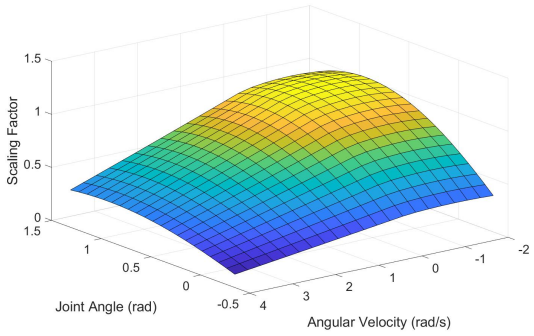

(a) Hip extension

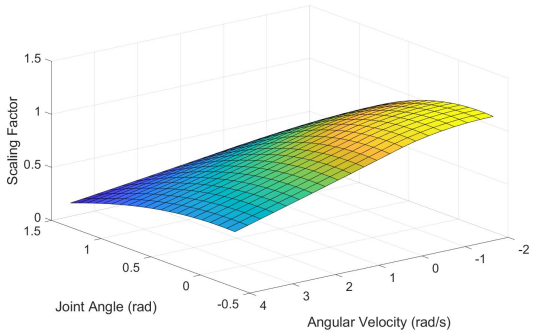

(b) Hip flexion

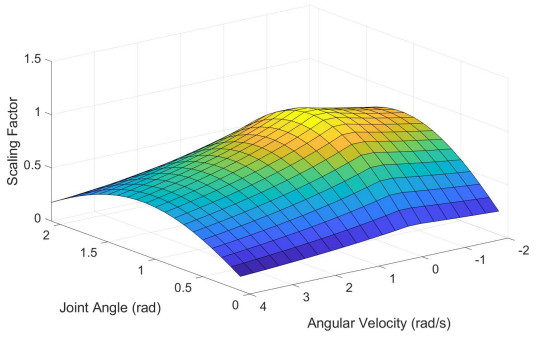

(c) Knee extension

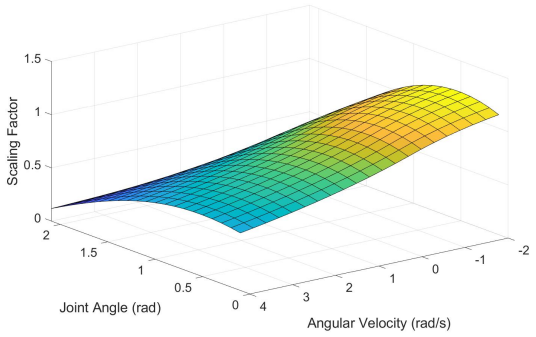

(d) Knee flexion

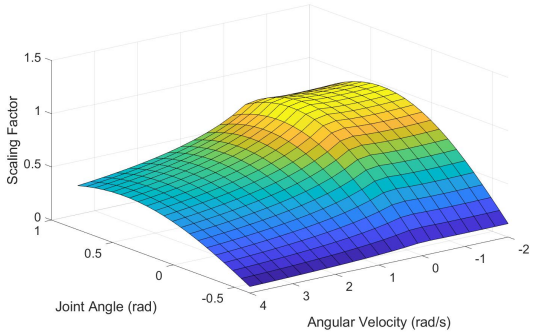

(e) Ankle plantar flexion

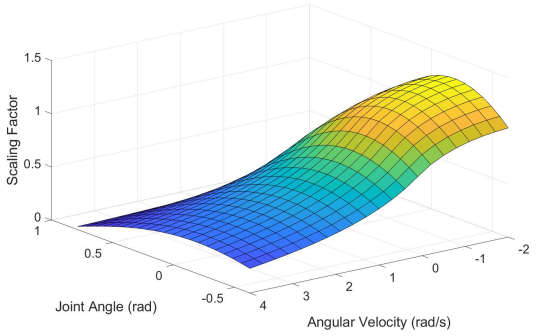

(f) Ankle dorsiflexion

Figure 3.4: Torque scaling for the lower limbs. The color is for visualization purposes only.

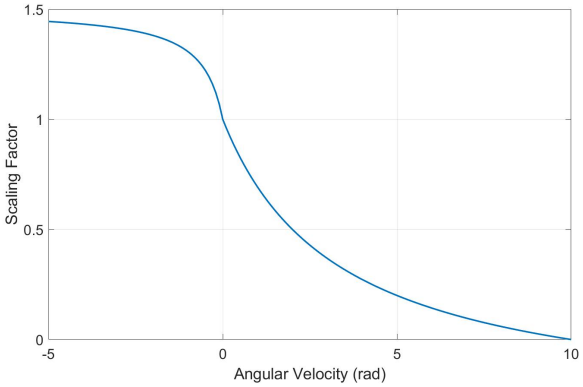

Figure 3.5: Torque scaling for the upper limbs

In actuality, the deactivation time is approximately two to three times that of activation depending on the muscle type, and both occur in an exponential fashion [62]. The bounds here allow for linear activation (although the exact rate could be less than linear if found to be more desirable) and the activation and deactivation rates were assumed to be the same to avoid separating the torques into flexion and extension and thus increasing the number of controls.

3.4.2 Passive Joint Torques

In addition to the active joint torques, passive joint torques were also included for each joint. Passive torques represent the passive forces that are generated by the stretching of muscle tissue, tendons, and ligaments. Although the passive torques perform a separate role to the active torque scaling and represent different physiological components, there is the potential that models based on fitting to experimental data have some amount of overlap between the phenomena the two torque models are capturing. Despite the difficulties in quantifying the degree to which the passive structures influence active torque scaling, passive torques were included because there are clearly distinguishable effects at the limits of the joint range of motion that were important to capture in the model. Riener and Edrich's [3] model for lower limb passive joint stiffness was chosen based on its ability to take into account adjacent joint angles, accounting for some of the effect of biarticular muscles. The equations for Riener and Edrich's lower limb passive joint torques are included below in Equations 3.10-3.12.

$$T_A = e^{(2.016-0.0843\theta_A-0.0176\theta_K)} - e^{(7.9763+0.1949\theta_A+0.0008\theta_K)} - 1.792 \tag{3.10}$$

$$T_K = e^{(1.8-0.046\theta_A-0.0352\theta_K+0.0217\theta_H)} - e^{(3.971-0.0004\theta_A+0.0495\theta_K-0.0128\theta_H)} - 4.820 + e^{(0.220-0.15\theta_K)} \tag{3.11}$$

$$T_H = e^{(1.4655-0.0034\theta_K-0.00750\theta_H)} - e^{(1.3403-0.0226\theta_K+0.0305\theta_H)} + 8.072 \tag{3.12}$$

where T_A is the passive torque for the ankle in N·m, T_K is the passive torque for the knee, T_H is the passive torque for the hip, θ_A is the ankle joint angle in degrees, θ_K is the knee joint angle, and θ_H is the hip joint angle. The plots in Figure 3.6 show the passive torque profiles for various adjacent joint angles. The active and passive joint torques were summed to get a total joint torque applied to each joint.

3.5 Dynamic Equations and Optimal Control: Implementing the Problem in GPOPS-II

The goal for this project was to identify the optimal joint torque activations for achieving the maximum distance in a fixed amount of time. In some previous joint torque models, the joint torque is fully activated every time it is excited. Rather than using this method, it was desired to find an optimal torque profile that did not require the joints being maximally activated every time. The General Purpose Optimal Control Software, Version II (GPOPS-II) optimal control package from Rao et al. [63] was used together with an interior-point optimizer (IPOPT) to solve the optimal control problem. GPOPS-II uses orthogonal collocation, which is a direct optimization method. In direct collocation, both the control and state variables are parameterized, which means the state and control are both approximated with a polynomial function. GPOPS-II turns the optimal control problem into a non-linear programming problem, which is then solved by the non-linear programming solver IPOPT.

One of the difficulties in working with this model was the cyclist and bicycle together form a closed kinematic chain due to the feet being fixed to a single crank and the hands being fixed to the handlebars (or in the case of the ergometer model, the hips being fixed at the seat location). This means that there are more coordinates than there are degrees of freedom. Therefore, the dynamic equations are a system of differential algebraic equations (DAEs) of the form

$$M\ddot{q} + \phi_q^T \lambda = F\,, \quad \phi(q) = 0 \tag{3.13}$$

where q are the generalized coordinates, M is the mass matrix, λ are the Lagrange multipliers, $\phi_q = \frac{\partial \phi}{\partial q}$ is the Jacobian matrix, and F are the torques and forces being applied. The combined cyclist and bicycle was modeled by fourteen generalized coordinates coupled by four algebraic constraints resulting in ten degrees of freedom. It was actuated by nine

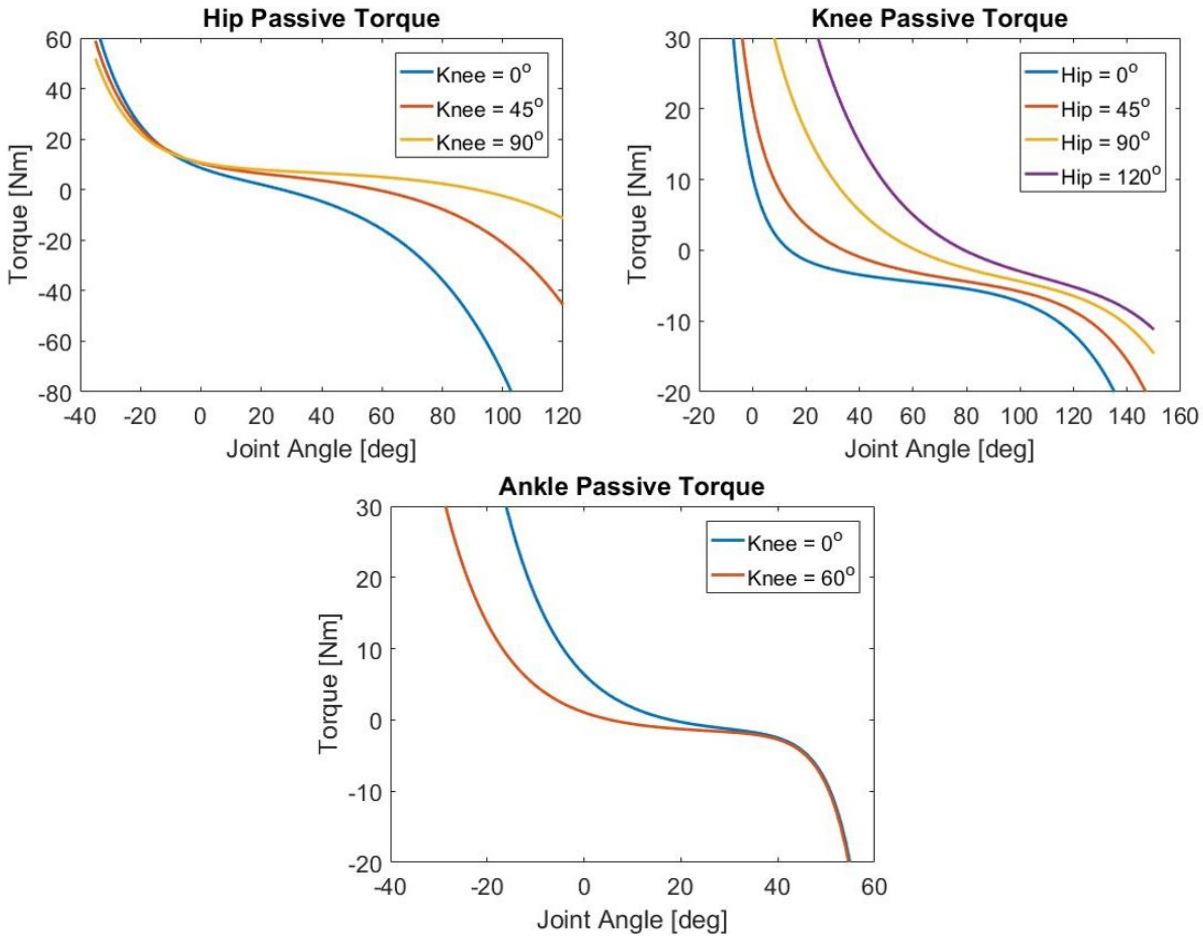

Figure 3.6: Passive torque plots generated using the passive torque functions from Riener et al. [3]. The ankle angle was 0 degrees for all knee passive torque tests.

active torque inputs applied at the cyclist model coordinates, meaning there were more actuators than degrees of freedom for the cyclist due to the closed kinematic chain. The problem was formulated such that the constraints were the position constraints for the foot/pedal joints.

Generally, the presence of the algebraic equations make DAEs more difficult to solve than ordinary differential equations (ODEs). In GPOPS-II, the dynamic equations can be left as DAEs with the constraint equations being handled as path constraints. This essentially separates the algebraic constraint equations from the differential equations. The differential equations with the reaction forces are included as the dynamic constraints. The next issue is handling the reaction forces. If they are included as states in the formulation, then a derivative is required. This derivative would have to be obtained by isolating the reaction force variables and then differentiating them, a process which is time-consuming due to the complexity of the model. Instead, the derivatives of the reaction forces were treated as controls, which allowed GPOPS-II to freely determine the reaction force derivatives, and therefore the reaction forces, that satisfy the dynamic equations and constraint equations at each time point.

The optimal control problem was formulated as such: find the states and controls that minimize the cost function subject to the dynamic constraints, event constraints, path constraints and integral constraints. Setting up the problem in GPOPS-II required specifying bounds and initial conditions for the 43 states (generalized coordinates and their derivatives, tire slip, active joint torques, and reaction forces) and 13 controls (joint torque rates of change and the reaction force derivatives). The dynamic equations for the model that were exported from MapleSim were input for the dynamic constraints in GPOPS-II. The desired objective function and the event constraints (constraints for continuation between phases in multi-phase problems) were also designated. The event constraints were set that the end of the pre-launch phase coincided with the beginning of the launch phase and all states were continuous from the end point of the pre-launch phase. The constraint equations were treated as path constraints with bounds of $\pm$ 0.05 mm. It is also required to specify an initial and final guess for the control and state variables, along with any intermediate guesses. In all the simulations, the initial and final guesses were set based on the experimental results, to give a reasonable starting point for the optimization. For some problems, such as matching known movements, intermediate guesses would be appropriate as well. However, since the problem in question was purely predictive, no intermediate guesses were used to avoid driving the simulation to a particular result. The mathematical statements of the optimal control problem for each simulation is given in the respective sections of the following chapters.

One of the difficulties with GPOPS-II is determining the correct number of mesh it-

erations and number of iterations within each mesh, as well as the tolerances for both of these. Additional parameters in the optimization setup include the initial number of mesh intervals, initial number of collocation points, scaling method, and mesh refinement method, among others. The state and control bounds and the initial guesses for the state and control and any intermediate guess points also must be determined. All of these factors affect how quickly the solver is able to converge on a solution, and trial and error was required to find the settings that work best.

An important final point to note was that the duration of the trial (e.g. simulating a six second trial) also affects the time required to find an optimal solution. This played a role in the length of simulations chosen. Furthermore, there is no fatigue built into the model so, for longer simulations, the model might assume techniques that are not physically realistic due to the energy expenditure required to maintain them.

Chapter 4

Ergometer Pedaling: Experiments and Simulations

4.1 Experimental Methods

To quantify the dynamics and kinematics of start-up ergometer pedaling, active marker motion capture technology (Optotrak Certus, Northern Digital Inc.) and an instrumented ergometer (SRM ergometer, SRM) were used to analyze seven (four male, three female) members of the Canadian Olympic program who take part in the team sprint event. All testing took place at the Mattamy National Cycling Centre in Milton, Ontario, and equipment was provided by Cycling Canada, except for the motion capture equipment. For motion capture, the right side of the cyclist was studied with markers placed on the hip, knee, ankle, heel, and toe (approximately where the center of the pedal was located), as well as the shoulder, elbow, wrist, and hand (see Figure 4.1). Two motion capture cameras collecting at 150 Hz were placed at approximately 45-degree angles to ensure no markers were occluded.

The SRM ergometer measured total torque applied to the crank from both legs at 200Hz. It has the ability to measure cadence as well, but can only do so once per pedal stroke. This may be sufficient when pedaling at a constant cadence, but during start-up pedaling, higher frequency measurements are needed to capture the variations throughout the entire pedal stroke. For this reason, the ergometer was outfitted with a modification developed by Jensen [64] that allowed for the measurement of crank angle, and therefore cadence, every five degrees. With the combination of these systems, high-frequency torque and cadence could be measured. This allowed for the calculation of a high-frequency

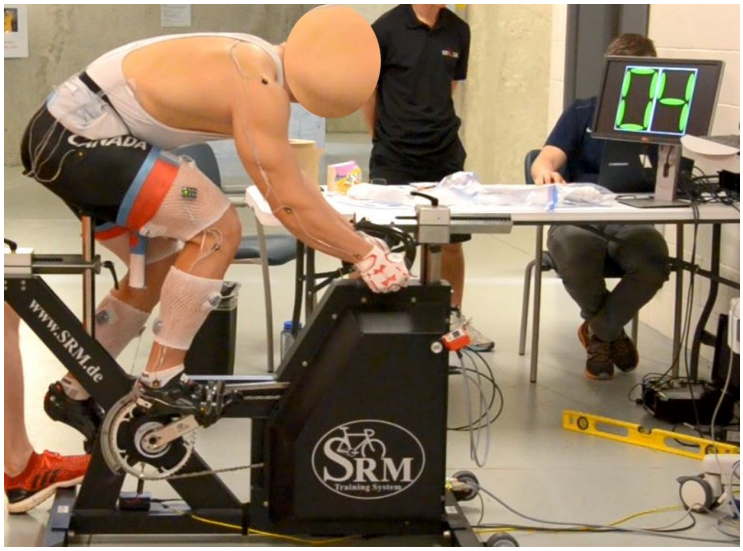

Figure 4.1: Experimental setup for ergometer pedaling

power, which is important for analyzing start-up pedaling. For the data collection, it was attempted to synchronize the motion capture system with the crank data automatically using a trigger. However, the trigger did not work properly, so the motion capture data start shortly after the trial has begun. Due to the limited availability of Olympic cyclists, and the time requirements of these tests, it was not feasible to repeat testing for these data. The motion capture data were manually synchronized with the ergometer data by aligning the crank angle and the position of the foot marker from the motion capture data.

The cyclists performed several tests as part of a larger study designed and conducted by Cycling Canada. Prior to starting the trials, the cyclists completed a self-selected warm-up routine. The ergometer was adjusted to match the setup of each cyclist's track bicycle in terms of the crank length and the saddle and handlebar position relative to the bottom bracket. The trials varied in length, ergometer settings (the ergometer has the ability to control the cadence, if desired), and cyclist position (seated vs. standing). In some tests the only resistance from the ergometer was the inertia of the flywheel. In other tests, the ergometer resistance would adjust so that the cyclist could not surpass a certain cadence, essentially matching the torque output of the cyclist. Each cyclist completed seven total trials, broken down as follows, with time to rest between each trial:

1. 2 six-second seated starts. In each of these trials the cyclist was instructed to remain seated and accelerate from a standstill to maximum cadence as quickly as possible.

The resistance at the crank was the flywheel inertia only.

2. 2 six-second standing starts. The objective was the same as the seated starts, but now the cyclist was instructed to get up off the seat and use the extra degrees of freedom to their advantage. Again, the only resistance was the flywheel inertia.

3. 1 fifteen-second seated start capped at 160 rpm. In these trials, the cyclist would accelerate from stand-still with only the resistance of the flywheel until they reached 160 rpm, at which point the ergometer would apply resistance to limit the cadence from going above 160 rpm.

4. 2 ten-second seated rolling starts capped at 50 rpm. The cyclist began pedaling and was instructed to pedal just below the 50 rpm threshold, then provide a countdown at which point they would maximally exert for 10 seconds controlled at 50 rpm by the ergometer.

For start-up pedaling, cyclists started in a self-selected stationary position. A digital clock counted down from 10 to 0, at which point they attempted to accelerate to top speed as quickly as possible. In the six second tests, the flywheel itself was the only resistance. The trial of interest for model validation and comparison was the six-second seated start. This test most closely replicated the ergometer pedaling model in which the hip position was fixed.

All joint angles reported here are the 2D angles in the sagittal plane. This is for direct comparison to the model, which was also limited to 2D motion in the sagittal plane. There was minimal concern with the angle of the trunk/pelvis during the seated ergometer pedaling. For this reason, hip angles were measured between the thigh vector and the vertical (see Figure 4.7). The knee angle was the angle between the thigh vector and shank vector defined by the 2D lines between the corresponding markers. The ankle angle was measured between the bottom of the foot (vector between heel and toe markers) and the shank vector (ankle and knee markers).

For the comparisons between simulation and experiment throughout this thesis, the correlation coefficient is used to assess the similarity between simulated and experimental curves. The correlation coefficient measures the linear dependence of two variables and is defined by equation 4.1

$$R = \frac{1}{N-1} \sum_{i=1}^{N} \left(\frac{A_i - \mu_A}{\sigma_A} \right) \left(\frac{B_i - \mu_B}{\sigma_B} \right) \tag{4.1}$$

where A and B are the two variables, N is the number of samples, μ_A and μ_B are the means of the two variables, and σ_A and σ_B are the standard deviations. For all calculations of the correlation coefficient throughout this thesis, the variables are compared relative to the total crank angle. Comparing versus the crank angle is better for making direct comparisons of the cycling biomechanics because it gives a common scale even when there are different pedaling rates, which is the case for the predictive simulations.

4.2 Data Tracking Simulation

The first set of ergometer simulations performed were to test the ability of the model to match experimental data. Oftentimes the first step in multibody modeling when experimental kinematic and dynamic data are available is to perform an inverse dynamics analysis. It was not possible in this case due to the lack of the required experimental data, namely the pedal forces. The SRM ergometer only measures total crank torque. Therefore, it is unknown how this torque breaks down between right and left sides, and the amount of radial forces (i.e. "wasted" forces) applied. At a minimum, 2D pedal forces would be required to conduct an inverse dynamics analysis. Additionally, due to the limitations of the experimental setup and number of cameras available, motion capture was only performed on the right leg and not both legs. The intent at the time of the data collection was not to use the data for inverse dynamics, only to give a general idea for comparison to models and simulations. The model was still able to be tested to assess its ability to match the available experimental data.

4.2.1 Modifications for the Ergometer Model

To model the ergometer, the bicycle frame and wheels were removed from the model, and the bottom bracket location was fixed, thus forcing the system to remain in the designated location. Extra inertia was then added to the crank to represent the effective load that the cyclist experiences from the inertia of the flywheel. The effective flywheel inertia was found as part of the optimization in the data tracking simulation. Finding the effective inertia was done by using the crank inertia as a parameter in the optimization with the objective to match the experimental kinematics and dynamics (crank torque and crank angle as well as right leg joint angles). The upper limbs were included in the same manner as the track bike simulations to allow the hip joint center to translate in the sagittal plane, as the hip joint center does have some movement, even during seated pedaling. These degrees of freedom in the cyclist model allowed for the matching of all three experimentally measured

joint angles. If the hip position had been fixed, only two of the four angles between the crank, right hip, knee, and ankle can be matched, as it would be a closed kinematic chain.

4.2.2 Problem Formulation and GPOPS-II Setup

Here the problem was formulated to drive the solution to match the experimental data from a single trial by Cyclist X. The objective function was different from the predictive simulations, but the formulation in GPOPS-II was essentially the same otherwise. The model was driven to match the experimental data for the right leg joint angles, the crank angle, and the crank torque, while minimizing the joint torques. The minimization of joint torques is included to drive the simulation towards a solution that represents the cyclist pedaling in a more efficient manner. The effective inertia was included as a parameter in the optimization to determine the value that best represents the experimental conditions. The objective function was

$$J = \frac{W_{\theta_C}(\theta_C - \theta_{C,exp})^2}{\sigma^2_{\theta,exp}} + \frac{W_T(T_C - T_{C,exp})^2}{\sigma^2_{T,exp}} + \sum_{i=1}^{3} \frac{W_{q,i}(q_i - q_{i,exp})^2}{\sigma^2_{q,exp}} + W_M \sum_{i=1}^{9} M_i^2 \quad (4.2)$$

- q_i are the three joint angles (right hip, right knee, right ankle)
- θ_C is the crank angle
- T_C is the crank torque
- M_i are the joint torques for each of the nine joints in the model
- W are weighting factors
- σ^2 are the variances for the experimental data used for normalizing the differences
- subscripts 'exp' correspond to experimental data

Left leg joint angles were ignored in the objective function because there was no knowledge about the left leg kinematics. In the simulation, the left leg was essentially driven by the hip position, which is the same as the right hip, and by matching the crank angle and crank torque. Based on this, there was essentially one lower body degree of freedom left uncontrolled. The bounds for the joint angles and angular velocities were set at the range of the experimental data plus 0.25 radians (≈15 degrees) to allow for the simulation to go outside the kinematic data as necessary. The iteration tolerance was met in the final mesh with a total computation time of 88 minutes on an Intel Core i7-6700 CPU at 3.40GHz with 16GB RAM.

4.2.3 Simulation Results

Figures 4.2, 4.3, and 4.4 demonstrate that the simulation is able to match the experimental data for Cyclist X. The correlation coefficients between the ergometer data tracking simulation and experiment are displayed in Table 4.1. All correlation coefficients are greater than 0.97, and the correlation coefficients for the tracked variables are all greater than 0.995. The optimal effective inertia for matching the experimental results was found to be 33.5 kg·m^2, which is within the expected range for an ergometer. For the joint kinematics, the only significant difference is in the knee angle when the crank is at top dead center and the knee is flexed. It also can be noted that matching the crank torque does not result in a match in crank angular velocity. In reality, there is the likelihood of there being bearing friction and other forces that would cause the net torque to be negative at times. The differences could also be due to measurement errors, not necessarily the simulation. If there are measurement errors between the different data streams, this would create difficulties in matching all the experimental results.

Table 4.1: Correlation coefficients between the ergometer data tracking simulation and experiment

Cadence	Crank Torque	Power	Hip Angle	Knee Angle	Ankle Angle
0.987	0.996	0.978	0.996	0.997	0.996

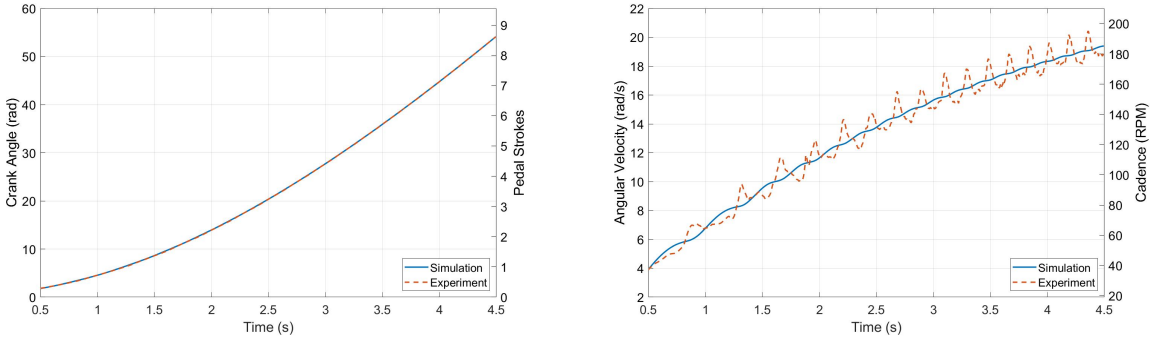

(a) Crank angle

(b) Crank angular velocity

Figure 4.2: Crank kinematics for the ergometer data tracking simulation

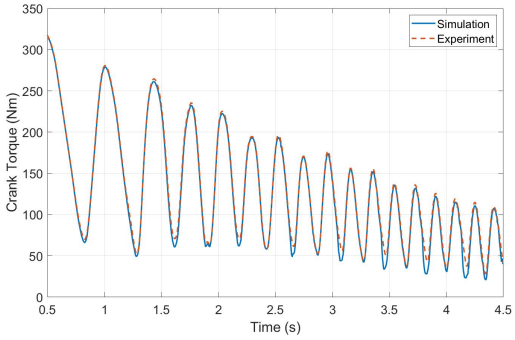

(a) Crank torque

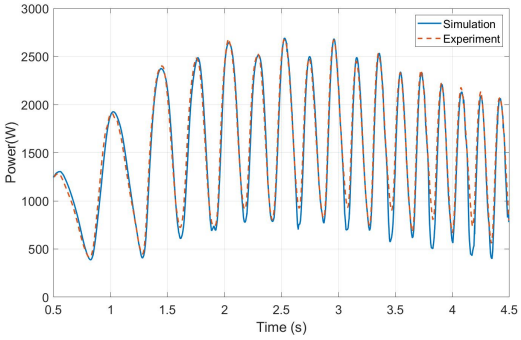

(b) Crank power

Figure 4.3: Crank torque and power for the ergometer data tracking simulation

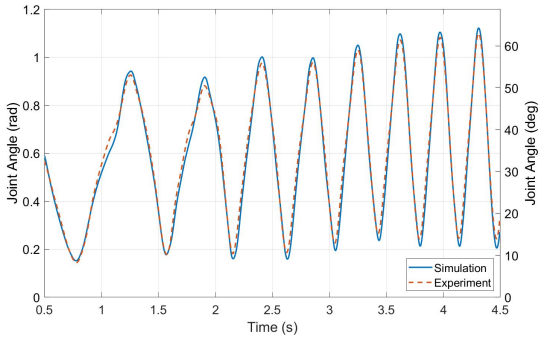

(a) Right hip joint angle

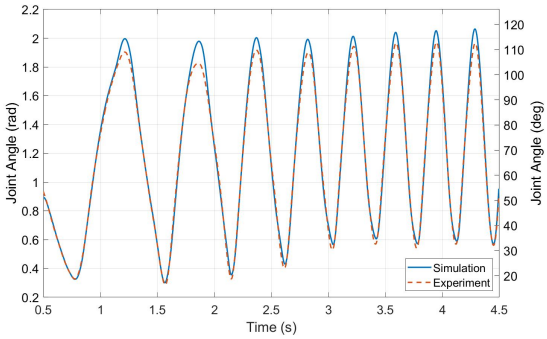

(b) Right knee joint angle

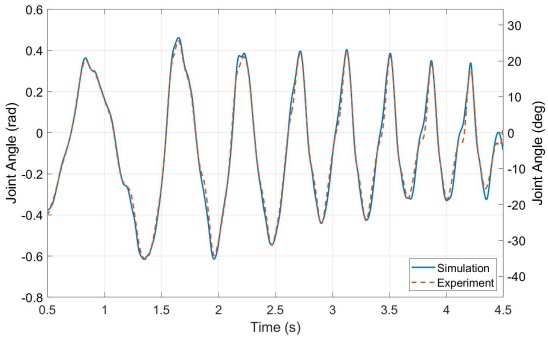

(c) Right ankle joint angle

Figure 4.4: Joint angles for the ergometer data tracking simulation

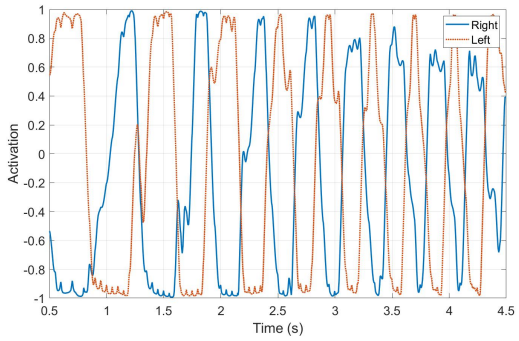

(a) Hip torque activation

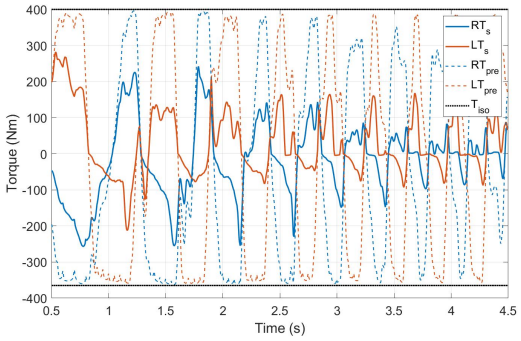

(b) Hip torque

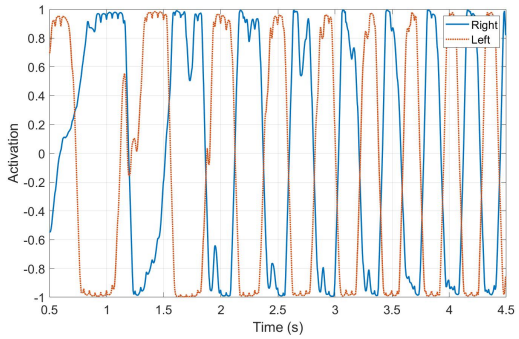

(c) Knee torque activation

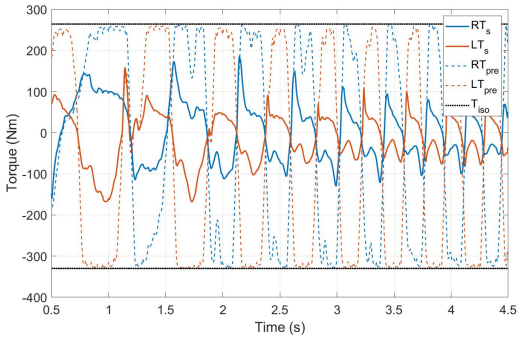

(d) Knee torque

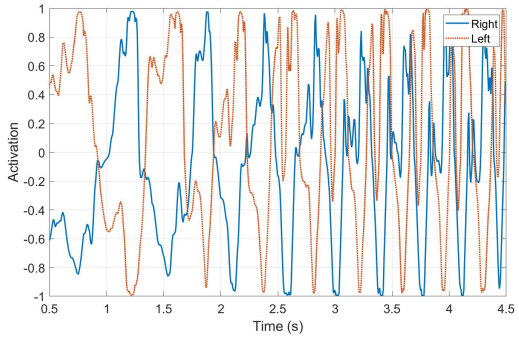

(e) Ankle torque activation

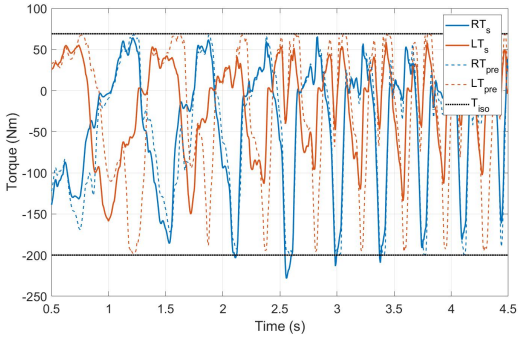

(f) Ankle torque

Figure 4.5: Joint torques for the ergometer data tracking simulation. T_s refers to the scaled torque, T_{pre} refers to the pre-scaled torque (i.e. before scaling based on joint angle and angular velocity), and T_{iso} refers to the isometric torques for flexion and extension.

In Figure 4.5, the joint torques and torque activations are plotted. The torques are being maximally activated for most excitations, especially for the knee joint. The ankle seems to take a more unique torque profile in the initial few pedal strokes. With the ankle there is also noticeable eccentric contractions as the muscles around the ankle joint act in a stabilizing manner. There was some difficulty in determining the weighting parameter for the joint torque term in the objective function. Based on this, it is reasonable to assume that future experimentation could result in a solution that can achieve the same outputs with smaller joint torques.

The main goal in this formulation was to ensure the model is capable of performing the task in a similar manner as the cyclist did in the experiments. We can see that the cyclist model is capable of completing the task and can be used to obtain the joint torques that were required. This confirmed that the parameters being used were reasonable and the torque capabilities of the model are in the correct range. Following the success of this setup, the next step was to perform purely predictive simulations of ergometer pedaling.

4.3 Predictive Simulation

4.3.1 Modifications for the Ergometer Model

The model used in the data tracking simulations was further modified and simplified for the predictive simulations of ergometer pedaling. For the predictive simulations, the head, arms, and trunk (HAT) were lumped together and fixed in a constant orientation (see Figure 4.6) because these segments do not move significantly relative to one another during seated pedaling. The hip joint centers were fixed at the location of the seat, as the cyclist remained seated while pedaling. This is the modeling approach used by many previous researchers, and it assumes the upper body has a negligible effect on seated pedaling. The orientation of the upper body only had an effect on the passive hip torque, for which a fixed 45 degrees was added to the hip joint angle. In the ergometer model, the joint coordinate system and sign convention is different for the hip angle than in the track model (see Figure 4.7). There is limited concern with the upper body motion, so the hip angle is measured relative to the vertical rather than the pelvis or trunk. The same method was used for modeling the ergometer as in the data tracking simulations. The effective inertia was set using the value found in the data tracking simulation. This fixed hip ergometer model had three degrees of freedom and was modeled using seven generalized coordinates coupled by four algebraic constraints.

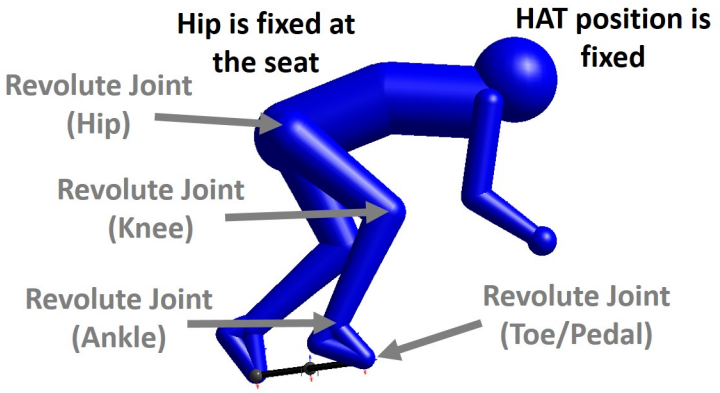

Figure 4.6: Picture of the ergometer model in MapleSim

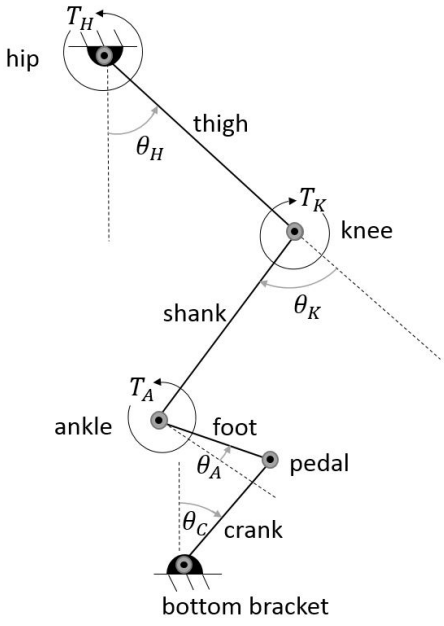

Figure 4.7: Diagram of the cyclist in the ergometer model

4.3.2 Problem Formulation and GPOPS-II Setup

The ability of the model to predict ergometer pedaling was tested and results are included here. The simulation was free to choose its fixed hip position within the given bounds, as well as its initial joint angles. The bounds were set so that there was no initial angular velocities for any of the joints or the crank itself. Initial torque bounds were set at ± 20 N·m to allow for the initial torques required to support the limbs in a stationary position. Initial state guesses were based on the crank angle being at 75 degrees. The bounds for joint angles and joint angular velocities throughout the simulation were set at values that would not restrict the natural motion of the cyclist. The time duration of the simulation was 5.5 seconds, a sufficient amount of time for comparisons with the experimental results while maintaining a reasonable computation time. The objective for the simulations was to achieve the maximum crank angle in the given time period. This was the objective for the cyclists in the ergometer experiments and also represents the objective on the track. Therefore, the following cost function was minimized, where $\theta_{c,f}$ is the final total crank angle.

$$J = \frac{1}{\theta_{c,f}} \tag{4.3}$$

Other cost functions have been used in optimizing pedaling that include some form of minimization of jerks and/or minimization of joint torques. These were considered, but ultimately not used for the predictive simulations because minimization of these led to less distance covered, which was the ultimate goal. The computation time was 127 minutes on an Intel Core i7-6700 CPU at 3.40GHz with 16GB RAM for the ergometer predictive simulation.

4.3.3 Simulation Results

The crank angle, cadence, crank torque, and power profiles were in a similar range and showed similar oscillatory patterns for the simulation and experiment on the ergometer (Figures 4.8 and 4.9). The correlation coefficients were 0.988, 0.952, and 0.873 for the cadence, crank torque, and power, respectively, when plotted versus the total crank angle (Table 4.2). The crank torque and power were plotted versus time and versus the total crank angle. Plotting versus time is useful for comparing the performance over time, and it can show how two cyclists differ if one is outperforming the other. However, in some cases, plotting versus time makes it more difficult to directly compare the biomechanics due to differing pedaling rates. Plotting versus the crank angle is better for making direct comparisons between the predictive simulation and the experimental result because it gives

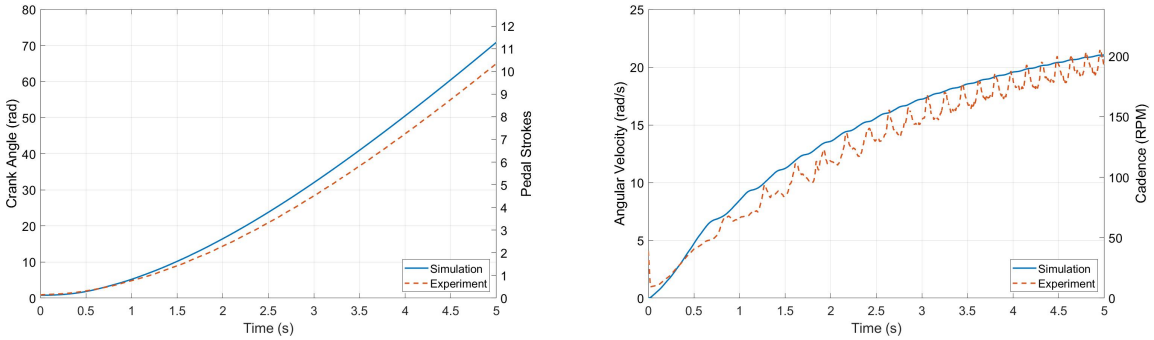

(a) Crank angle

(b) Crank angular velocity

Figure 4.8: Crank kinematics for the ergometer predictive simulation

a common scale that allows for a direct comparison. When plotting versus crank angle, the trends relative to the crank angle can be easily compared even if they are pedaling at different rates.

It was interesting to see the similarities in the initial crank angle between the simulation and experiment. The model started with a slightly lesser crank angle than the experiment. It started with a crank angle of 0.806 rad (46.2 degrees) whereas in the experiment the cyclist chose to start with a crank angle of 0.873 rad (50.0 degrees). The guess for the initial crank angle was 1.15 rad so the simulation indeed found the smaller initial crank angle to be more optimal. The initial crank angle chosen would likely be dependent on the position in which the maximum torque can be generated and the position that allows for the most torque to be generated during the first downstroke. One hypothesis would be that the model tends toward the position that allows for maximum torque throughout the first downstroke, not necessarily for the maximum torque to be generated in the initial position. While the initial position might be less powerful, the extra torque is more important. Additionally, the model could be positioning in this way so that joint torques are maximum when the crank is in position for generating the maximum torque. It is important to note that the position in which maximum torque can be generated is dependent on the joint angle scaling. Differences in this would lead to different maximum torque positions for the cyclist. The crank angular velocity remained slightly above the experimental cadence, resulting in a greater final crank angle (79.4 versus 73.2 rad, or just under one full pedal stroke). The simulated oscillations in the cadence were smaller and not as sharp as in the experimental results.

One of the more noticeable aspects of these plots in Figure 4.9 is that the first crank

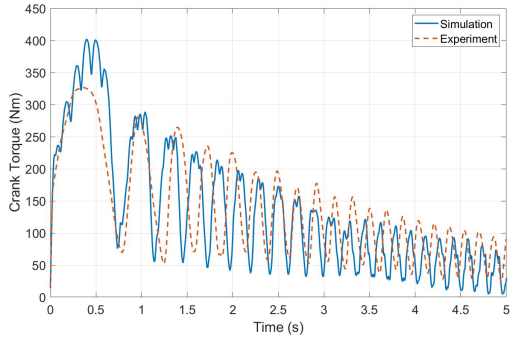

(a) Crank torque versus time

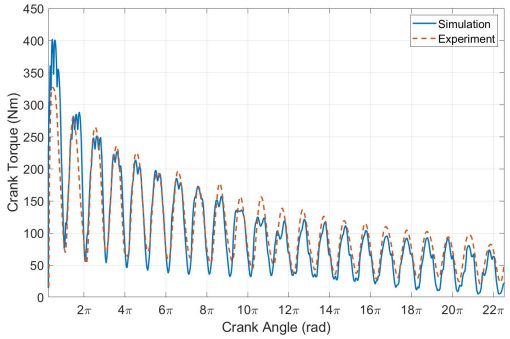

(b) Crank torque versus total crank angle

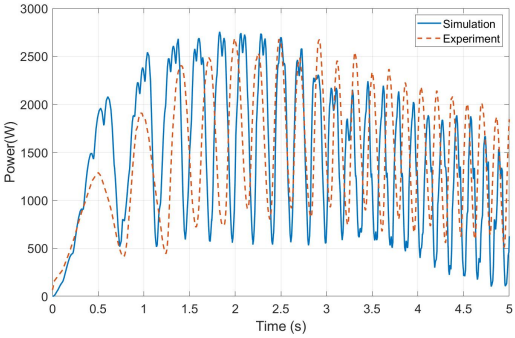

(c) Power versus time

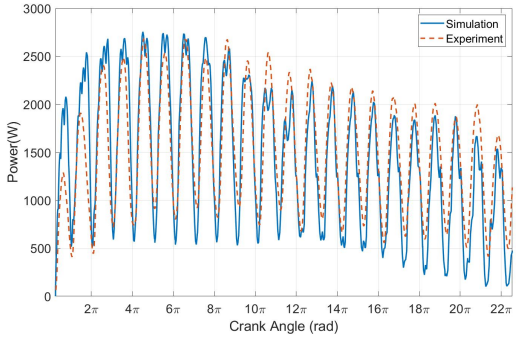

(d) Power versus total crank angle

Figure 4.9: Crank torque and power for the ergometer predictive simulation

Table 4.2: Correlation coefficients between the ergometer predictive simulation and experiment

Cadence	Crank Torque	Power	Hip Angle	Knee Angle	Ankle Angle
0.988	0.952	0.873	0.937	0.977	0.717

torque peak is larger in the simulation. In the simulation, the peak crank torque is approximately 400 N·m, whereas in the experiment the crank torque reaches a maximum around 325 N·m. This could be due to differences in the torque parameters versus the actual strength of the cyclist. The subsequent peaks seem to be similar, if slightly less in some cases. The valleys also seem to be slightly deeper as well. Some of these differences could be attributed to the simplified method of modeling the ergometer. The similar trends in crank torque and cadence naturally lead to a similar power profile as well.

Figure 4.10 contains joint angles over time and joint angles versus the total crank angle. The hip angle profiles are fairly similar between the experiment and simulation, with a correlation coefficient of 0.937. For both experiment and simulation, the hip range of motion increases from approximately 45 degrees to approximately 50 degrees as the trial goes on, with the most noticeable change being an increase in flexion angles. The maximum extension occurs in the first pedal stroke, and extension decreases for several pedal strokes before increasing slightly towards the end. The first push results in a greater extension, as the model is trying to generate maximum torque in the first downstroke, but then the model becomes more controlled in subsequent pedal strokes. There is less knee extension at bottom dead center in the first few pedal strokes in the model than in the experiment, by about 15 degrees. Following from that observation, there is a decrease in the experimental range of motion by about 15 degrees over the course of the trial as the cyclist transitions to less knee extension. In general, there is about 10 degrees more knee flexion at top dead center than in the experiment. Despite the initial pedal strokes, the correlation coefficient of 0.977 indicates the curves are quite similar for the duration of the trial. Overall, the simulations seem to take a more consistent approach throughout the simulation, whereas there is a noticeable change in the experimental knee and hip kinematics after the first three pedal strokes.

The ankle goes through a larger range of motion in the simulations than in the experiments. This is evidenced by the correlation coefficient of 0.717, which is the lowest of the three joint angles. Initially, they are more similar, with ranges of motion of 67 degrees and 60 degrees for the simulation and experiment respectively. The discrepancy in range of motion is more noticeable later in the simulation when the ankle is still going through a range of motion of approximately 45 degrees while the experimental range of motion has decreased below 30 degrees. The simulated ankle continues to display greater plantar flexion when the crank is at bottom dead center. The results seem to indicate that the cyclists in the experiments are not incorporating the ankle as much as would be advantageous. To follow up on this point it must be determined whether there are assumptions being made in the model that would account for why the ankle is moving in this manner rather than the technique used in experiments. This could possibly be due to the passive torque model

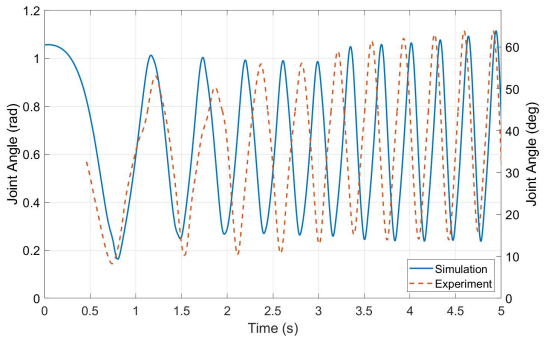

(a) Right hip angle versus time

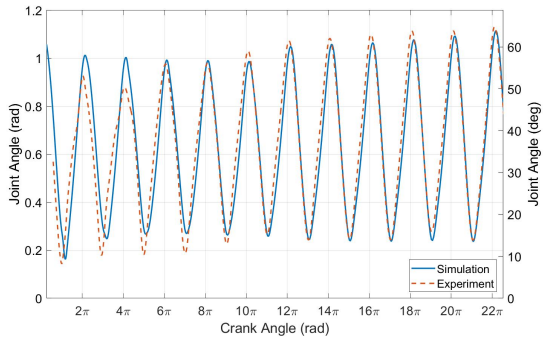

(b) Right hip angle versus total crank angle

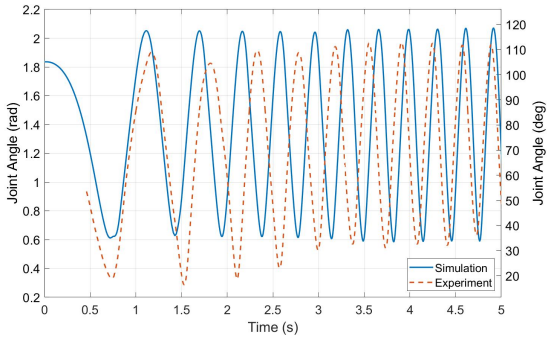

(c) Right knee angle versus time

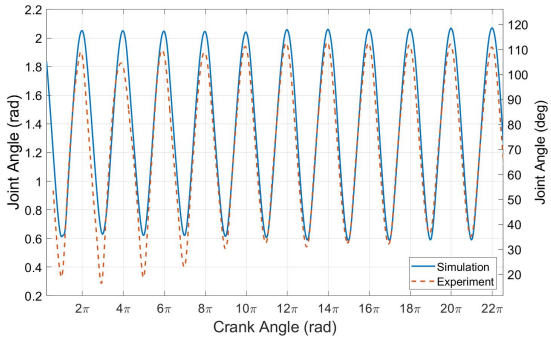

(d) Right knee angle versus total crank angle

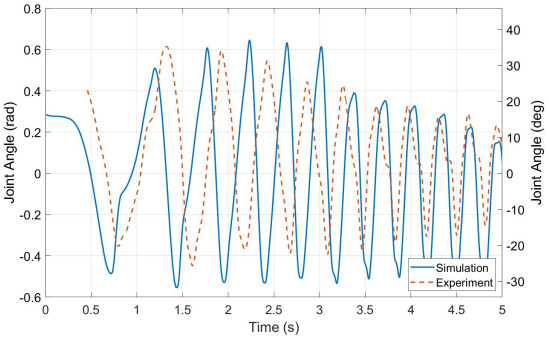

(e) Right ankle angle versus time

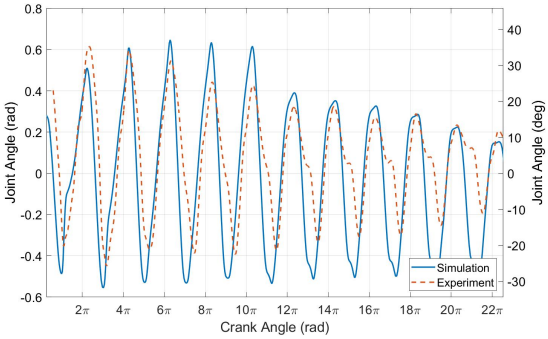

(f) Right ankle angle versus total crank angle

Figure 4.10: Comparison of the lower limb joint angles between the ergometer experiment and predictive simulation

or the method of active torque scaling. In reality, it can be difficult to continuously exert that much force in the ankle. At higher cadences, it can be difficult to control the ankle through a large range of motion in a stabilized manner due to the rapid, precise movements that would be required. Instead, a more controlled and more easily repeatable movement is used. This is seen in both the simulation and experiment with the transition from more ankle motion to more hip motion over the course of the trial.

Figure 4.11 contains a comparison of average simulated joint angles for ergometer pedaling to the average joint angles from the six-second seated experimental trials as well as the joint angles from a single trial for Cyclist X. The averages and standard deviations reported in Figure 4.11 include each cyclist's two six-second seated starts (14 trials total among all the cyclists). The averages are found over each 5 degree increment of the crank angle. This is done to show how the simulation compares to the average, as well as how it compares to the cyclist on which the model is based. Overall, there are similar trends in the joint angles between the ergometer simulations and experiments, with the largest differences seen in the ankle angle. The greatest variability between the experimental trials is for the ankle angle, so it would be reasonable to expect to see the largest differences between the experiments and simulations for the ankle angle as well. The hip and knee are fairly similar between simulations and experiments, especially in the upstroke. Both see greater flexion in the downstroke. The simulated ankle on the other hand has greater amounts of plantar flexion in general.

The optimal kinematics are sensitive to the limb lengths and the fixed hip position. A primary cause of differences between the simulations and experiments is the constraint on the hip joints to remain fixed. Even during seated pedaling, the hips are moving, which affects the biomechanics. Start-up pedaling from a seated position is a difficult task so a cyclist prefers to rise from the seat to attain a mechanically efficient body position and use their mass to aid in driving the pedal downward. In this simulation, however, the cyclists hips are fixed, which makes start-up pedaling significantly more difficult because they cannot adjust their body position and use gravity to their advantage.

In Figure 4.12, the torque activations showed that in the initial few pedal strokes, each limb was generating close to the maximum possible torque when the muscles were activated. There does seem to be a bit of noise at the peaks of the active joint torques so it is possible that with a lower iteration tolerance this would reach the maximum at all points. As the cyclist increased pedaling rate, the torque activations did not reach maximum as they did not have time to activate fully before being deactivated again. At around 3.5 seconds into the simulation, the hip flexor torque activations decrease greatly. This is likely indicating that at higher cadences the primary focus is on generating maximum extensor torque for the downstroke, and there is less of a contribution from the leg pulling up on the pedal.

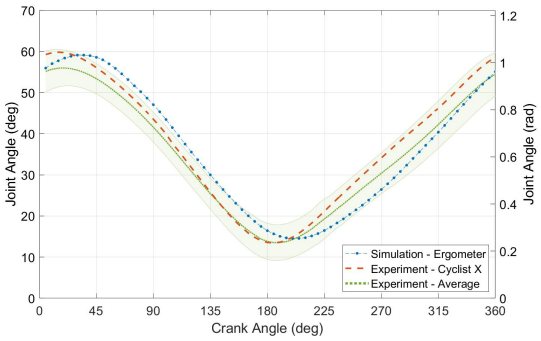

(a) Average right hip joint angle

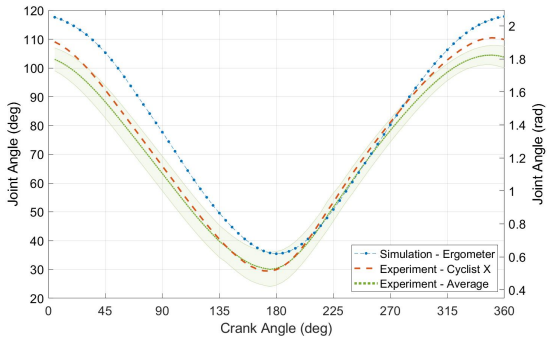

(b) Average right knee joint angle

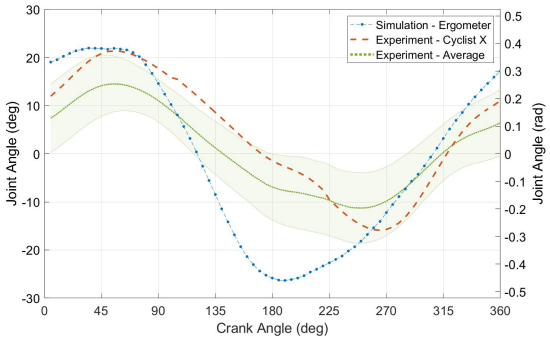

(c) Average right ankle joint angle

Figure 4.11: Average joint angles for each 5 degree increment of the crank angle for the ergometer experiments and predictive simulation. The shaded area represents ±1 standard deviation for the average of all the cyclists' trials (N=14).

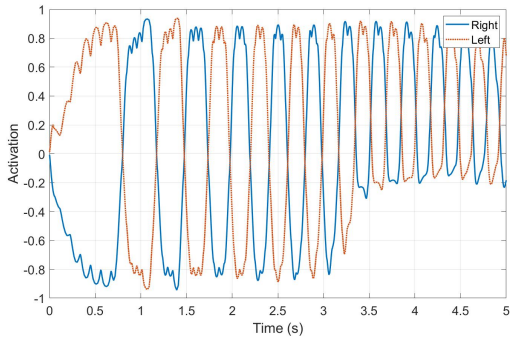

(a) Hip torque activation

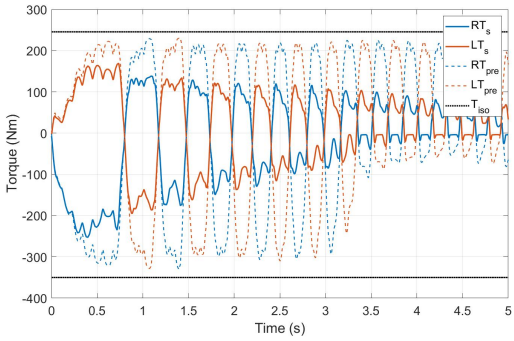

(b) Hip torque

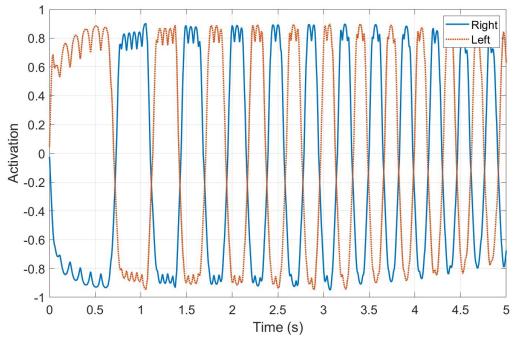

(c) Knee torque activation

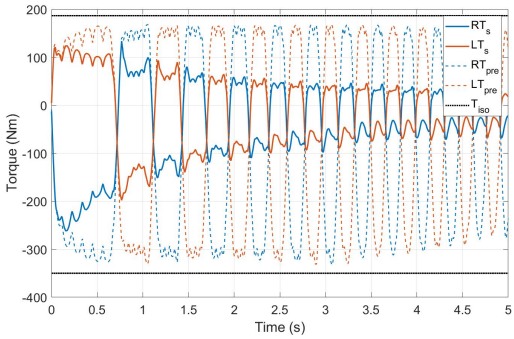

(d) Knee torque

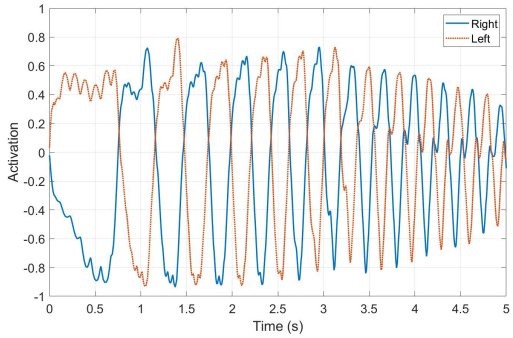

(e) Ankle torque activation

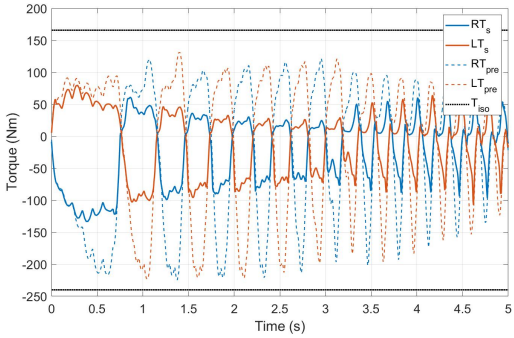

(f) Ankle torque

Figure 4.12: Joint torques for ergometer predictive simulation. T_s refers to the scaled torque, T_{pre} refers to the pre-scaled torque, and T_{iso} refers to the isometric torques for flexion and extension.

This corresponds with the findings of Martin and Brown [18] who noted that favoring the more powerful extension movements increases power production in cycling. An additional point they mention is that it is common to see people reduce the complexity of their movements when fatigued. In cycling, this can help explain the reduced ankle movement as cyclists primarily focus on hip and knee flexion and extension.

The net joint torques decreased as the joint angular velocity increased and the joint angle became less optimal for generating torque (Figure 4.12). The ankle motion is generally ≈45 degrees out of phase with the hip and knee so at times the ankle torque acts opposite to joint rotation in a stabilizing manner. This eccentric torque causes the active torque to spike, especially later in the simulation (around 3.5 seconds and on). Another important point to consider is that the torque scaling model is not necessarily designed to handle large joint angular velocities such as those being seen here. It is difficult to achieve those angular velocities for an isolated joint on a dynamometer, so the scaling at higher angular velocities is primarily an extrapolation of the scaling that occurs at lower angular velocities. This could result in some inaccuracies in the joint torque scaling. For additional plots containing the passive joint torques, the pedal forces, and the constraint errors, see Appendix B.

The primary purpose of these simulations was to ensure the cyclist model was a reasonably accurate representation of a real-life cyclist. These results indicate that the nature of the model, the bounds chosen, and the parameters being used are representative. The next step was to analyze cycling on the track.

Chapter 5

Standing Starts: Experiments and Simulation

5.1 Standing Start Experiments

5.1.1 Experimental Methods

Experimental data were collected on a single male member of the Canadian track cycling team who participates in the team sprint event. The team had limited availability so it would be of interest to test more cyclists in the future. Electrogoniometers from Biometrics, Ltd. (pictured in Figure 5.1) were used with adapters from Delsys (Trigno Wireless EMG, Delsys Inc.) to wirelessly transmit the data. Electrogoniometers were attached at the joints of interest in the model (both ankles, knees, and hips, single elbow and wrist). While it would have been interesting to see the kinematics of both arms, it would have required purchasing additional goniometers, and it was deemed that the cost would have outweighed the benefit of having the additional measurements, which were assumed to be similar. Electrogoniometers cannot measure shoulder angles so there was no reliable way to measure it. Attempts were made to estimate the joint angle from video, but the video quality was not high enough. The cyclist performed six standing starts on the track at the Mattamy National Cycling Centre in Milton, ON. The automatic gate and track timing system was used, which records time stamps at track landmarks (start/finish line, front pursuit line, 200 m, 100 m, etc.). For these purposes, the only ones that were within the trial were the start/finish line and front pursuit line so the time stamps available were the gate release and 15 m.

Figure 5.1: An example of the electrogoniometers from Biometrics, Ltd. that were used in the experiments [4]

Crank data were collected at 80 Hz using instrumented cranks from 4iiii Innovations, Inc. The crank sensors operated independently of each other so independent right and left side crank torques were collected. These were then summed together to get the total crank torque that is displayed in the figures. Inertial Measurement Units, or IMUs, (Mbientlab, Inc.) containing a magnetometer, three-axis accelerometer, and three-axis gyroscope collecting at 100Hz were placed on the crank and on the frame. The angular velocity from the IMU on the crank was used for a high-frequency cadence measurement. This was integrated to get the crank angle and was adjusted based on a magnetic reed switch in the 4iiii's system to account for measurement drift over time. The reed switch was triggered once per pedal stroke so the IMU data were able to be calibrated accordingly. The acceleration data from the IMU on the frame was integrated to get an approximation of frame position and velocity. These curves were not calibrated with other measurements so there is a potential for some integration drift in these approximations.

Prior to the experiments, the cyclist completed a self-selected, typical warm-up routine to ensure he was completely warm and loose for the tests. The cyclist used his personal bicycle, a Look L96 model. The cyclist's feet were clipped into the pedals, as is typical in track cycling. The bicycle started fixed in the gate, which uses a pneumatic clamping mechanism that clamps the bike on the seat post, just below the seat. The bicycle was then released automatically as the clock hit zero. The cyclist was quite familiar with this setup as it closely resembles the starting conditions of a team pursuit race and is a setup that is used in their practices. The cyclist was instructed to use his normal technique and give high effort up until the first turn (approximately the first 25 meters). After each trial,

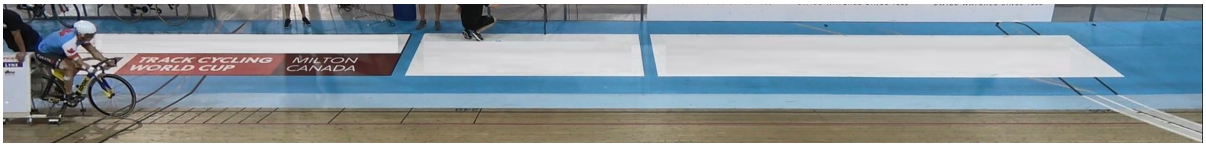

Figure 5.2: Experimental setup for standing starts

the cyclist was given time to rest so fatigue would not play a role. Figure 5.2 displays the setup used in the experiments.

One of the challenges with this data collection was synchronizing all the data streams. Post-testing, the data streams were synchronized using the accelerometer data. An EMG sensor from the Delsys system was placed on the crank to allow for the synchronization of electrogoniometer data through the accelerometer in the EMG sensor. This meant that the IMU, crank arms, and Delsys (i.e. electrogoniometer) streams all had accelerometer data in their data streams. The track timing system was visually synchronized by attempting to match the point where the crank began moving to the time stamp of the gate release.

There are several points to note regarding the electrogoniometers used. These electrogoniometers are strain gauge based so the output is a voltage. This voltage then has to be converted to a joint angle, a calibration process that was performed manually. The next point is that the angle obtained from the voltage output is a relative angle between the two endblocks. This means the angles are highly dependent on accurate placement of the endblocks. To account for differences in placement, a calibration measurement was obtained where the cyclist was asked to place each joint in a neutral angle (standing straight up with arms straight at sides). The offsets measured in these positions was subtracted from all the joint angle measurements so that the neutral position would correspond to zero joint angles.

The ankle angle was difficult to measure in these experiments because the distal endblock had to be attached to the heel of the shoe. This is not an ideal surface because of the nature of the cyclist's shoes so the attachment was slightly loose. Furthermore, the two ankle goniometers appeared to be faulty, so the ankle measurements were not successful. A comparison to the simulation could be made from measurements that were obtained from previous standing start experiments, under similar conditions. The ankle angle measurements displayed here for comparisons with the predictive simulation are from previous testing that was conducted to assess the efficacy of electrogoniometers for track cycling standing starts. These conditions were not identical, but the other joint angle ranges appear to be similar so it can give an idea of what these joint angles look like in experiments.

There are several difficulties with using electrogoniometers; however, there are limited tools available for measuring joint angles in the field over a 30 m distance. IMUs were considered, but drift was an issue. Electrogoniometer measurements would not be recommended for conducting an inverse dynamics analysis or for comparing small differences between cyclists or between different days of the same cyclist. However, for a single cyclist on a single set of experiments it is a useful tool for comparison and to get a general idea of the kinematics being used.

5.1.2 Experimental Results

A selection of experimental results are displayed here. In trial 1, the cyclist momentarily lost balance during the trial, causing the bicycle to swerve and slow down. This was not representative of an effective standing start so trial 1 was ignored for data analysis. Additionally, due to the faulty ankle electrogoniometers, there was no ankle joint data to analyze for these experiments.

Figure 5.3 contains the measured bicycle positions, bicycle velocities, crank angular velocities, and crank angles for trials 3 and 4. Due to a faulty IMU, there were no IMU data recorded for the other trials so results are not available for those. For the frame x position in Figure 5.3a, the markers represent the measured times from the time stamps in the track timing system. A time stamp was recorded at 15 m so the $*$ markers in the figures are the times at which the 15 m line was crossed. In comparison with the time stamps obtained from the track timing system, the position curve approximation is a slight underestimation of the actual position due to integration drift.

One of the first things to notice with the experimental results is the cyclist's consistency. Figure 5.4 displays the joint angles for trials 2-5, and they are quite similar for all the trials, especially for the hips and knees. An Olympic-level cyclist will have practiced this motion many times and have developed the "muscle-memory" to be able to consistently repeat the technique. The largest variability is seen in the wrist angle. Some of this variability can be attributed to measurement error, as the endblock on the hand was difficult to keep secured so there was the possibility of slight movement over the duration of the six trials. The secondary peaks seen in the hip angles correspond to the cyclist thrusting the hips back in the reset motion. Interestingly, these peaks were more pronounced in the right side than the left side, indicating that while the cyclist was consistent, he was not performing the motions symmetrically. This leads into the second point of interest in these results.

The second thing to note is that there are noticeable asymmetries between the right and left side. In Figure 5.5 one can see asymmetries in the hip and knee joint angles. As

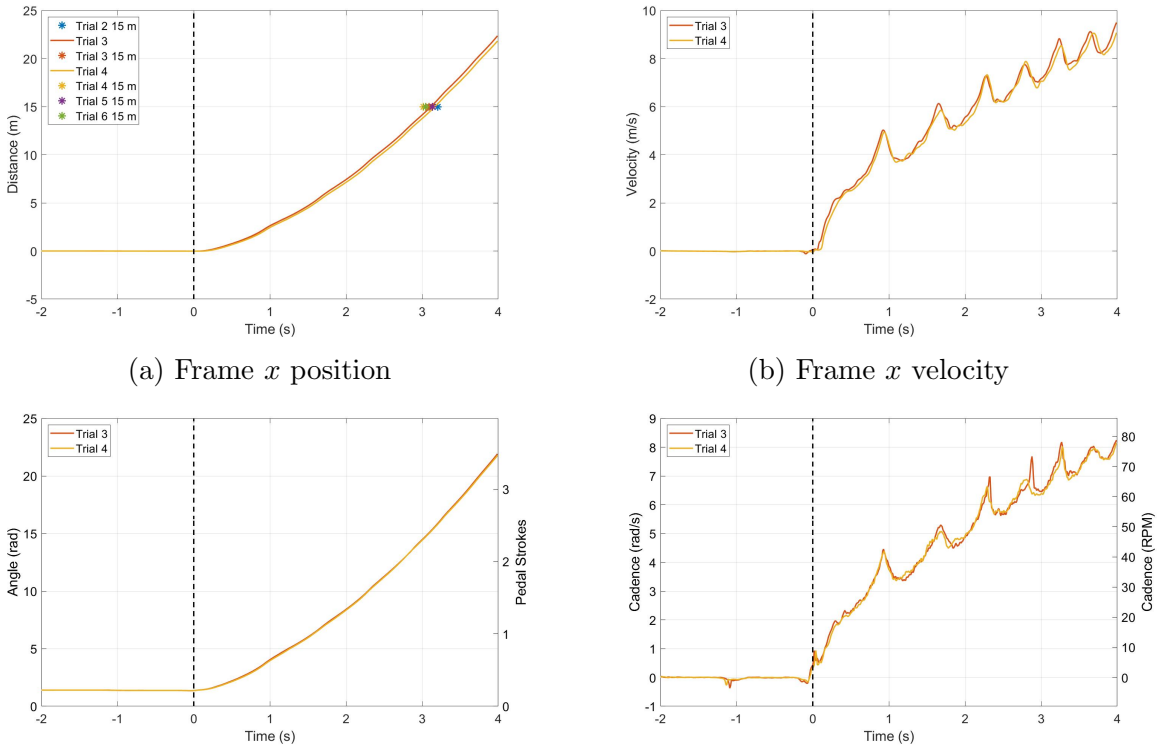

(a) Frame x position

(b) Frame x velocity

(c) Crank angle

(d) Crank angular velocity

Figure 5.3: Experimental kinematics for the bicycle

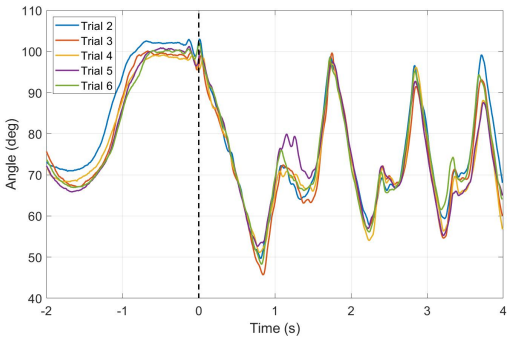

(a) Right hip joint angle

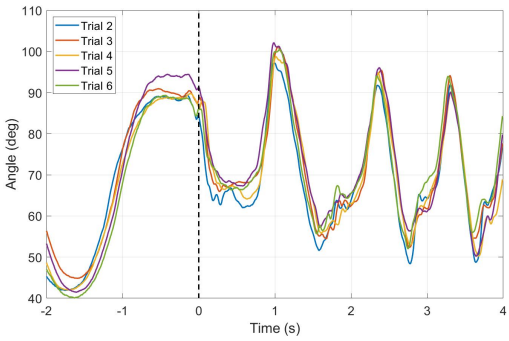

(b) Left hip joint angle

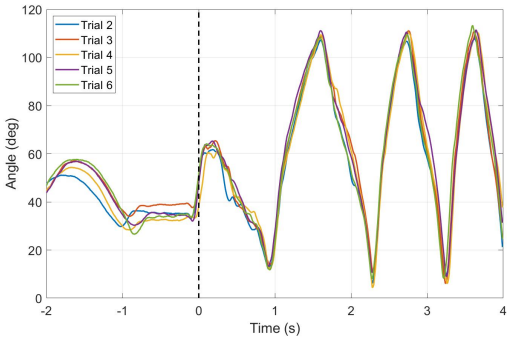

(c) Right knee joint angle

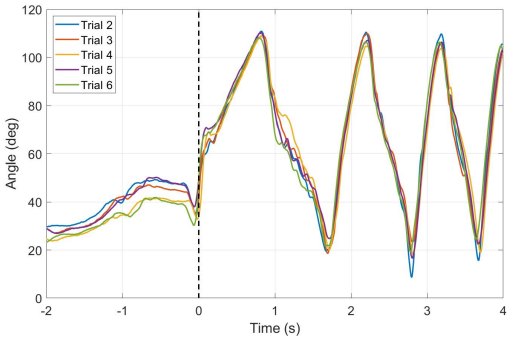

(d) Left knee joint angle

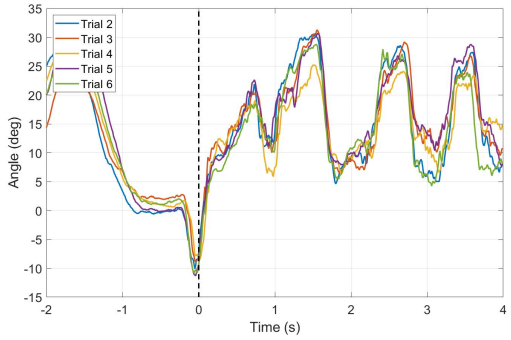

(e) Wrist joint angle

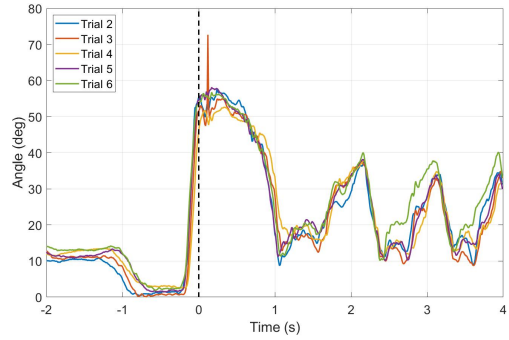

(f) Elbow joint angle

Figure 5.4: Experimental joint angles for the standing starts

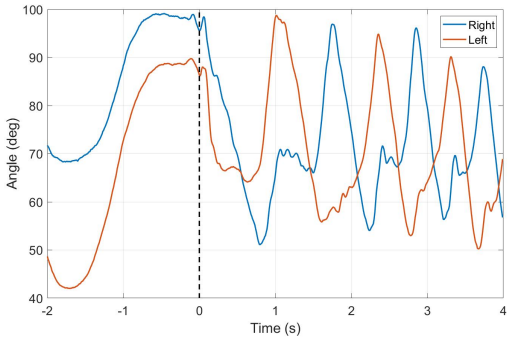

(a) Right and left hip joint angles

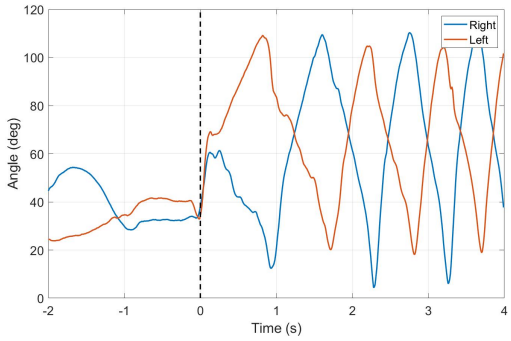

(b) Right and left knee joint angles

Figure 5.5: Experimental hip and knee joint angles: comparison between legs

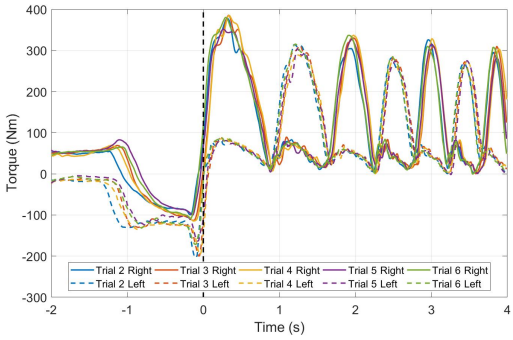

(a) Right and left crank torque

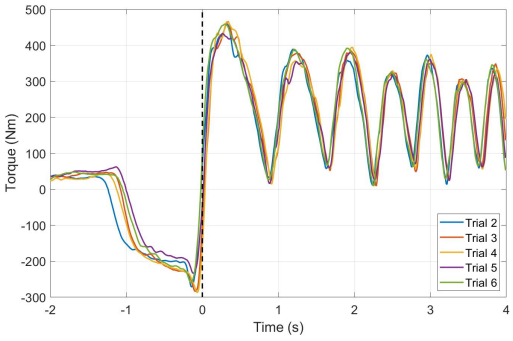

(b) Combined crank torque

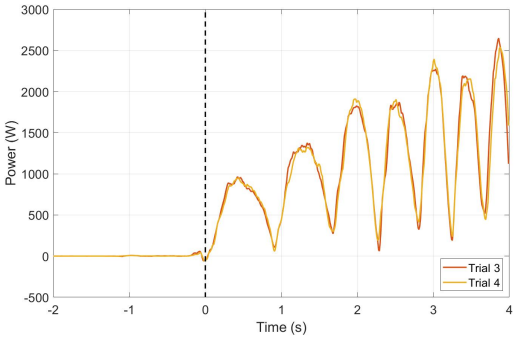

(c) Power

Figure 5.6: Experimental crank torque and power

mentioned there are intermediate peaks in the right hip joint angles that are not seen in the left hip joint angles. In general, the range of motion for the right knee is greater. The right knee is fully extended close to bottom dead center, where as the left leg does not undergo as much extension. When making comparisons between the legs, it is important to keep in mind there is potential for measurement errors due to sensor placement and the initial calibration. The calibration is an inexact process so the measured joint angles could be offset from the actual joint angles. However, the overall range of motion is not susceptible to that error, as sensor placement errors result in a shift of the entire curve and not distortion of the curve. For this reason, the electrogoniometer measurements are more useful for comparing ranges of motion and the shapes of the curves as opposed to the exact values.

Figure 5.6 displays an additional asymmetry with the right side producing more torque than the left side. Both are following similar patterns; however, the peaks for the right side are larger, even in the subsequent pedal strokes. The decrease in torque is expected as the angular velocity increases, but the left crank torque is still consistently smaller. All of these asymmetries are potentially related in that the greater torque being generated in the right leg results in a greater range of motion for the right leg joints.

The key takeaways are that an Olympic-level cyclist is able to perform the standing start technique in a repeated manner. This indicates that if an optimal technique was suggested, it would be possible for this technique to be repeated consistently. However, the primary challenge with adopting any changes in technique would be in overcoming the existing "muscle-memory." The noticeable asymmetries are a second takeaway from these experimental results. This is not something that is incorporated in the model, as both sides are given equal torque parameters.

5.2 Predictive Simulation

5.2.1 Problem Formulation and GPOPS-II Setup

Simulations were run using the combined cyclist and bicycle model and GPOPS-II for solving the optimal control problem as discussed in Chapter 3. The problem was formulated as a two-phase problem, separated into the launch and pre-launch phases (refer to Chapter 1 for a more detailed description of these standing start phases). In the pre-launch phase, the bicycle is treated as being completely fixed, leaving the model with only the cyclist degrees of freedom. This assumption is not entirely true, as from video analysis one can

see the bicycle actually pivots slightly about the fixation point when the cyclist rocks back and launches forward. The gate contains a pressurized clamping mechanism that clamps down on the main post several centimeters below the seat. It is fairly rigid, but does not completely fix the bicycle in place, as there is some movement of the entire gate and also some slight rotation within the clamp. It was attempted to more accurately model the bicycle in the pre-launch phase by incorporating the vertical movement and pitch. However, when using this formulation, GPOPS-II ran out of memory, so this modeling approach was abandoned.

The time duration of the simulation was 5 seconds, with the pre-launch designated to last 1 second and then continuing into 4 seconds of the launch phase. Initial state guesses for both phases were based on the crank angle being at 75 degrees and the bicycle being stationary. The initial guesses for the cyclist should only play a role in how the cyclist starts the pre-launch phase, which seems to be largely irrelevant as they proceed into a similar "coiled" position regardless of where they start. The initial guesses for the launch phase could also play a role in the solution, but the optimal solution of the pre-launch phase seems to be uninfluenced by the initial guess for the launch phase. The bounds for joint angles and joint angular velocities were set at values that would not restrict the natural motion of the cyclist. However, during both phases, path constraints were placed on the position of the hip joint center that limited it going through the seat or seat post. The most important initial states and bounds were for the frame vertical position/velocity and pitch angle/angular velocity. The bicycle needed to be starting in a vertical position that is quite precise in terms of the bicycle resting on the track. Otherwise the stiffness and damping of the tire would cause significant oscillations for the frame position and orientation in the initial seconds of the simulation. These oscillations can be seen in the tire normal forces, which then affects the amount of tire slip and the amount of longitudinal tire forces. From there, these oscillations propagate throughout the results and oscillations are seen in the other states such as crank angular velocity and overall frame horizontal velocity.

There was a tuning process required in generating these simulations in order to find the bounds, mesh numbers, tolerances, and other parameters in the GPOPS-II setup. These all affected the solution that was obtained and the time it took to achieve that solution. They were tested in a trial and error type formulation during the tuning process, but they were not tested as extensively as desired due to the length of the simulation. Disconcertingly, the results seemed to vary with some changes to these parameters. For a large problem such as this, GPOPS-II seems to be fairly sensitive to the bounds and parameters. An alternative explanation is that the problem was set up in such a way that it was not able to sufficiently converge to an optimal solution in every simulation.

The objective for the simulation was to achieve the maximum distance in the given time period. This represents the objective on the track, where the cyclist wants to cover the maximum distance possible in the initial portion of the event to get up to top speed as quickly as possible. Therefore, the following cost function was minimized, where x_f is the final distance traveled.

$$J = \frac{1}{x_f} \tag{5.1}$$

As mentioned with the ergometer simulation, other cost functions have been used in optimizing pedaling that include some form of minimization of jerks and/or minimization of joint torques. As with the ergometer simulation, these were considered but ultimately not used because minimization of these led to less distance covered, which was the ultimate goal. These additional objectives would play more and more of a role the longer the simulation continues. In a standing start, the primary objective is to achieve top speed as quickly as possible. The lead cyclist only completes one lap and their teammates look for them to get out in front quickly and set the pace. For this reason, efficiency of the motion is not as much of a concern for the first few seconds of the standing start. Beyond the first few seconds, fatigue becomes more of a factor to consider so the cyclist begins to take efficiency into account more.

An additional component of the objective function was considered for the pre-launch phase in order to help drive the solver to the optimal solution for the pre-launch. In the end, this was not needed because the solver was able to find that launching forward at the end of the pre-launch helped achieve maximal distance. It is rather interesting to see the ability of the solver to find key characteristics of a standing start solely based off the goal of achieving maximal distance. Entering the project, it was anticipated that more complex objective functions might be needed. More complex objective functions could still give results that more closely match the experiments, but a fairly representative simulation can be achieved with a simple objective function.

The computation time was 670 minutes ($\approx$11 hours) on an Intel Core i7-6700 CPU at 3.40GHz with 16GB RAM for the track standing start simulation. The subsequent figures contain the results of the simulation. After seeing some variabililty among the solutions obtained during the tuning process, the conclusion was reached that it is likely these results have not completely converged to an optimal solution. While they may not be a global optimal result, they still present a highly-effective method of completing a standing start. These uncertainties with the results are largely due to the lengthy computation time and the difficulties posed by tuning the GPOPS-II setup.

One of the challenges with this simulation was the interface between the two phases. The state trajectories found by GPOPS-II tended to have an unnatural jump at the end

of each phase, especially with the joint kinematics for the pre-launch phase, which causes issues for the start of the next phase. Additional difficulty seems to be coming from the tire vertical stiffness and damping. As mentioned, if the bicycle does not begin with the correct initial conditions there tends to be oscillations in the frame vertical position and pitch angle. The solution that is found seems to be more sensitive to these variables than would be expected. It seems that the solver has some difficulty finding solutions that meet the bounds for the vertical position/velocity and pitch angle/angular velocity, states that are heavily dependent on the tire stiffness and damping.

A final note is that the optimal trajectories towards the end of the simulated trial are less reliable and less meaningful than those during the main portion of the trial. The initial portion was fairly consistent throughout the tuning process, but results varied somewhat in terms of the hip positions later in the simulation. Based on the objective function, at the end of a trial, the model may attempt to maneuver itself in a way that will increase the final distance slightly at the expense of future performance (e.g. driving the bicycle frame forwards in the last second of the simulation). An updating prediction horizon would be needed for longer simulation lengths.

5.2.2 Simulation Results

Figure 5.7 contains still frames of standing starts in the experiment and simulation. This gives a side-by-side, qualitative comparison of the experiment and simulation from the pre-launch through the initial drive and reset of the launch phase. There are qualitative similarities between the two. Both rock their hips back in the pre-launch in a similar nature. It seems in the experiment, the cyclist may extend back slightly farther, with greater shoulder and elbow extension.

One of the most noticeable differences between simulation and experiment is that the simulation tends to be farther forward, with a more elevated hip position at gate release than the actual cyclist during the experiments. This difference is likely due to the fact that the simulation can time the gate release perfectly. In experiments on the other hand, the cyclist would tend to err on the side of caution to make sure the gate is fully released at the end of their pre-launch. They do not want to have fully launched themselves forward only for the gate not to have been released and to have lost all forward momentum in an inefficient position.

The drive phase is fairly similar between the two, but this is where the planar nature of the model results in some differences. The cyclist tends to have a more out of plane elbow flexion, coming from shoulder rotation. While the trunk is in a similar position and

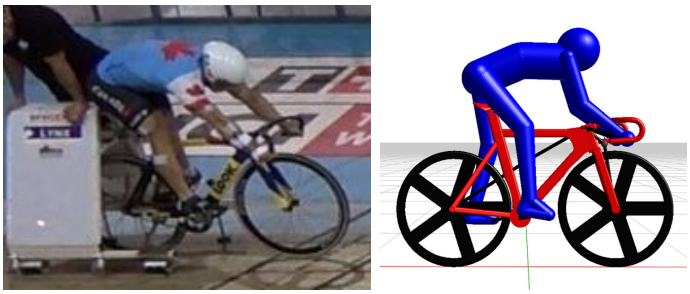

(a) Pre-launch

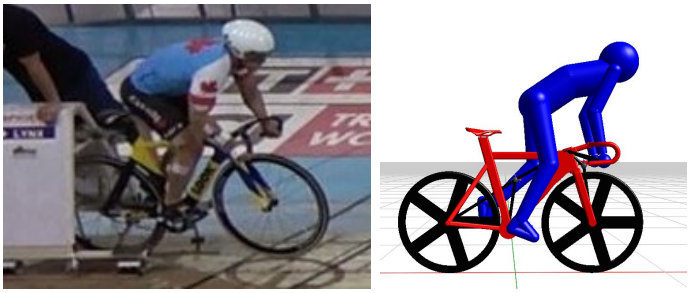

(b) Gate Release

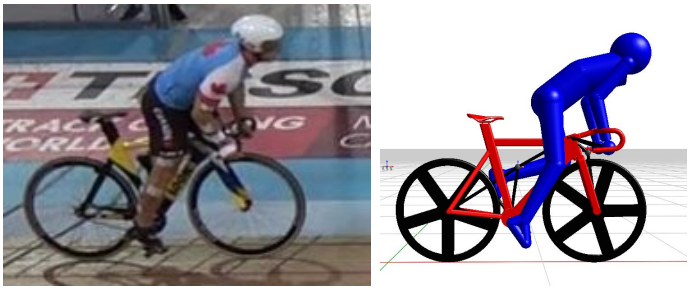

(c) Drive

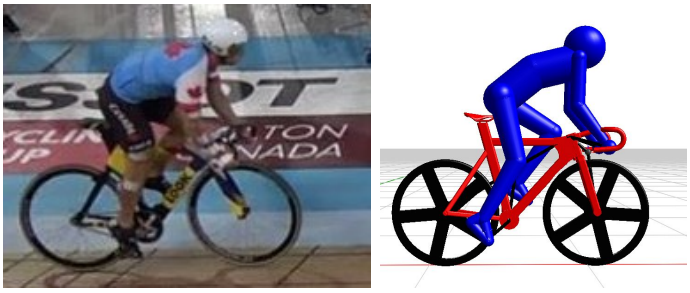

(d) Reset

Figure 5.7: Images from standing start simulation and experiment

orientation for both, the arm kinematics to achieve it are different. Furthermore, we can see the angle of the spine changing in the experiments as well, which cannot be captured by this model. Continuing from the drive to the reset position, the cyclist has shifted the hips back to assume a more mechanically efficient position. Here the general pose is also similar between the two and seems to be occurring at a similar 45-degree crank angle. From this qualitative comparison, we can see the technique being used is fairly similar between the two, with the most noticeable area for improving the real-life technique being the timing of the pre-launch. This model is not able to provide suggestions on better ways to achieve that timing.

Moving on from those images, a more quantitative comparison of the simulation and experiment can be presented. The general notation for all plots will be to use solid blue curves for simulation and dashed red curves representing experimental results. The black vertical dashed line represents the gate release, separating the end of the pre-launch phase and beginning of the launch phase. Table 5.1 contains the correlation coefficients, which will be discussed for the corresponding figures. Additional plots not presented in this chapter for the standing start simulation can be found in Appendix C. Figure 5.8 contains the bicycle kinematics, including the x position and speed of the frame center of mass. The experimental speed of the frame was obtained by integrating the acceleration from the accelerometer that was fixed to the frame. With the bicycle kinematics, we can see the simulation clearly outperforming the experiments. This is primarily due to the ability of the simulation to almost perfectly transfer all of its initial momentum generated in the pre-launch phase to the bicycle when it is released from the gate. The cyclist weighs more than 10x that of the bicycle, so the velocity of the trunk is mostly converted to translational velocity of the combined system. The correlation coefficient for the bicycle speed is 0.973, indicating that when compared relative to the crank angle, the simulation and experiment are strongly related for this variable.

The transfer of momentum is optimized because the simulation is able to abruptly stop the upperbody motion relative to the frame. This is unrealistic due to the complicated nature and difficult timing of such a maneuver. One difficulty with predictive simulations is that the model can be manipulated in very precise ways to maximize performance that might not be feasible in real life due to the precision that would be required for such a movement. Another example of this is the possibility the simulated cyclist could be manipulating the bicycle to have optimal wheel normal forces. By manipulating the body position and bicycle orientation to reduce the front wheel normal force, the simulation could be experiencing less resistance at the front wheel while being able to generate larger amounts of torque at the rear wheel. This is something that a human cyclist would have more difficulty executing precisely. Looking at the wheel normal forces plotted in Appendix

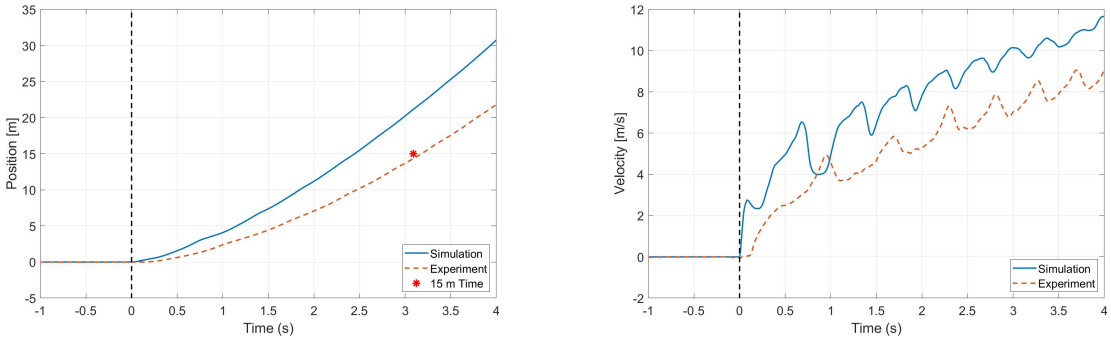

(a) Frame x position

(b) Frame x velocity

Figure 5.8: Frame kinematics

C, this does not appear to be the case in this simulation, but there were instances in other simulations that indicated this might be occurring. In some simulations, oscillations occurred at the beginning so the bicycle was not always perfectly balanced on the ground. In general, caution must be taken in utilizing the results because the simulation can be quite precise with its movements.

The peaks in the bicycle velocity and crank angular velocity correspond to the cyclist reset maneuver. The cyclist shifting the weight backward thrusts the bicycle forward underneath them. At the same time, this motion is driving the crank forward, both through the pushing against the crank and through the fixed gear connection. Due to the nature of the fixed gear ratio, the crank angular velocity and bike velocity are directly related. Figure 5.9 contains the crank kinematics, including total crank angle and crank angular velocity, or cadence. The crank angular velocity displays a similar initial jump as the bicycle movement as a result of the fixed gear ratio. After the initial jump, the crank angular velocity seems to follow a similar trend to the experiments, with peaks and valleys as the cyclist goes through the drive and reset process. The similar trends between the two result in a correlation coefficient of 0.962 for the crank angular velocity. In these results and some subsequent results, there will be the appearance of some "noise" in the simulated data. This is caused by the bicycle bouncing slightly, as was mentioned in the previous section.

When examining the crank kinematics we can look at one of the key points of interest for Cycling Canada: what should the initial crank angle be? The initial crank angle chosen by the simulation was 83 degrees. The initial crank angle for the cyclist in the experiments was approximately 75 degrees. It is unclear what are the driving factors determining the

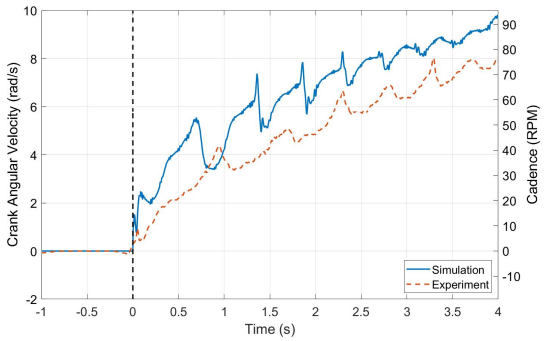

(a) Crank angular velocity versus time

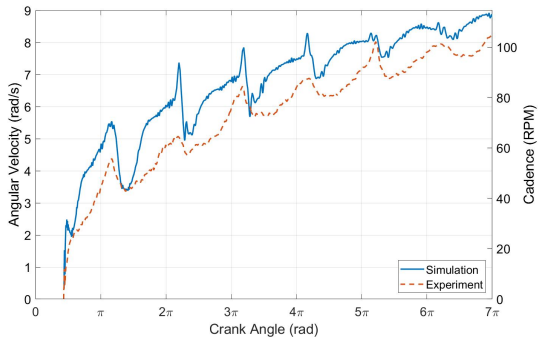

(b) Crank angular velocity vs. total crank angle

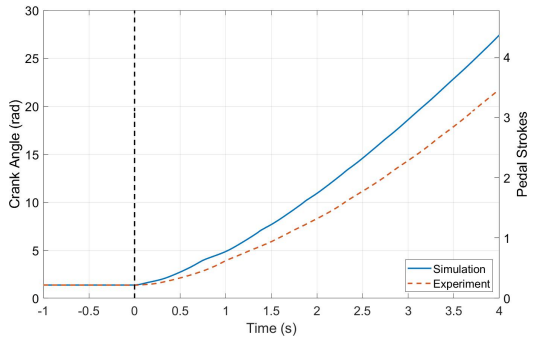

(c) Crank angle versus time

Figure 5.9: Crank kinematics

optimal initial crank angle being computed in the simulation. Various initial crank angles were seen throughout the parameter tuning process, all starting with the same initial guess of 75 degrees. A sensitivity analysis would be useful to examine what parameters are having the strongest effect on the initial crank angle. One might expect that the initial crank angle chosen should be the crank angle that allows for the most torque to be generated throughout the first downstroke. The predominant factors for this would be the joint angles that are optimal for generating torque and what crank angle puts the body in the most efficient position for transferring propulsive energy to the crank. An additional factor in the initial crank angle could be at what point after the gate release the initial reset motion has to take place. Since there is such a large initial velocity in the simulation, this could be playing a larger role than it should be.

For more insight into what is occurring at the crank, we can look at Figure 5.10, which contains the crank torque and power. Here the correlation coefficient is 0.828 for the crank torque and 0.765 for the power. From the experimental results it was noted there was a significant right and left asymmetry in the torque production. This is something that is not included in the model so the crank torque profile is more consistent. The simulation generate greater crank torque than in the experiments at the beginning and less crank torque than in the experiments towards the end. It is possible this is due to the nature of the torque scaling with angular speed, and that an Olympic cyclist may have less of a decrease in torque production at higher angular velocities. As mentioned before, the simulated behavior at the end is not necessarily indicative of what should be done to achieve success beyond five seconds.

Figures 5.11 and 5.12 contain the right and left leg joint angles plotted versus time and versus the total crank angle, respectively. Plotting with respect to time is useful for seeing how the joint angles change during the pre-launch and to see the time differences in the profiles due to the higher cadences seen in the simulation. Plotting against the total crank angle is more useful for a direct comparison of the joint kinematics between the simulation and experiment as it aligns them on a common scale. The correlation coefficients for the hip angles are 0.748 and 0.708 for the right and left hip, respectively. Comparisons between experimental and simulated hip angles can be difficult due to the nature of the trunk. In the model, the spine was given a fixed angle of 25 degrees. In reality, this angle is varying, which would affect the pelvis angle, resulting in different hip angles. One of the key features of the hip angle is the intermediate peaks that result from the reset motion. For the right hip, there is a larger intermediate peak at a 45-degree crank angle, and a smaller intermediate peak at 225 degrees. In the simulation, this intermediate peak only occurs once versus the multiple times that are seen in the experiments, indicating the cyclist performed more reset motions in the experiment than the simulation did.

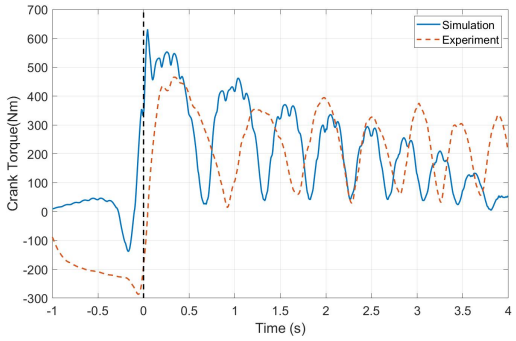

(a) Crank torque versus time

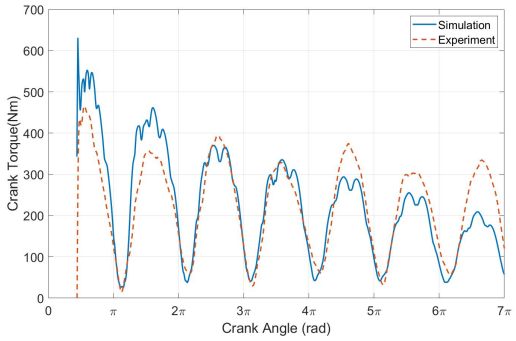

(b) Crank torque versus total crank angle

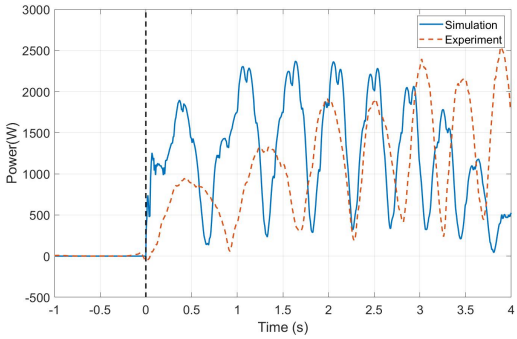

(c) Power versus time

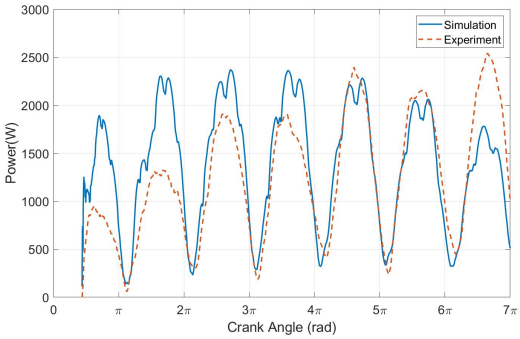

(d) Power versus total crank angle

Figure 5.10: Comparison of simulated and experimental crank torque and power for standing starts

Table 5.1: Correlation coefficients between the standing start simulation and experiment

Speed	Cadence	Crank Torque	Power
0.973	0.962	0.828	0.765

R. Hip	L. Hip	R. Knee	L. Knee	R. Ankle	Elbow	Wrist
0.748	0.708	0.930	0.872	-0.102	0.067	-0.105

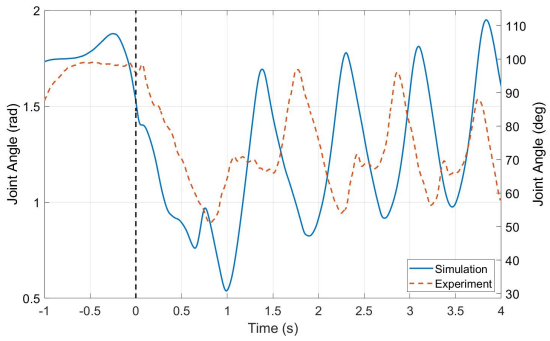

(a) Right hip angle versus time

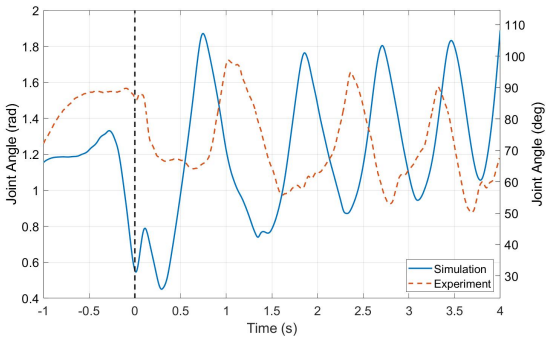

(b) Left hip angle versus time

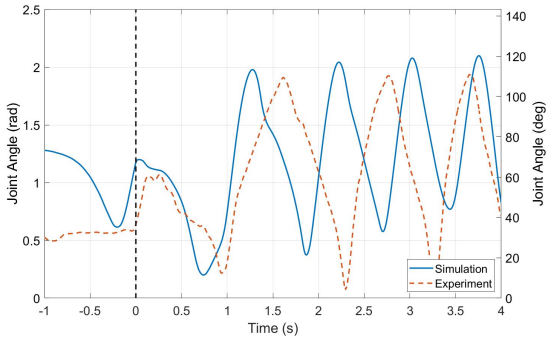

(c) Right knee angle versus time

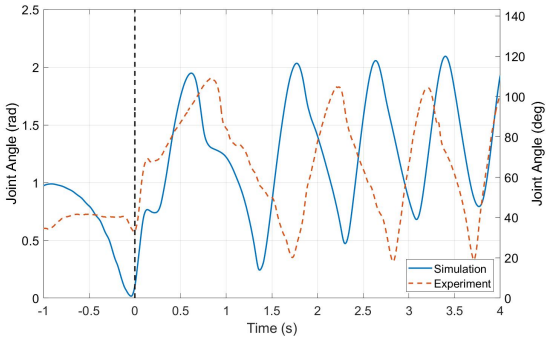

(d) Left knee angle versus time

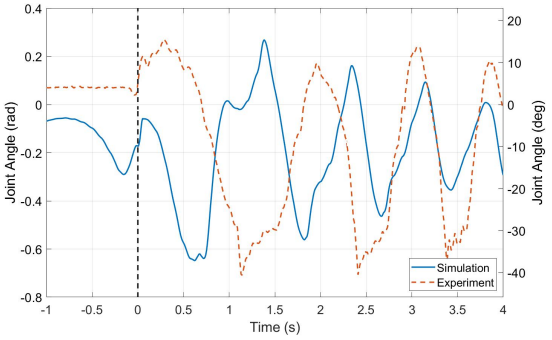

(e) Right ankle angle versus time

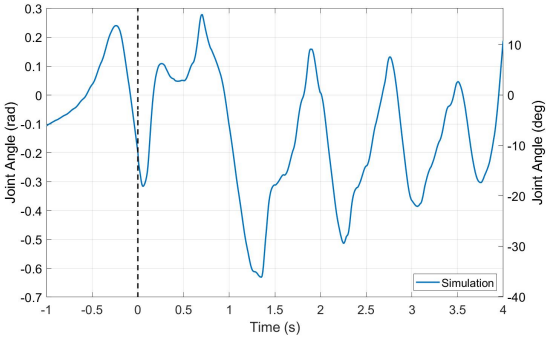

(f) Left ankle angle versus time

Figure 5.11: Lower limb joint angles versus time for standing starts

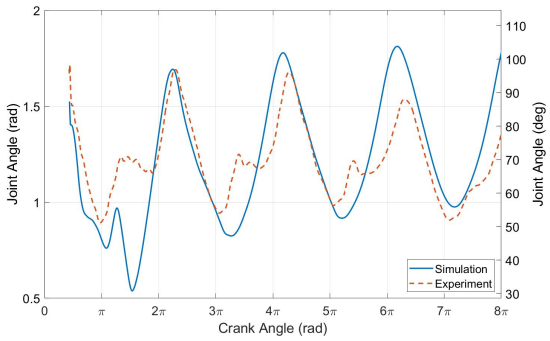

(a) Right hip angle versus total crank angle

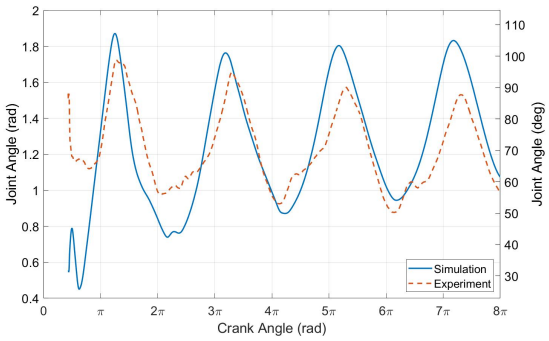

(b) Left hip angle versus total crank angle

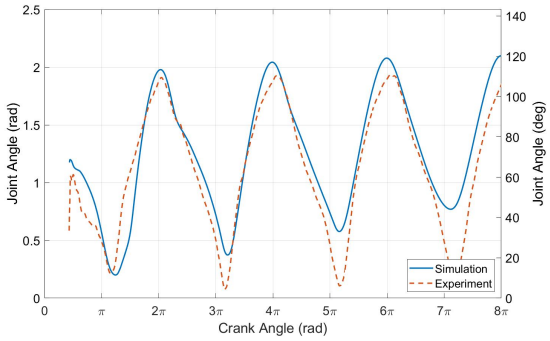

(c) Right knee angle versus total crank angle

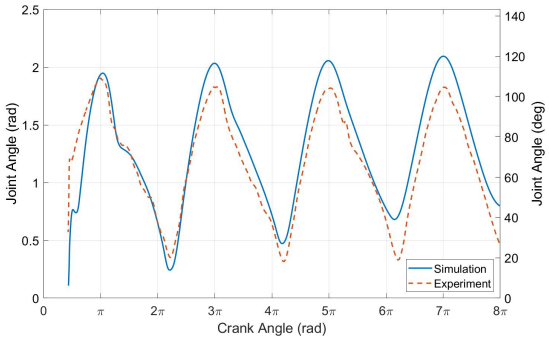

(d) Left knee angle versus total crank angle

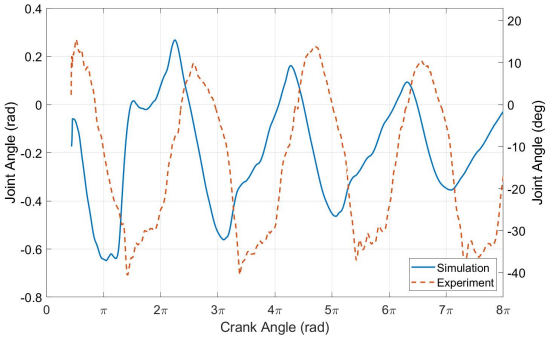

(e) Right ankle angle versus total crank angle

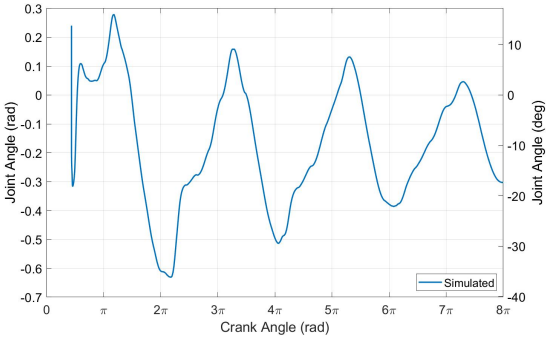

(f) Left ankle angle versus total crank angle

Figure 5.12: Lower limb joint angles versus total crank angle for standing starts

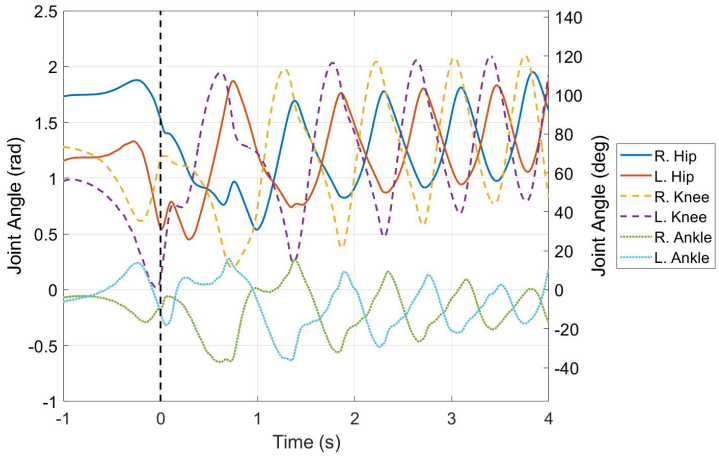

Figure 5.13: Lower limb joint angles for the standing start simulation

The knee and ankle angles are the best for comparison; unfortunately, the ankle angle measurements were not successful. Comparing with the ankle angles from the preliminary testing, there was more ankle dorsiflexion in the simulation. The experimental ankle joint angle is not perfectly aligned with the crank angle since it came from a different experiment. As a result, the correlation coefficient of -0.102 for the right ankle indicates there is no relationship between the experiment and simulation. The main use of this experimental ankle angle is for comparison of the range of motion and general trends of the joint kinematics. The knee has the most similarity between the experiment and simulation with correlation coefficients of 0.930 and 0.872 for the right and left knee, respectively. For the knee, there is less flexion in the experiments than at the end of the simulation due to the hip position gradually trending lower over the course of the simulation. Overall, the simulation appears to be more symmetric than the experimental results, a characteristic that is made clearer in Figure 5.13. A final point to note is that the size of the cyclist relative to the bicycle could play a role in the optimal kinematics as well. The cyclist model was scaled using anthropometric data to match the experimental cyclist, but it is possible the cyclist's relative limb lengths were not the same as those for the average population. Overall, these joint angles are useful to see as a comparison and confirm that the simulation is in similar ranges.

Figure 5.14 contains the upper limb joint angles for all three joints. There are significant differences seen between the upper limb joint angles in the simulation and in the experiment. Correlation coefficients for the elbow and wrist were 0.067 and -0.105, respectively. The upper limbs go out of plane much more than the lower limbs so the planar

modeling is much more effective for the lower body, but not as good of a representation for the upper body. The physiological nature of the shoulder, elbow, and wrist joints allows for significantly more movement out of plane than what is included in the model. The fixation method of the hand also constrains the attachment angle, when in reality, the hand orientation can change on the handlebars in addition to the wrist deviation. To further compare with the lower limb, the foot being clipped into the pedal gives a much better representation in the model so that is one fewer potential source of discrepancy in the joint angles due to modeling for the lower limb joints.

For the elbow and wrist, the joint angles do seem to be in a similar range despite these modeling issues. The experimental results are showing less elbow flexion, likely because the arms are able to go out of the plane. The wrist angle is difficult to measure using the electrogoniometers, so of all the joints, it has the greatest likelihood of measurement error. There is limited surface to fix the endblocks and the cyclist sweating made it difficult to secure in place. These joint angles may be significantly different between the simulation and experiment, but that does not say anything definitively about the hip joint center translational kinematics, which matters more than the individual upper limb joint angles when it comes to being in the optimal position for overcoming the mechanical inefficiencies. The same hip position could be obtained with different combinations of joint angles depending on whether they are going out of the plane versus staying in the plane. Ideally, an exact measure of hip position and velocity during the experiments would be used for comparison, but this was not possible using the existing sensors.

A final observation about the upper limb joint angles is that it seems like the elbow is somewhat redundant. The wrist and and shoulder angles follow oscillatory patterns that relate to the hip movement, whereas the elbow angle seems to have other oscillatory movements as well. Figure 5.14f shows the upper limb joint angles plotted together to get a sense of the trends relative to each other. The torques for the upper limbs (Figure 5.15) are primarily the shoulder torques, as they are the strongest of the three. The torque values displayed in Figure 5.15 represent the combined torque of both arms due to the simplification made to lump the arms together for symmetric movement.

Figure 5.16 contains the joint torques and torque activations for each lower limb joint. The torques are being close to maximally activated for most excitations of the hip and knee joints. There are certain points during extension in the first pedal stroke that each joint undergoes a slight decrease in activation before returning to maximal activation. For the ankle joint torques there is a period of eccentric contraction as was seen in the ergometer simulation, indicating there are times when it is acting in a stabilizing manner. This would correspond with the findings of previous researchers [40] that during portions of the crank cycle, the ankle is acting primarily as an energy transfer mechanism.

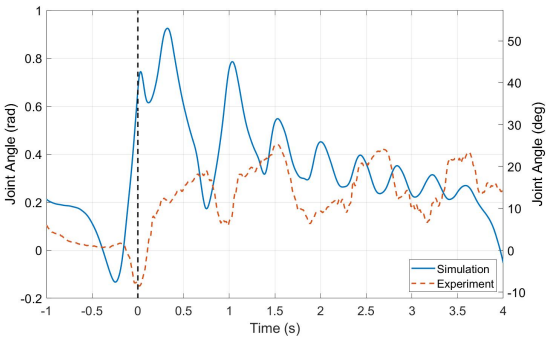

(a) Wrist angle versus time

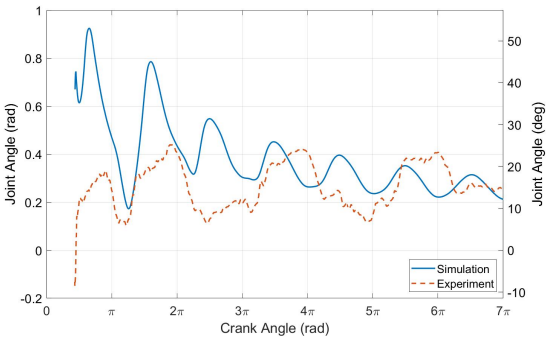

(b) Wrist angle versus total crank angle

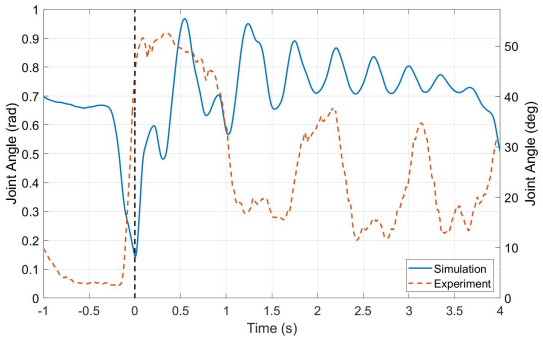

(c) Elbow angle versus time

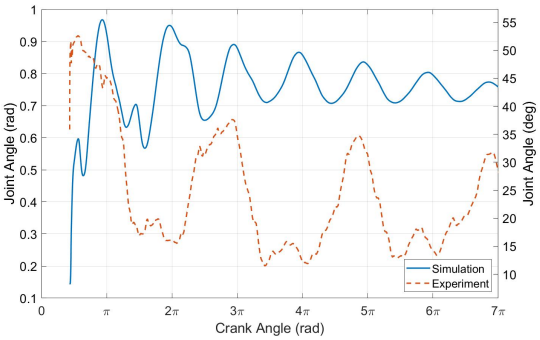

(d) Elbow angle versus total crank angle

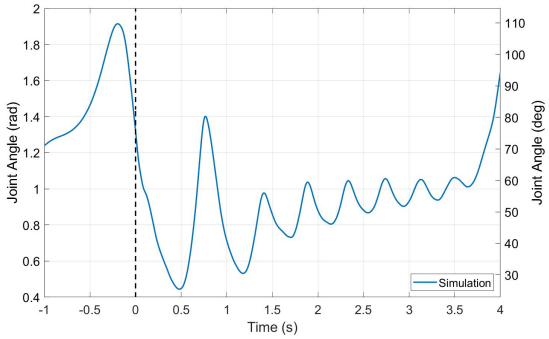

(e) Shoulder angle versus time

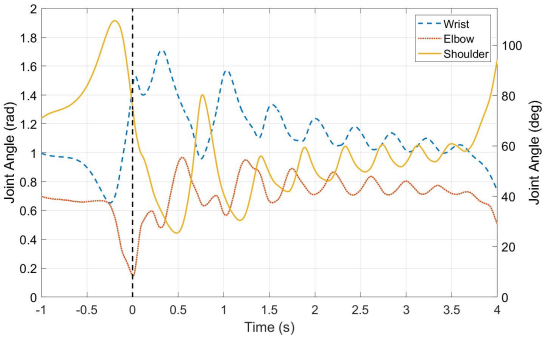

(f) All upper limb joint angles

Figure 5.14: Upper limb joint angles

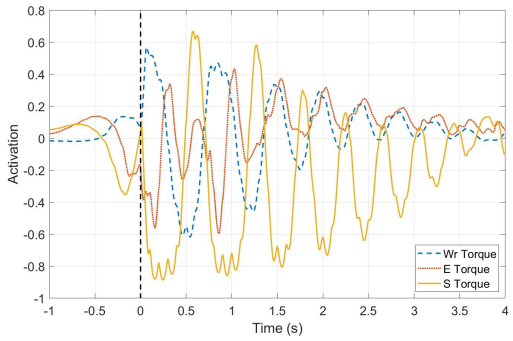

(a) Upper limb torque activations

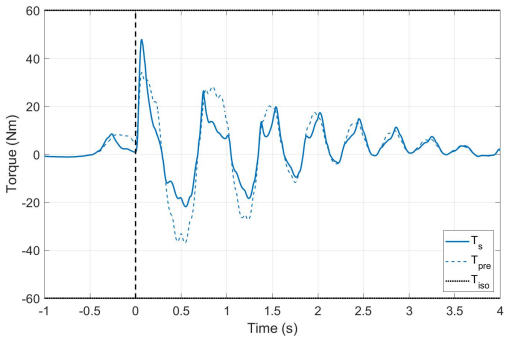

(b) Wrist torque

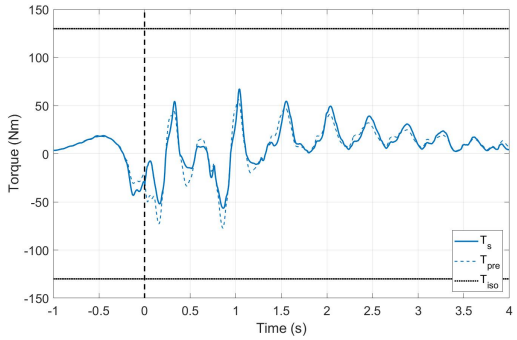

(c) Elbow torque

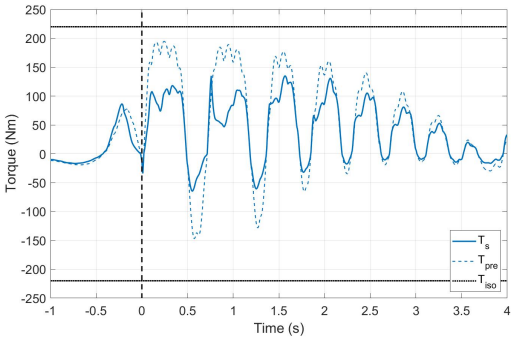

(d) Shoulder torque

Figure 5.15: Upper limb joint torques and activations. T_s refers to the scaled torque, T_{pre} refers to the pre-scaled torque, and T_{iso} refers to the isometric torques for flexion and extension.

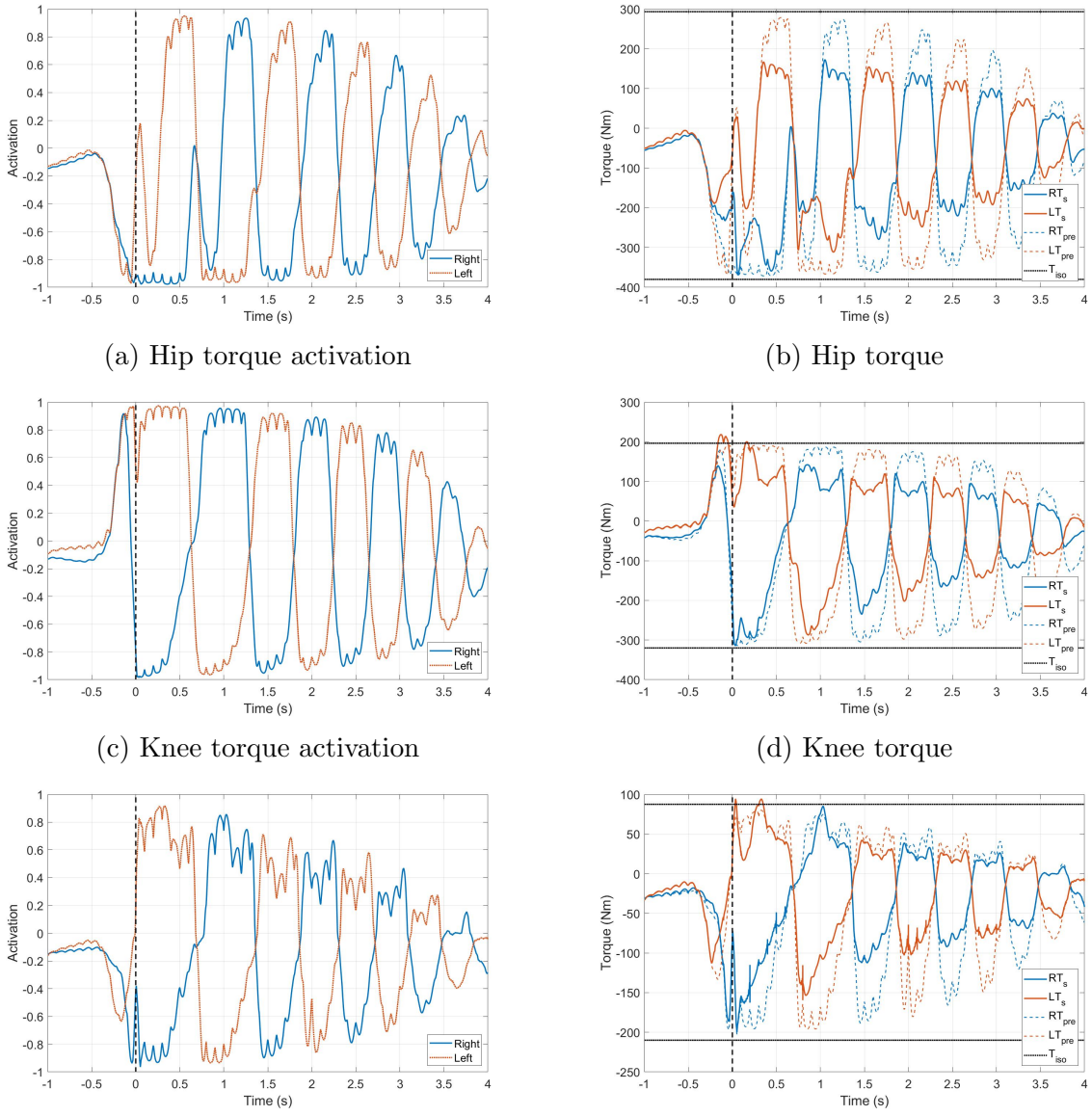

(a) Hip torque activation

(b) Hip torque

(c) Knee torque activation

(d) Knee torque

(e) Ankle torque activation

(f) Ankle torque

Figure 5.16: Lower limb joint torques and activations. T_s refers to the scaled torque, T_{pre} refers to the pre-scaled torque, and T_{iso} refers to the isometric torques for flexion and extension.

The hips tend to utilize the maximum activation rate when switching from flexion to extension. However, it undergoes a more gradual activation going from extension to flexion, indicating the hip torque is not as much of a driving factor during the upstroke. We can see similar trends with the knee torques. The results of vanSoest and Casius [36] and Bobbert et al. [28] indicated the importance of activation/deactivation dynamics to the results and this can be seen here. A faster activation and deactivation rate would allow for faster transition from flexion to extension, which plays a role in the maximum amount of torque that can be produced.

Figure 5.17 is the hip joint center kinematics. The simulation starts by rocking the hips back and stretching the upper body so that the hips are above the seat and almost as far back as possible. The simulation then launches the body forward to its forward-most position. The simulation tends to reach its peak reset position at approximately 45 degrees past top dead center (TDC) with each leg. It begins the reset motion at about 45 degrees prior to reaching top dead center (crank angle of 315 degrees). The reset motion takes place as the crank passes through TDC so that the simulated cyclist can overcome the mechanical inefficiency. In this reset motion, the cyclist shifts the bike forward underneath them, a motion that can be seen in the peaks in translational bike velocity. Completing this motion, it is in the full reset position at a crank angle of 45 degrees and is prepared for driving the hips forward again.

From the earlier qualitative comparison with the still images of the experiments, the experimental crank angle also appeared to be at approximately 45 degrees when in the reset position. The patterns in the hip joint angles seem to confirm this as well. Visually, it seems like the cyclist in the experiments may be farther back when in the reset position. The higher crank angular velocity means we do not see the same amount of hip movement in the simulation as in the experiments. At higher crank angular velocities, the technique becomes less effective as it is more difficult to go through the drive-reset motion at that speed in that amount of time. Unfortunately, a limitation for these comparisons is the lack of quantitative experimental measures of the hip position relative to the crank, so a direct comparison can not be made to the experiments.

Looking at the overall outcome of the simulation gives an idea of the optimal standing start technique. Based on the results of these experiments and simulation, it seems that the standing start technique being currently used is close to what was found by the optimal simulation. It seems that this cyclist in particular might be able to improve his starts by better timing his pre-launch with the gate release. From analyzing the experimental results, the cyclist may also improve performance by reducing the right/left asymmetries that were observed. This could be done by focusing on strengthening the weaker leg. Both seem to be performing the drive and reset motion at similar points in the pedal stroke.

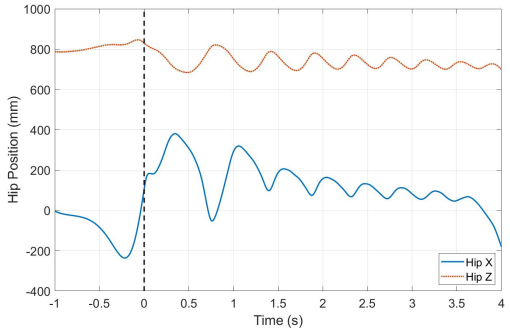

(a) Hip position versus time

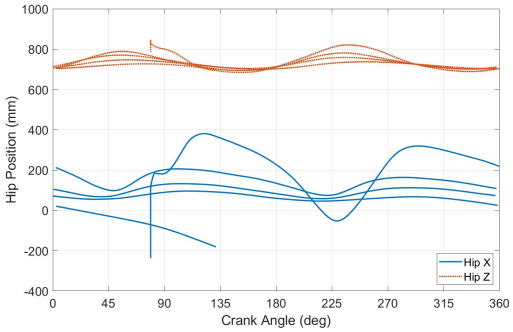

(b) Hip position versus relative crank angle

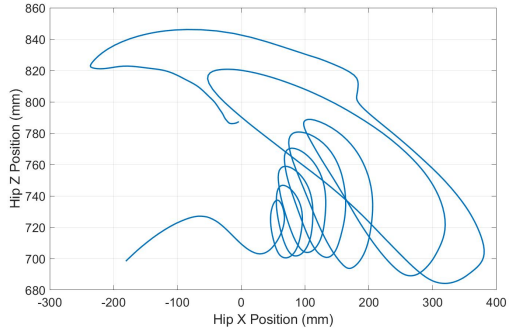

(c) Hip position in the vertical (sagittal) plane

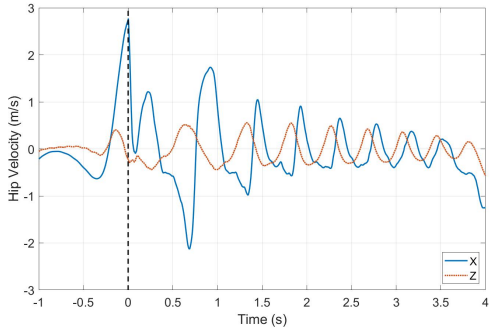

(d) Hip velocity relative to the bicycle

Figure 5.17: Hip joint center kinematics for the standing start simulation

The simulation and experiments are close enough in nature that any differences seen can not be clearly distinguished as improvements that should be made without questioning the effects of the assumptions and simplifications that have been made in the model.

Chapter 6

Conclusions

6.1 Project Summary

A two-legged cyclist and bicycle model was developed for predictive simulations using optimal control methods. First, the cyclist model was validated by simulating maximal start-up pedaling on an ergometer while in a seated position. The validation of the model appeared to be successful in that it could successfully replicate experimental results using an experimental data tracking approach, and produced similar results when using a predictive simulation. Predictive simulations were then performed for start-up cycling on a track bicycle. The model was able to replicate key features of the standing start technique, including the pre-launch, drive, and reset motions. A shortcoming of the predictive simulation is long CPU times, which is expected for the optimal control solution of complex multibody dynamics

The purposes of this study were two-fold. One was to provide feedback to the Canadian track cycling team on the technique being used in standing starts. The second was to evaluate the modeling and simulation methods being used to determine whether they are an effective way of modeling human movement. The secondary objective was successful in terms of its ability to find a technique that resembles that being used in real life. In one sense this was a positive because it indicated that our model was working well, but on the other hand, it was not going to produce groundbreaking changes to the standing start technique. The expectation was to find smaller details of the technique that could be corrected. It was expected for a sport that has been around for many years, the big-picture technique is fairly refined, but details need to be refined and better understood.

In its current form the model can be a useful tool. Additional uses of the model could be in testing cyclist set up such as handlebar position and crank length, or seat position in steady-state pedaling. It can provide insight into which groups of muscles are being used predominantly in which phases of the pedaling motion. There is the potential to observe the effects of varying joint strengths and how that affects the optimal technique. Additional benefits could be gained from understanding which joint torques are playing the largest roles throughout the standing start.

6.2 Limitations

There are some limitations to the results presented in this study. One is the use of joint torques rather than a full musculoskeletal model for the lower limbs. The joint torque model simplifies the neuromuscular components of a musculoskeletal model, in the process ignoring individual muscle properties and simplifying the activation dynamics, force-length scaling, and force-velocity scaling. Furthermore, the method of scaling the active joint torques does not take into account the effects of biarticular muscles. To represent a biarticular muscle, a joint torque would need to be scaled based off the joint angle and angular velocity of both joints that the muscle is acting on. Developing such a torque scaling function for all joints in the model would require a more comprehensive protocol for the dynamometer experiments than what has previously been used. There is also some uncertainty in the joint torque model with regards to the inclusions of passive torques and joint damping along with the active torques. Distinguishing the separate effects of each of these during dynamometer experiments can be difficult, so it is possible active torque scaling is already incorporating some of the effects of the passive torques and joint damping. Using a full musculoskeletal model would help solve some of these issues, but the additional state variables required make a full musculoskeletal model impractical for use in a predictive simulation of this scale.

More testing is needed on Olympic-level cyclists, as well as their bicycles, to ensure the model accurately represents their characteristics. One of the challenges of studying Olympic cyclists is knowing their capabilities. Their body types and muscle strength would be on the extreme end when compared to the average population, so more data are needed on Olympic-level athletes to create more representative models. To obtain more accurate results, it is desirable to obtain dual-energy X-ray absorptiometry (DXA) scans of the athletes, which would allow for the determination of person-specific anthropometric information, including limb segment lengths, masses, center of masses, and moments of inertia [65].

As mentioned, there were several assumptions and simplifications that were made in the development of the bicycle model. Center of mass and moment of inertia are estimated based on the geometry of the SolidWorks bicycle model so there is likely some error there. These errors were not a significant concern because the bicycle is fixed to remain upright, so only x location of the center of mass comes into play for the normal force experienced by wheels. Even then, the mass of the cyclist is ten times the frame mass so it likely would not have significant effects. Other aspects such as chain friction, bearing friction, wheel drag, and frame stiffness could also have an effect, although it is likely minimal and would not affect the optimal technique. The lack of aerodynamic drag forces is also a limitation of this work. However, as mentioned previously, these forces are small for the low velocities seen during the standing.

Some of the biggest uncertainties in the bicycle model lie with the tire model. For traveling in a straight line as this model does, the tire models are probably sufficiently accurate. The default tire model assumes the tires are traveling on a flat surface so there was no camber included as would be seen on the track. The tire stiffness and damping parameters should also be examined further. At times it seemed like the optimal result was overly dependent on meeting the bounds for vertical position. While it was not entirely accurate, the bicycle model was a reasonable approximation of a generic track bicycle.

The primary limitation of developing a more complex and accurate model is the computation time required. The longer simulation times are a result of looking at start-up pedaling, not steady-state pedaling, and using predictive simulation as opposed to data tracking. There was not a sensitivity study or convergence study to analyze how close to optimal these results truly are. The conclusion reached was that they give a general picture of the optimal technique, but conclusions can not be drawn without some degree of uncertainty. The "sub-optimal" results that were output were sometimes different from one simulation to the next. It is also possible, or even very likely, that similar results with similar objective function values could be attained with shorter run time. Extensive additional effort was not able to be put into finding the optimal number of meshes, iterations and tolerances as this would have been a time consuming process based on the simulation lengths.

6.3 Future Work

One of the main drawbacks to this method is the length of the optimal control process. As optimal control techniques continue to improve and take advantage of improved computing power, this will become less of an issue. Some of these recommendations for future work

would be dependent on faster run times, because simulations are already taking quite long, so adding to the complexity of the model is not recommended at the moment.

The primary recommendation is to investigate methods of improving the CPU times. Direct collocation seems to be the best method for optimal control of human movements, but there could be alternative methods available that work well. One possibility is to try using optimal control via indirect methods to see if it is more efficient. Currently, with the method of exporting the dynamic equations, automatic differentiation with adiGator does not work. Investigating a method to allow for the use of automatic differentiation with adiGator would be useful to increase computational efficiency. Another possibility for improving computation time is to examine additional modeling simplifications that would make the problem easier to solve. A large part of the difficulties with the optimal control seem to be coming from the stiffness and damping of the tires. It is possible that alternative methods of modeling these would allow for more efficient simulations. In addition to, and in the process of investigating methods of running simulations faster, more time should be spent exploring and understanding the nuances of the GPOPS-II software. This would help place more faith in the results that are being achieved and in deeming them the optimal technique that should be used by the team, as well as finding the optimal setup for finding the optimal solution efficiently.

Future work could be done to address some of the limitations that were presented. DXA scans could be used to get subject-specific mass and moment of inertia properties. A dynamometer could be used to develop a subject-specific torque scaling model for an Olympic cyclist. Passive torque functions could also be obtained. At a minimum, the maximum isometric torque values could be obtained to use as the bounds for the joint torques in the optimization. The primary challenge with this is the availability of the athletes. Olympic cyclists have busy training schedules so it can be difficult to find time to do experimental testing.

In addition to the dynamometer testing, a muscle model could be implemented in place of the joint torque model. The first step in this process would likely be to add the muscles but have them grouped into flexors and extensors so the number of controls stays the same. This would still increase the number of states, but maintaining the same number of controls could help keep computation times reasonable. The most practical method would be to only include lower limb muscles and leave the upper limbs actuated by joint torques. With regards to skeletal dynamics, the fidelity could be improved by adding a more complex knee joint that has translational degrees of freedom as a function of knee flexion angle, as was used in some previous pedaling models.

For tires, experimental testing could be done to obtain parameters specifically for track

cycling tires, rather than the parameters for road cycling tires that have previously been reported. This would require the development of a test rig specifically for bicycle tires. For the bicycle frame, work could be done to more accurately determine moment of inertia and center of mass locations for the frame. For an even more accurate bicycle model, a method of approximating energy lost due to bicycle frame deformation could be incorporated. Track cycling frames are designed to be quite stiff though, so this would likely have minimal effect and would not be a top priority.

It would be of interest to do more extensive testing with the cyclists on the track. Testing with more cyclists would enable a comparison between different cyclists to see how much the technique varies. In addition to measuring crank torque as was done in this study, it would be interesting to measure the exact pedal forces to study the forces that are directed radially inwards on the crank arm, as well as lateral forces out of the sagittal plane. The radial forces could be compared to simulations to see how the two compare in terms of efficiency of force production. More work could be done to evaluate using IMUs for measuring joint kinematics. Improved sensor fusion techniques would allow for more accurate kinematic measurements with minimal drift, while being less invasive and more durable than electrogoniometers.

The model could be tested in some of the applications mentioned previously using various aspects of the bicycle design and setup as part of the optimization: handlebar position, crank length, gear ratio or, in the case of steady-state pedaling, seat position. Varying physiological parameters could help for analyzing the effects of varying muscle strengths and how that affects the optimal technique. The key with these applications is knowing that the solver has converged and that the differences in the optimal solutions are due to the change in parameter and not just that the solver is converging to a different local optimum. Beyond using it for standing starts, this model could be fairly easily adapted to various other cycling applications by changing the height/weight, torque bounds, and bicycle setup.

Progressing into more complex modeling modifications, one could add a degree of freedom for bicycle roll and a controller for balance. While adding a single degree of freedom might not sound complicated initially, the incorporation of roll would add several complications. A controller for balancing and steering would be required, which would be difficult due to the oscillating leg masses and the trunk oscillating front to back. Doing so might also require a controller for lean to accurately incorporate the cyclist's ability to balance. These additions would present added difficulties with the tire models, as they would require lateral dynamics and camber forces to be included. The slope of the track would need to be considered as well, as tire forces would change with the addition of a camber angle. This starts getting quite complicated very quickly, and would likely cause a significant increase

in computation times.

Aerodynamics could be included within the standing start to get a more accurate estimation of distance traveled. Applying a generic aerodynamic drag to the entire model would not affect the technique being used, only the performance output. A proper aerodynamic model that could affect the technique would have to account for different body positions. One interesting potential application for a model such as this would be to investigate the optimal cycling position. In their review on aerodynamics in cycling, Crouch et al. [66] mention the lack of research on the relationship between aerodynamics and biomechanical efficiency for determining the optimal body position. Certain body positions are more aerodynamic but are less conducive to maximum power generation. Making this modification would be necessary for carrying out the simulation to study track cycling beyond the first 5-10 seconds of the race.

References

[1] J. L. Hicks, T. K. Uchida, A. Seth, A. Rajagopal, and S. L. Delp, "Is my model good enough? Best practices for verification and validation of musculoskeletal models and simulations of movement," *Journal of Biomechanical Engineering*, vol. 137, no. 2, p. 020905, 2015.

[2] A. Zignoli, F. Biral, B. Pellegrini, A. Jinha, W. Herzog, and F. Schena, "An optimal control solution to the predictive dynamics of cycling," *Sport Sciences for Health*, vol. 13, no. 2, pp. 1–13, 2017.

[3] R. Riener and T. Edrich, "Identification of passive elastic joint moments in the lower extremities," *Journal of Biomechanics*, vol. 32, no. 5, pp. 539–544, 1999.

[4] Biometrics Ltd., "Twin-Axis Electrogoniometers for Joint Movement Analysis," 2015.

[5] R. Fatovic, "Milton Velodrome," 2015.

[6] LOOK Cycle International SAS, "Look Track Bicycle," 2018.

[7] M. Patton, "Personal Communication," 2017.

[8] R. Lukes, J. Hart, and S. Haake, "An analytical model for track cycling," *Proceedings of the Institution of Mechanical Engineers, Part P: Journal of Sports Engineering and Technology*, vol. 226, no. 2, pp. 143–151, 2012.

[9] J. C. Martin, A. S. Gardner, M. Barras, and D. T. Martin, "Modeling sprint cycling using field-derived parameters and forward integration," *Medicine and Science in Sports and Exercise*, vol. 38, no. 3, pp. 592–597, 2006.

[10] T. Olds, K. I. Norton, and N. P. Craig, "Mathematical model of cycling performance.," *Journal of Applied Physiology*, vol. 75, no. 2, pp. 730–737, 1993.

[11] L. Underwood and M. Jermy, "Mathematical model of track cycling: The individual pursuit," *Procedia Engineering*, vol. 2, no. 2, pp. 3217–3222, 2010.

[12] N. Flyger, A. Froncioni, D. T. Martin, F. Billaut, J. Robert, and J. C. Martin, "Modelling track cycling standing start performance: combining energy supply and energy demand," *Proceedings of the International Conference on Biomechanics in Sports*, vol. 31, 2012.

[13] I. Janssen and J. Cornelissen, "Pedal Forces During the BMX and Track Sprint Cycling Start," *Sports Science and Innovation , Sportcentrum Papendal , Arnhem , The*, pp. 793–796, 2014.

[14] J. Padulo, G. Laffaye, W. Bertucci, A. Chaouachi, and D. Viggiano, "Optimisation of starting conditions in track cycling," *Sport Sciences for Health*, vol. 10, no. 3, pp. 189–198, 2014.

[15] J. Padulo, L. P. Ardigò, M. Milic, and D. W. Powell, "Electromyographic analysis of riding posture during the bicycling start moment," *Motriz: The Journal of Physical Education*, vol. 22, no. 4, pp. 237–242, 2016.

[16] R. R. Bini and F. Diefenthaeler, "Mechanical work and coordinative pattern of cycling: a literature review," *Kinesiology*, vol. 41, no. 1, pp. 25–39, 2009.

[17] M. Wangerin, S. Schmitt, B. Stapelfeldt, and A. Gollhofer, "Inverse dynamics in cycling performance," in *Advances in Medical Engineering* (T. Buzug, D. Holz, J. Bongartz, M. Kohl-Bareis, U. Hartmann, and S. Weber, eds.), no. 114, p. 476, Berlin, Heidelberg: Springer, 2007.

[18] J. C. Martin and N. A. T. Brown, "Joint-specific power production and fatigue during maximal cycling," *Journal of Biomechanics*, vol. 42, no. 4, pp. 474–479, 2009.

[19] H. Yamazaki and A. Matsuda, "Joint Torque Evaluation of Lower Limbs in Bicycle Pedaling," *Procedia Engineering*, vol. 147, pp. 263–268, 2016.

[20] C. C. Raasch, F. E. Zajac, B. Ma, and W. S. Levine, "Muscle coordination of maximum-speed pedaling," *Journal of Biomechanics*, vol. 26, no. 96, 1993.

[21] C. C. Raasch and F. E. Zajac, "Locomotor strategy for pedaling: muscle groups and biomechanical functions.," *Journal of Neurophysiology*, vol. 82, no. 2, pp. 515–25, 1999.

[22] R. R. Neptune and M. L. Hull, "Evaluation of performance criteria for simulation of submaximal steady-state cycling using a forward dynamic model.," *Journal of Biomechanical Engineering*, vol. 120, no. 3, pp. 334–41, 1998.

[23] A. V. Hill, "The Heat of Shortening and the Dynamic Constants of Muscle," *Proceedings of the Royal Society B: Biological Sciences*, vol. 126, no. 843, pp. 136–195, 1938.

[24] M. Millard, T. Uchida, A. Seth, and S. L. Delp, "Flexing computational muscle: modeling and simulation of musculotendon dynamics," *Journal of Biomechanical Engineering*, vol. 135, no. 2, p. 021005, 2013.

[25] L. H. Ting, S. A. Kautz, D. A. Brown, and F. E. Zajac, "Phase reversal of biomechanical functions and muscle activity in backward pedaling," *Journal of Neurophysiology*, vol. 81, no. 2, p. 544, 1999.

[26] M. L. Kaplan and J. H. Heegaard, "Predictive algorithms for neuromuscular control of human locomotion," *Journal of Biomechanics*, vol. 34, no. 8, pp. 1077–1083, 2001.

[27] D. G. Thelen, F. C. Anderson, and S. L. Delp, "Generating dynamic simulations of movement using computed muscle control," *Journal of Biomechanics*, vol. 36, no. 3, pp. 321–328, 2003.

[28] M. F. Bobbert, L. J. Casius, and A. J. Van Soest, "The relationship between pedal force and crank angular velocity in sprint cycling," *Medicine and Science in Sports and Exercise*, vol. 48, no. 5, pp. 869–878, 2016.

[29] R. M. Alexander, "Optimum take-off techniques for high and long jumps.," *Philosophical Transactions of the Royal Society of London. Series B, Biological Sciences*, vol. 329, no. 1252, pp. 3–10, 1990.

[30] D. Balzerson, J. Banerjee, and J. McPhee, "A three-dimensional forward dynamic model of the golf swing optimized for ball carry distance," *Sports Engineering*, vol. 19, no. 4, pp. 237–250, 2016.

[31] W. McNally and J. McPhee, "Dynamic Optimization of the Golf Swing Using a Six Degree-of-Freedom Biomechanical Model," *Proceedings*, vol. 2, no. 6, p. 243, 2018.

[32] M. R. Yeadon and M. A. King, "Evaluation of a torque driven simulation model of tumbling," *Journal of Applied Biomechanics*, vol. 18, pp. 195–206, 2002.

[33] F. C. Anderson and M. G. Pandy, "Dynamic Optimization of Human Walking," *Journal of Biomechanical Engineering*, vol. 123, no. 5, p. 381, 2001.

[34] S. Porsa, Y.-C. Lin, and M. G. Pandy, "Direct methods for predicting movement biomechanics based upon optimal control theory with implementation in OpenSim," *Annals of Biomedical Engineering*, vol. 44, no. 8, pp. 2542–2557, 2016.

[35] F. De Groote, A. L. Kinney, A. V. Rao, and B. J. Fregly, "Evaluation of Direct Collocation Optimal Control Problem Formulations for Solving the Muscle Redundancy Problem," *Annals of Biomedical Engineering*, vol. 44, no. 10, pp. 2922–2936, 2016.

[36] A. J. K. van Soest and L. J. R. Casius, "Which factors determine the optimal pedaling rate in spring cycling?," *Medicine and Science in Sports and Exercise*, pp. 1927–1934, 2000.

[37] S. D. Farahani, W. Bertucci, M. S. Andersen, M. de Zee, and J. Rasmussen, "Prediction of crank torque and pedal angle profiles during pedaling movements by biomechanical optimization," *Structural and Multidisciplinary Optimization*, vol. 51, no. 1, pp. 251–266, 2015.

[38] R. Redfield and M. L. Hull, "Prediction of pedal forces in bicycling using optimization methods," *Journal of Biomechanics*, vol. 19, no. 7, pp. 523–540, 1986.

[39] H. Gonzalez and M. L. Hull, "Multivariable optimization of cycling biomechanics," *Journal of Biomechanics*, vol. 22, no. 11-12, pp. 1151–1161, 1989.

[40] B. J. Fregly and F. E. Zajac, "A state-space analysis of mechanical energy generation, absorption, and transfer during pedaling," *Journal of Biomechanics*, vol. 29, no. 1, pp. 81–90, 1996.

[41] S. Kautz and M. Hull, "Dynamic optimization analysis for equipment setup problems in endurance cycling," *Journal of Biomechanics*, vol. 28, no. 11, pp. 1391–1401, 1995.

[42] A. K. Lai, A. S. Arnold, A. A. Biewener, T. J. Dick, and J. M. Wakeling, "Does a two-element muscle model offer advantages when estimating ankle plantar flexor forces during human cycling?," *Journal of Biomechanics*, vol. 68, pp. 6–13, 2017.

[43] B. M. Ashby and S. L. Delp, "Optimal control simulations reveal mechanisms by which arm movement improves standing long jump performance," *Journal of Biomechanics*, vol. 39, no. 9, pp. 1726–1734, 2006.

[44] M. G. Pandy, F. C. Anderson, and D. G. Hull, "A Parameter Optimization Approach for the Optimal Control of Large-Scale Musculoskeletal Systems," *The American society of mechacnial engineers*, vol. 114, no. 1992, pp. 450–460, 1992.

[45] N. Mehrabi and J. McPhee, "Predictive Simulation of Cycling with Muscle Fatigue," in *The 4th Joint International Conference on Multibody System Dynamics*, 2016.

[46] A. L. Schwab and J. P. Meijaard, "A review on bicycle dynamics and rider control," *Vehicle System Dynamics*, vol. 51, no. 7, pp. 1059–1090, 2013.

[47] J. D. G. Kooijman, A. L. Schwab, and J. P. Meijaard, "Experimental validation of a model of an uncontrolled bicycle," *Multibody System Dynamics*, vol. 19, no. 1-2, pp. 115–132, 2008.

[48] A. L. Schwab, J. P. Meijaard, and J. D. G. Kooijman, "Lateral dynamics of a bicycle with a passive rider model: Stability and controllability," *Vehicle System Dynamics*, vol. 50, no. 8, pp. 1209–1224, 2012.

[49] B. Connors and M. Hubbard, "Modelling and Stability Analysis of a Recumbent Bicycle with Oscillating Leg Masses," *The Engineering of Sport 7*, pp. 677–685, 2008.

[50] R. S. Sharp, "On the Stability and Control of the Bicycle," *Applied Mechanics Reviews*, vol. 61, no. 6, pp. 1–24, 2008.

[51] A. E. Dressel and A. Rahman, "Measuring sideslip and camber characteristics of bicycle tyres," *Vehicle System Dynamics*, vol. 50, no. 8, pp. 1365–1378, 2012.

[52] A. Doria, M. Tognazzo, G. Cusimano, V. Bulsink, A. Cooke, and B. Koopman, "Identification of the mechanical properties of bicycle tyres for modelling of bicycle dynamics," *Vehicle System Dynamics*, vol. 3114, no. January 2013, pp. 1–16, 2012.

[53] V. E. Bulsink, A. Doria, D. van de Belt, and B. Koopman, "The Effect of Tyre and Rider Properties on the Stability of a Bicycle," *Advances in Mechanical Engineering*, vol. 7, no. 12, pp. pp 1–19, 2015.

[54] J. Bierman, "Tire Test - Vittoria Corsa Speed (tubular)," 2017.

[55] H. B. Pacejka, *Tire and Vehicle Dynamics, 2nd edition.* Butterworth-Heinemann, 2 ed., 2005.

[56] N. Petrone and F. Giubilato, "Methods for evaluating the radial structural behaviour of racing bicycle wheels," *Procedia Engineering*, vol. 13, pp. 88–93, 2011.

[57] P. de Leva, "Adjustments to Zatsiorsky-Seluyanov's Segment Inertia Parameters," *Journal of Biomechanics*, vol. 29, no. 9, pp. 1223–1230, 1996.

[58] D. E. Anderson, M. L. Madigan, and M. A. Nussbaum, "Maximum voluntary joint torque as a function of joint angle and angular velocity: Model development and application to the lower limb," *Journal of Biomechanics*, vol. 40, no. 14, pp. 3105–3113, 2007.

[59] M. Kordi, S. Goodall, P. Barratt, N. Rowley, J. Leeder, and G. Howatson, "Relation between Peak Power Output in Sprint Cycling and Maximum Voluntary Isometric Torque Production," *Journal of Electromyography and Kinesiology*, vol. 35, pp. 95–99, 2017.

[60] A. van Soest and M. Bobbert, "The contribution of muscle properties in the control of explosive movements," *Biological Cybernetics*, vol. 69, no. 3, pp. 195–204, 1993.

[61] B. A. Garner and M. G. Pandy, "Musculoskeletal model of the upper limb based on the visible human male dataset," *Computer Methods in Biomechanics and Biomedical Engineering*, vol. 4, no. 2, pp. 93–126, 2001.

[62] J. M. Winters, "An improved muscle-reflex actuator for use in large-scale neuromusculoskeletal models," *Annals of Biomedical Engineering*, vol. 23, no. 4, pp. 359–374, 1995.

[63] A. V. Rao, D. a. Benson, C. Darby, M. a. Patterson, C. Francolin, I. Sanders, and G. T. Huntington, "GPOPS II: A MATLAB Software for Solving Multiple-Phase Optimal Control Problems Using hpAdaptive Gaussian Quadrature Collocation Methods and Sparse Nonlinear Programming," *ACM Transactions on Mathematical Software*, vol. 37, no. 2, pp. 1–39, 2010.

[64] M. Jensen, *Neuromechanical Measurement of the Effect of Carbohydrate Mouth Rinse on Human Performance in Strength and Elite Cycling Endurance*. PhD thesis, University of Victoria, 2018.

[65] B. Laschowski and J. McPhee, "Body segment parameters of Paralympic athletes from dual-energy X-ray absorptiometry," *Sports Engineering*, vol. 19, no. 3, pp. 155–162, 2016.

[66] T. N. Crouch, D. Burton, Z. A. LaBry, and K. B. Blair, "Riding against the wind: a review of competition cycling aerodynamics," *Sports Engineering*, 2017.

APPENDICES

Appendix A

Additional Details on Model Development and Optimal Control

A.1 Model Degrees of Freedom

For the model used in the ergometer pedaling predictive simulation, the legs+crank form a closed kinematic chain with three total degrees of freedom. This is generally thought of as one for each leg (either the hip, knee, or ankle) and one for the crank angle. For the model used in the ergometer pedaling data-tracking simulation, the upper body was included to allow for the matching of all three right leg joint angles. The cyclist has five degrees of freedom among the two legs and the upper body and there is one degree of freedom for the crank. For the data-tracking approach it makes the most sense to think of these degrees of freedom being the right hip, knee, and ankle (which are tracking the experimental data), the crank (also tracking the experimental data). This leaves two degrees of freedom among the upper body and the left leg that are essentially up to the model to find the best values for tracking the previously mentioned experimental data as well as the crank torque while minimizing the joint torques required. The combined cyclist and bicycle model has ten total degrees of freedom. Just as with the data-tracking model, the cyclist has five degrees of freedom. The bicycle has five degrees of freedom, with the rear wheel connected to the crank by an ideal gear

Ergometer data-tracking model

1. Crank
2. Right hip
3. Right knee
4. Right ankle
5. Left ankle
6. Wrist

Ergometer predictive model

1. Crank
2. Right ankle
3. Left ankle

Combined bicycle and cyclist model

1. Horizontal frame translation
2. Vertical frame position
3. Frame pitch
4. Front wheel
5. Crank
6. Wrist
7. Elbow
8. Shoulder
9. Right ankle
10. Left ankle

A.2 GPOPS-II Bounds

Table A.1 contains the state bounds that were used in GPOPS-II. In some cases, the bounds are not necessarily physical or physiological bounds, but were set in such a way to allow the solver to find the optimal solution more quickly. Reducing the bounds to the expected ranges limits the range of possible solutions that could be searched by the solver, thus speeding up the computation time. However, if the bounds are too restrictive, the solver may have difficulty finding the optimal solution due to the restrictive nature of the bounds.

Table A.1: Bounds used in GPOPS-II

State	Lower	Upper
Frame x Position (m)	0	60
Frame x Velocity (m/s)	0	25
Frame z Position (m)	-0.005	0.001
Frame z Velocity (m/s)	-0.1	0.1
Frame Pitch Angle (rad)	-0.03	0.03
Frame Pitch Angular Velocity (rad/s)	-0.7	0.7
Front Wheel Angle (rad)	0	190
Front Wheel Angular Velocity (rad/s)	0	75
Crank Angle (rad)	0	55
Crank Angular Velocity (rad/s)	0	20
Wrist Angle (rad)	0.45	1.75
Wrist Angular Velocity (rad/s)	-6	6
Elbow Angle (rad)	0	1.45
Elbow Angular Velocity (rad/s)	-8	8
Shoulder Angle (rad)	0.1	2
Shoulder Angular Velocity (rad/s)	-9	9
Hip Angle (rad)	0.5	2.7
Hip Angular Velocity (rad/s)	-9	9
Knee Angle (rad)	0.05	2.7
Knee Angular Velocity (rad/s)	-10	10
Ankle Angle (rad)	-0.8	0.65
Ankle Angular Velocity (rad/s)	-9	9

Appendix B

Additional Plots for the Ergometer Simulations

B.1 Additional Plots for the Ergometer Data Tracking Simulation

Figure B.1 contains the passive torques for the lower limbs. The hip and knee have less than 20 N·m of passive torque so it is not playing a significant role. The right ankle has slightly more, peaking at around 40 N·m. The left ankle has large amounts of passive torque in the first few pedal strokes. This is likely because there were no data recorded for the left leg, so it is being partially driven by the right leg hip position. This results in the left leg needing to produce joint angles that are somewhat more unnatural.

Figure B.2 contains the pedal forces in the crank reference frame. The forces are presented in the frame of the crank, with the radial direction referring to parallel to the crank arm, and propulsive referring to perpendicular to the crank arm. There were surprisingly large amounts of radial forces being applied, in some cases reaching peaks that were as much as twice the propulsive force peaks.

Figure B.3 displays the constraint error. The constraints were for the revolute joint connecting the foot/pedal to the crank. There is no noticeable constraint error for a majority of the simulation; however, there was a sharp jump to 0.6 mm of error at the last time point. It was noticed in most simulations that the solver had trouble maintaining the constraints at the final time point. It was unclear why this was an issue.

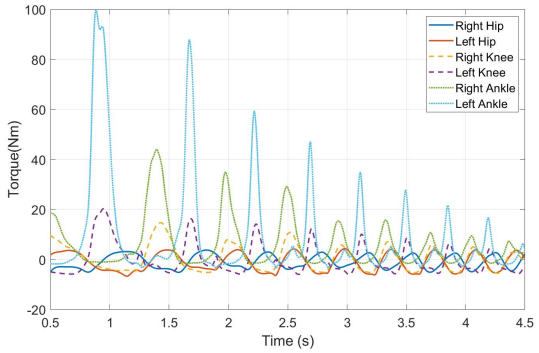

Figure B.1: Passive hip, knee, and ankle torques for data tracking simulation

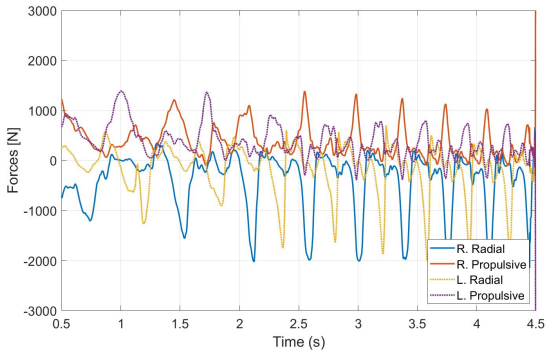

Figure B.2: Pedal forces for data tracking simulation

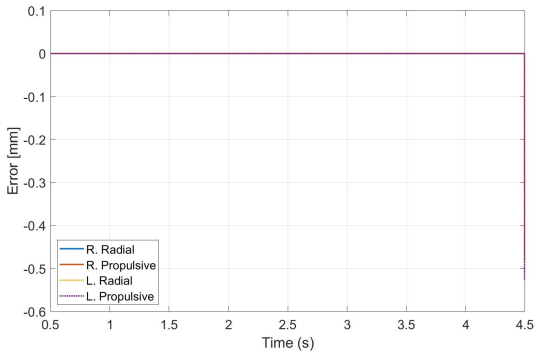

Figure B.3: Constraint error for data tracking simulation

B.2 Additional Plots for the Ergometer Predictive Simulation

Figure B.4 contains the passive torques for the lower limbs. When given freedom, the model uses a technique that does not result in large passive torques. Hip and knee passive torques both remain less than 10 N·m. There is more ankle passive torque, but it remains under 35 N·m.

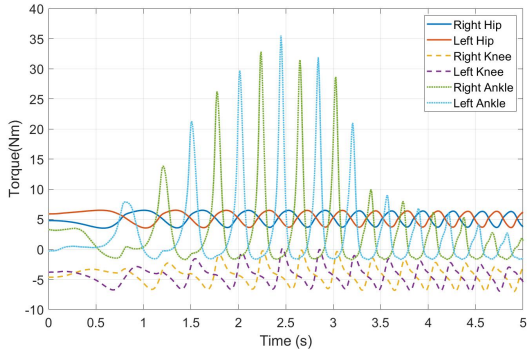

Figure B.4: Passive hip, knee, and ankle torques for the ergometer predictive simulation

Figure B.5 contains the pedal forces in the crank reference frame. As with the data-tracking simulation, there were larger radial pedal forces than propulsive pedal forces. This was more inefficient than was expected, as it was thought that minimizing the wasted forces would be optimal. An experimental analysis of pedal forces would be useful to further investigate pedal forces in maximal start-up cycling.

Figure B.6 displays the constraint error. The constraint error remains under $1\text{x}10^{-10}$ mm throughout the 5-second portion of the simulation that was displayed in all plots.

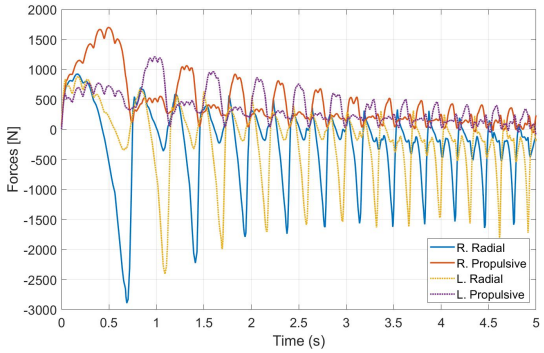

Figure B.5: Pedal forces for the ergometer predictive simulation

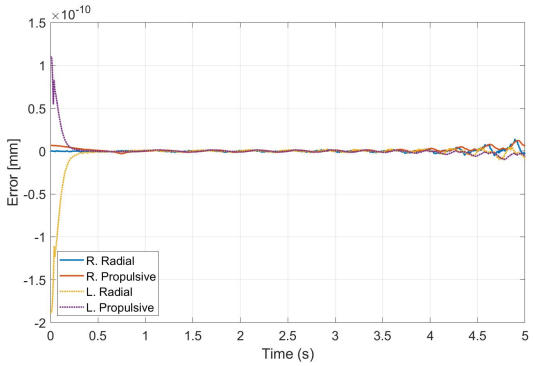

Figure B.6: Constraint error for the ergometer predictive simulation

Appendix C

Additional Plots for the Standing Start Simulation

C.1 Additional Plots for the Bicycle

Figure C.1 is the vertical position and frame rotation (frame pitch angle). There are oscillations of approximately 2mm in the vertical position of the frame center of mass. Very small oscillations in the frame pitch angle are seen as well. The most concern is with the initial spikes seen in both. This is due to the position and orientation starting in a position where the tire spring stiffness is compressed, resulting in transient behavior.

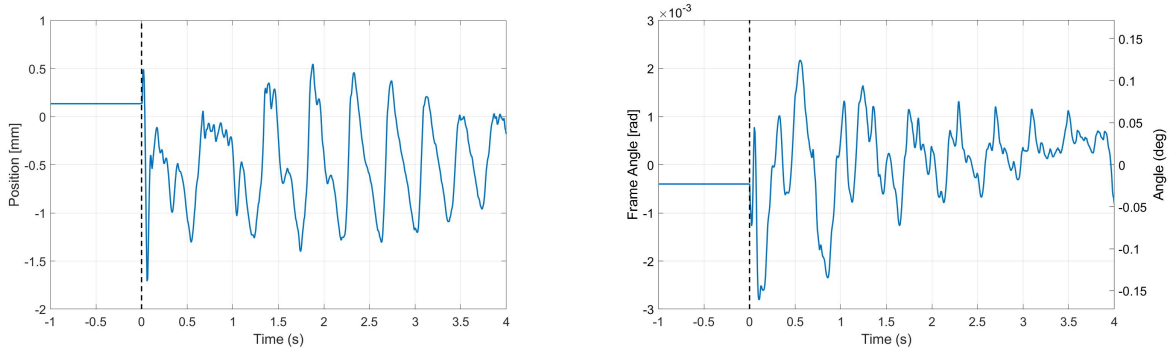

(a) Vertical position of the frame center of mass

(b) Pitch angle of the frame

Figure C.1: Bicycle frame motion

Figure C.2 are the wheel normal forces plotted versus time and versus the crank angle relative to TDC throughout the standing start simulation. The bicycle is not included in the pre-launch phase so the vertical forces prior to gate release are plotted as being the same as the instant of gate release, even though that is not actually the case. The vertical forces would be changing throughout the pre-launch phase. There are fairly large oscillations in the vertical forces as the cyclist model shifts its weight longitudinally relative to the bicycle.

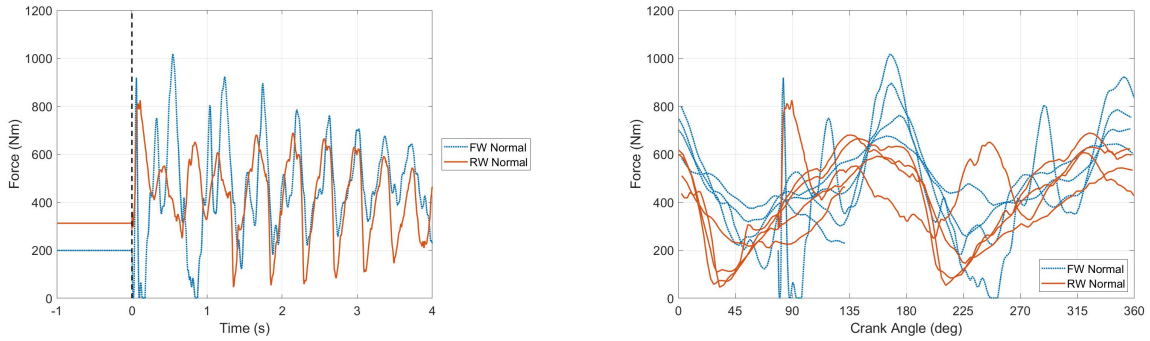

(a) Wheel normal forces versus time

(b) Wheel normal forces versus crank angle

Figure C.2: Wheel normal forces

Figure C.3 is the tire slip. The large amounts of slip are seen in the driven wheel (i.e. the rear wheel). The rear wheel slip follows a profile similar to the crank torque, as it is the applied torque that results in acceleration and wheel slip. The front wheel has considerably less slip as it is the non-driven wheel.

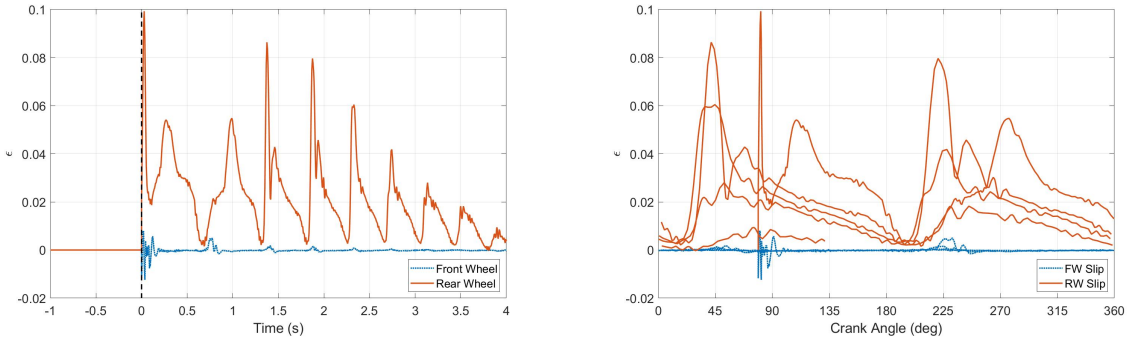

(a) Tire slip versus time

(b) Tire slip versus the relative crank angle

Figure C.3: Tire slip

C.2 Additional Plots for the Cyclist

Figure C.4 contains the velocity of the center of mass of the entire system (cyclist+bicycle). This shows that the velocity of the center of mass of the system is continuous between phases. The jump in bicycle velocity is coming from the transfer of the momentum from the cyclist to the bicycle when the bicycle is released from the gate.

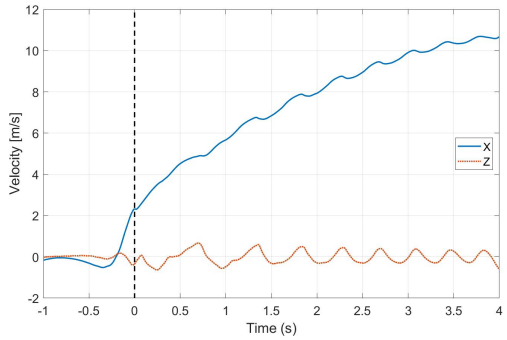

Figure C.4: System center of mass velocity

Figure C.5 contains the lower leg joint angles plotted against the crank angle relative to TDC. This shows whether or not the motion is repetitive. The experimental results indicate the cyclist was fairly repetitive from one pedal stroke to the next. The simulation was much less repetitive in nature, but the profiles generally followed the same trend in each pedal stroke.

Figure C.6 contains the upper limb joint angles plotted against the crank angle relative to TDC. Similar to the lower limb, the experimental results indicate the cyclist was fairly repetitive from one pedal stroke to the next. The simulation was much less repetitive in nature, but the profiles generally followed the same trend in each pedal stroke. The elbow did not seem to follow a consistent pattern between pedal strokes, indicating that its motion may be redundant to the overall motion. Generally in all the figures, the peaks/valleys are seen at approximately 45 degrees and 225 degrees for the crank, when the cyclist is in the reset position. The first two pedal strokes in the simulation are the only ones with a noticeable reset maneuver. The drive and reset maneuver is not as visibile in the experimental wrist and elbow angles. It seems these joints are generally more stable, and it is likely the drive/reset would be more visible in the shoulder angle if it could be accurately measured for the experiments.

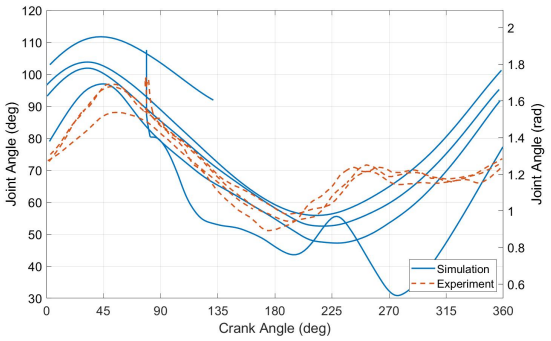

(a) Right hip angle versus crank angle

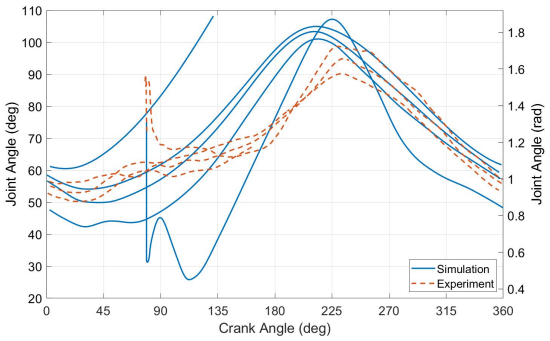

(b) Left hip angle versus crank angle

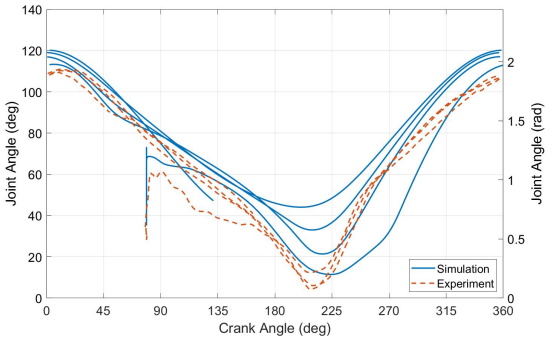

(c) Right knee angle versus crank angle

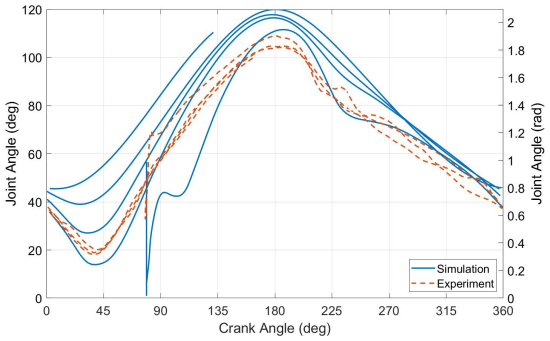

(d) Left knee angle versus crank angle

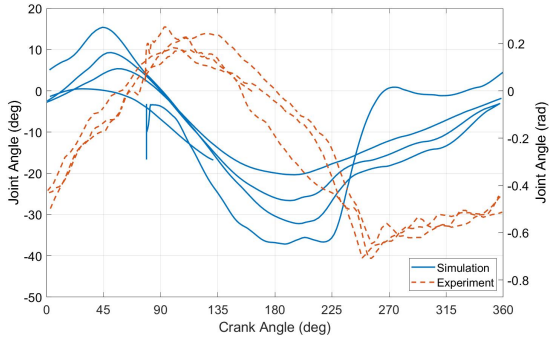

(e) Right ankle angle versus crank angle

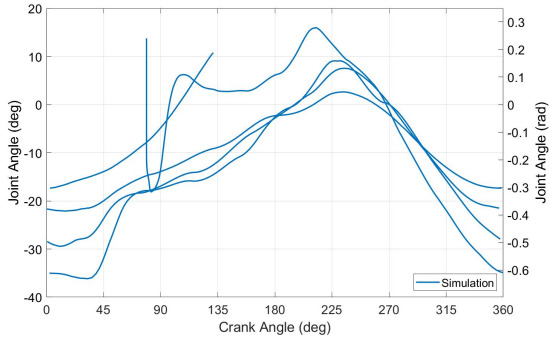

(f) Left ankle angle versus crank angle

Figure C.5: Lower limb joint angles versus relative crank angle

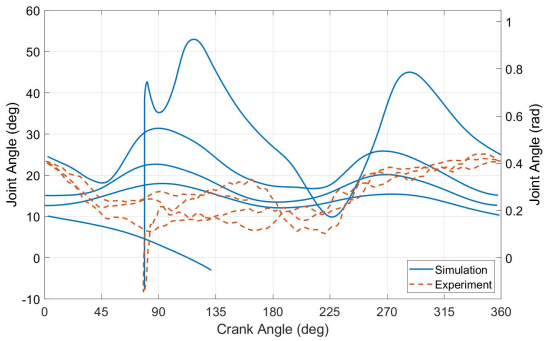

(a) Wrist angle versus relative crank angle

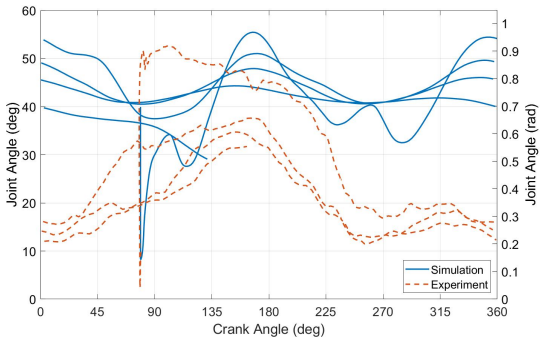

(b) Elbow angle versus relative crank angle

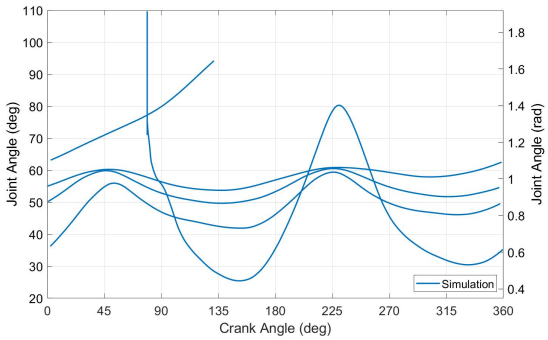

(c) Shoulder angle versus relative crank angle

Figure C.6: Upper limb joint angles

Figure C.7 has the lower limb joint torques plotted against the crank angle relative to TDC. The joint torques follow a fairly consistent pattern in the simulations. They are not being maximally activated in later pedal strokes, potentially because of the difficulty in controlling the motion at higher speeds and applying that large of a torque and then deactivating to a lower torque is difficult to perform.

Figure C.8 contains joint angles and angular velocities of for the lower limbs. From Figure C.8a there does not appear to be any noticeable asymmetries. The simulation seems to be fairly consistent between pedal strokes as well (Figure C.8b). Similarly, the angular velocities seem to be fairly consistent between legs as well (Figure C.8c).

Figure C.9 contains the passive joint torques for the lower limbs in the standing start simulation. The largest passive torques occurred in the ankle right at the gate release. The simulation was attempting to use the full range of motion for the ankle, which resulted in the larger ankle passive torques. As with the ergometer pedaling, there were less than 20 N·m of passive torque for the hips and knees.

Figure C.10 displays the crank torque and power versus the crank angle relative to TDC. The profiles for both the experiment and simulation follow the expected double-peak pattern. The peaks in the torque occur for each leg during the downstroke. The peaks in the simulation are slightly after the peaks in the experiments. This could be experimental error, as the crank angle is approximated from the cadence. It could also be due to a difference in technique. The cyclist seems to trend slightly farther forward, which would result in a larger crank angle being the most optimal for generating torque.

Figure C.11 is the pedal forces for both pedals in the propulsive (perpendicular to the crank arm) and radial (parallel to the crank arm) directions. Unlike in the ergometer pedaling, the propulsive pedal forces are greater than the radial pedal forces. In the first few pedal strokes, the opposite leg is able to pull up during the upstroke to add to the propulsive torque. As the cadence increases, this is no longer possible and the drive leg is responsible for nearly all the propulsive force.

Figure C.12 contains the constraint error. There were some issues with the interface between the pre-launch and launch phases. The initial mesh fraction after the phase switch has the largest constraint error, before the constraint error is reduced throughout the rest of the launch phase.

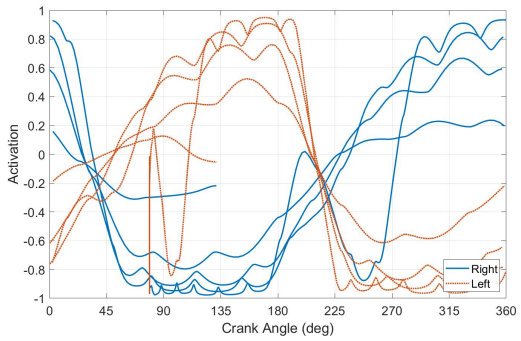

(a) Hip joint torque activation

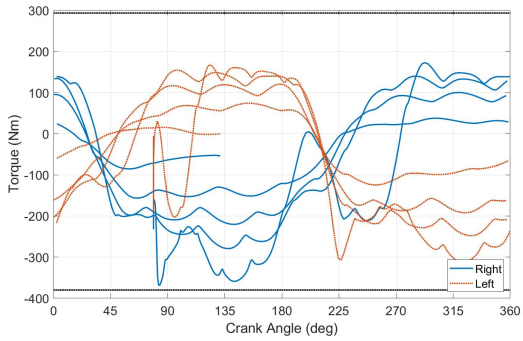

(b) Hip joint torque

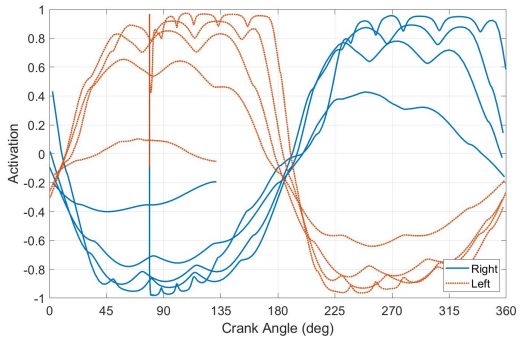

(c) Knee joint torque activation

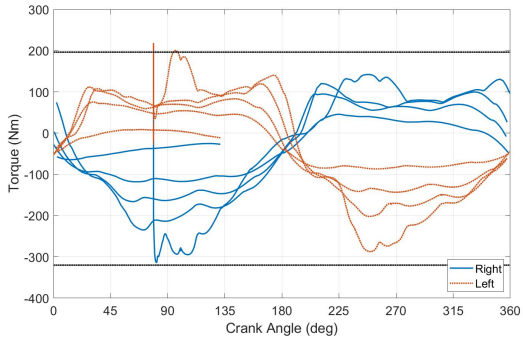

(d) Knee joint torque

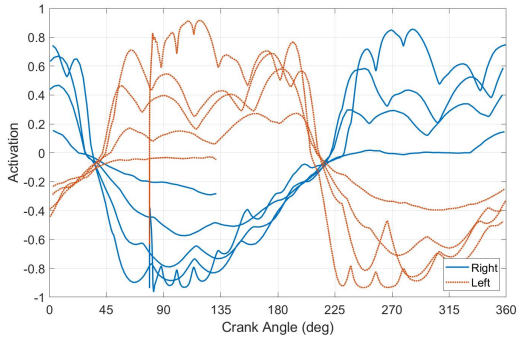

(e) Ankle joint torque activation

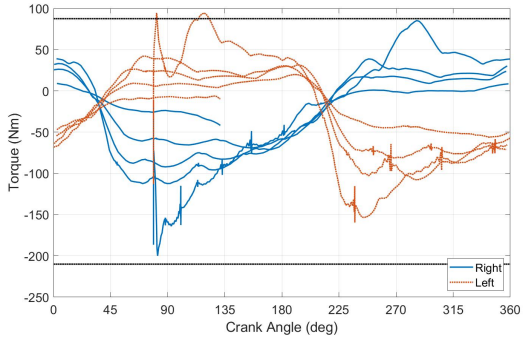

(f) Ankle joint torque

Figure C.7: Lower limb joint torques and activations versus relative crank angle

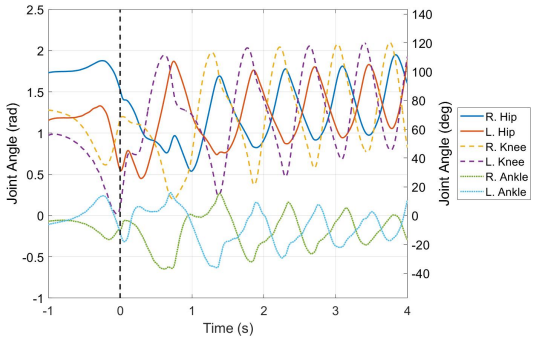

(a) All lower limb joints versus time

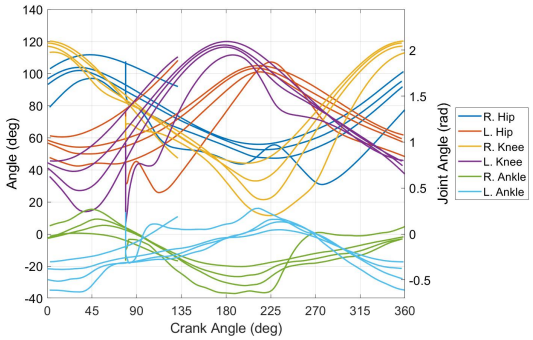

(b) All lower limb joints versus crank angle

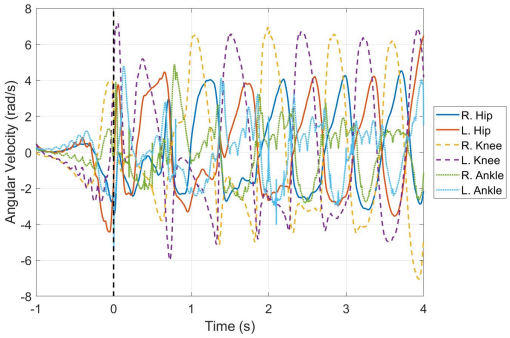

(c) Angular velocities for all lower limb joints

Figure C.8: Lower limb joint angles and angular velocities

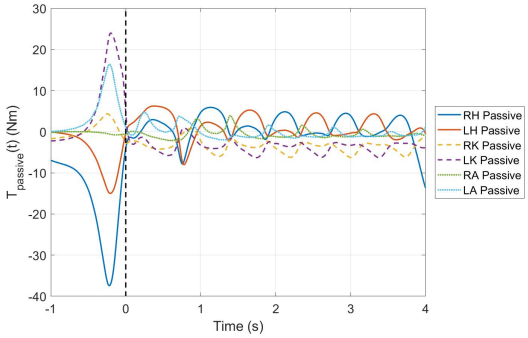

Figure C.9: Passive hip, knee, and ankle torques for track predictive simulation

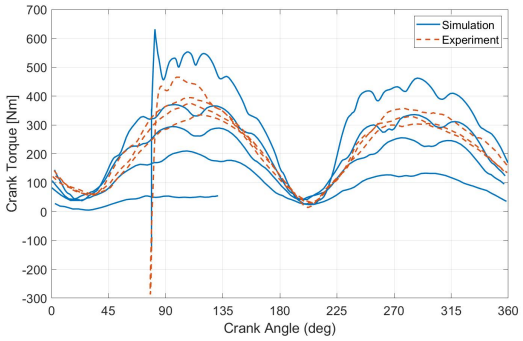

(a) Crank Torque

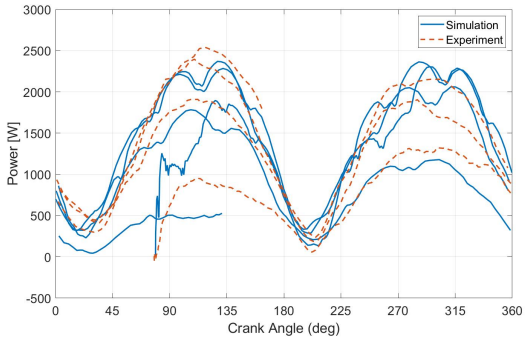

(b) Power

Figure C.10: Crank torque and power versus relative crank angle

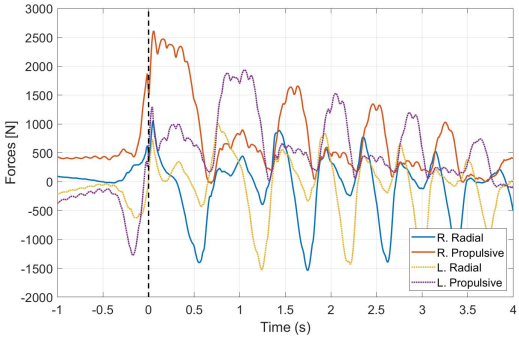

(a) Pedal forces

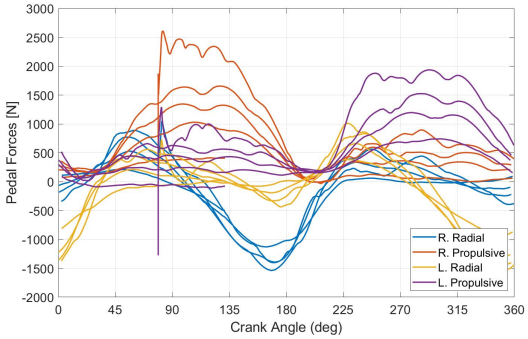

(b) Pedal forces

Figure C.11: Pedal forces for the predictive simulation

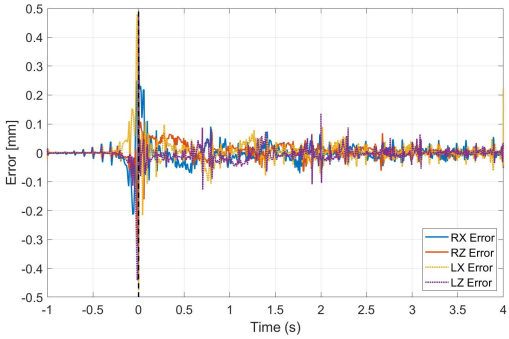

Figure C.12: Constraint error for track predictive simulation